

# PERFORMANCE EVALUATION OF CASCADED MULTILEVEL CONVERTER BASED STATCOM

**.A DISSERTATION**

*Submitted in partial fulfillment of the  
requirements for the award of the degree*

*of*

**MASTER OF TECHNOLOGY**

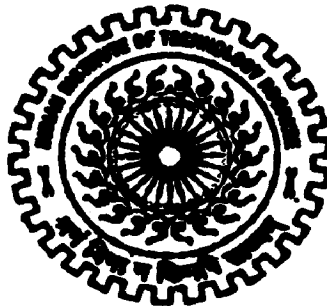
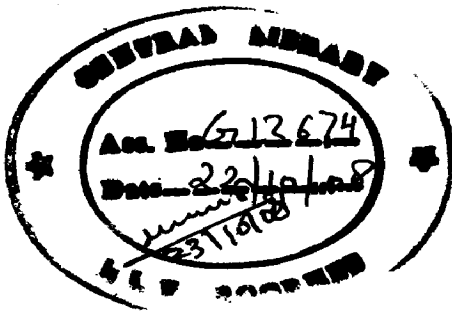
*in*

**ELECTRICAL ENGINEERING**

**(With Specialization in Power System Engineering)**

**By**

**PARAMARSHI BANERJEE**



IP

**DEPARTMENT OF ELECTRICAL ENGINEERING  
INDIAN INSTITUTE OF TECHNOLOGY ROORKEE  
ROORKEE - 247 667 (INDIA)  
JUNE, 2008**

## CANDIDATE'S DECLARATION

---

I hereby declare that the work that is being presented in this dissertation report entitled "**Performance Evaluation of Cascaded Multilevel Converter based STATCOM**" submitted in partial fulfillment of the requirements for the award of the degree of Master of Technology with specialization in "Power System Engineering", to the Department Of Electrical Engineering, Indian Institute Of Technology, Roorkee, is an authentic record of my own work carried out under the esteemed guidance of Dr. Biswarup Das & Dr. Pramod Agarwal, Department of Electrical Engineering.

I have not submitted the matter presented in this dissertation report for the Award of any other degree or diploma.

Date: 28-06-08


Place: Roorkee


*Paramarshi Banerjee*  
(PARAMARSHI BANERJEE)  
En. No. : 064003

---

## CERTIFICATE

This is to certify that the above statement made by the candidate is correct to the best of my knowledge.

  
(Dr. BISWARUP DAS)  
Associate Professor,

  
(Dr. PRAMOD AGARWAL)  
Professor,

Department of Electrical Engineering,  
Indian Institute of Technology,  
ROORKEE - 247 667

## Acknowledgement

---

*I write "He" (capital 'h') to pronoun both of my Guides.*

*Paramarshi Banerjee*  
*En. No. 064003*

# ABSTRACT

---

In this thesis the voltage control performance of the Cascaded Multilevel Converter (CMC) based STATCOM has been studied. Specifically, a 21 level CMC based STATCOM has been considered and its performance for controlling the bus voltage under fault conditions has been investigated in a practical power distribution system. For determining the switching angles of the CMC based STATCOM, an optimization methodology based on Sequential Quadratic Programming technique, has been used so as to minimize the THD of the STATCOM output voltage. Subsequently, a feedback linearization based on non-linear control law has been designed for the STATCOM voltage regulator. However it was found that under severe fault conditions, the performance of the non-linear voltage controller is quite unsatisfactory. To achieve satisfactory performance of the STATCOM voltage controller, Fuzzy Control systems have been proposed in this thesis. Two different fuzzy control systems namely indirect and direct have been developed in this thesis for this purpose. In the indirect control scheme, the angle difference between the STATCOM bus voltage and the STATCOM output voltage ( $\delta$ ) is used as the control signal, whereas the direct control system, both the modulation index and the angle  $\delta$  are used as control signals. The performances of these two developed control schemes have been studied with severe symmetrical and unsymmetrical faults. From detailed non-linear simulation studies it has been observed that the performance of the direct fuzzy control system is considerably superior to that of the indirect control scheme.



# Table of Contents

---

Acknowledgement	III
Abstract	IV
Nomenclature	VI
List of Figures	VII
List of Tables	X
Chapter 1 Introduction	1
1.1 The Problem	1
1.2 STATCOM Operation	3
1.3 Requirement of exchange of real power	4
1.4 STATCOM operating characteristics	5
1.5 Transient response	7
1.6 Literature Review	9
1.7 Organization of the thesis	11
Chapter 2 Multilevel Converters	13
2.1 Types of Multilevel Converters	13
2.2 Optimal Pulse Width Modulation	17
2.3 Optimization by Genetic Algorithm	21
2.4 A new initial condition algorithm for THD minimization	23
Chapter 3 Mathematical Modelling	27
3.1 The Distribution system	27
3.2 System start up	27
3.3 Vector representation of instantaneous 3-phase quantities	29
3.4 Equivalent circuit and equations	30
3.5 Exact linearization via feedback	31
Chapter 4 Indirect Fuzzy Control	37
4.1 Fuzzy PI controller	37
4.2 Performance of indirect fuzzy controller	40
Chapter 5 Direct Fuzzy Control	47
5.1 Direct fuzzy controller design	47
5.2 Performance of direct fuzzy controller	47
Chapter 6 Conclusion	55
References	57
Appendix A	59
Appendix B	61
Appendix C	67

# Nomenclature

---

AC	Alternating Current
CMC	Cascaded-Multilevel Converter
DC	Direct Current
DCMC	Diode-Clamped Multilevel Converter
ETO	Emitter Turn Off thyristor
FACTS	Flexible AC Transmission Systems
FCMC	Flying Capacitor Multilevel Converter
FPIC	Fuzzy Proportional Integral Controller
GA	Genetic Algorithm
GA	Genetic Algorithm
GTO	Gate Turn-Off thyristor
IEEE	Institute of Electrical and Electronics Engineers
IGBT	Insulated Gate Bipolar Transistor
IGCT	Insulated Gate Commutated Thyristor
SHEPWM	Selected Harmonic Elimination Pulse Width Modulation
SPWM	Sinusoidal Pulse Width Modulation
SQP	Sequential Quadratic Programming
STATCOM	Synchronous Static Compensator
SVC	Static VAr Compensator
THD	Total Harmonic Distortion
TVA	Tennessee Valley Authority
VSC	Voltage Source Converter

# List of Figures

---

Fig. 1.1(a)	VSC connected to ac network	3
Fig. 1.1(b)	Equivalent Circuit	3
Fig. 1.2(a)	Power exchange between the STATCOM and the ac system	4
Fig. 1.2(b)	Vectorial representation between voltage and current	4
Fig. 1.3	Modulating charge and discharge to of capacitor to control their voltages	5
Fig 1.4 (a)	Natural V-I characteristics of a STATCOM	6
Fig. 1.4(b)	Family of V-I characteristics of a STATCOM	6
Fig. 1.5(a)	Controlled V-I characteristics of a STATCOM	8
Fig. 1.5(b)	Response of a STATCOM to a system voltage change	8
Fig. 1.6(a)	TVA STATCOM inverter valve layout	9
Fig. 1.6(b)	±100 SDG&E Talega STATCOM	9
Fig 2.1	Diode Clamped Multilevel Converter	13
Fig 2.2	Flying Capacitor Multilevel Converter	14
Fig 2.3	Cascaded Multilevel Converter	15
Fig. 2.4 (a)	Waveform of the output voltages of the inverter cells	17
Fig. 2.4 (b)	synthesis of output phase voltage	17
Fig 2.5	Variation of %THD obtained by GA with set 1	22
Fig 2.6	Variation of %THD obtained by GA with set 2	23
Fig 2.7	Variation of % THD obtained by SQP	24
Fig 2.8	Constrained Satisfaction	25
Fig 2.9	No. of iterations of SQP	25
Fig 3.1	Single Line Diagram of Distribution system	27
Fig 3.2 (a)	$V_{rms}$ without modulation index ramp	28
Fig 3.2 (b)	$V_{rms}$ with ramped modulation index	28
Fig 3.2 (c)	$V_{dc}$ (3 phase) with ramped modulation index	28
Fig 3.3	Equivalent circuit of STATCOM	30

Fig 3.4	Control system for d-axis	33
Fig 3.5	Pole placement for d-axis control system	33
Fig 3.6	Step response for d-axis control system	34
Fig 3.7	Control system for q-axis	34
Fig 3.8	Step response for q-axis control system	34
Fig 3.9	$V_{dc}$ response in infinite bus for exact linearization	35
Fig 3.10	$V_{dc}$ response in Infinite Bus for approx linearization	35
Fig 3.11	$V_d$ plot for the distribution grid	36
Fig 3.12	$V_{dc}$ in grid for exact linearization on enabling control system	36
Fig 3.13	$V_{dc}$ in grid for approx linearization on enabling control system	36
Fig 4.1	Fuzzy PI controller	38
Fig 4.2	Fuzzy Logic Rule Definition	39
Fig 4.3	Indirect Fuzzy controller	40
Fig 4.4	Optimization block for step response	40
Fig 4.5	Optimized step response for Indirect Fuzzy controller	40
Fig 4.6	$V_{rms}$ without STATCOM for 3Ph-G fault	41
Fig 4.7	$V_{rms}$ with indirect controlled STATCOM for 3Ph-G fault	41
Fig 4.8	3-Ph DC link voltage with indirect control for 3Ph-G fault	41
Fig 4.9	Output of indirect controller (delta) for 3Ph-G fault	42
Fig 4.10	$I_q$ with indirect control for 3Ph-G fault	42
Fig 4.11	$I_d$ with indirect control for 3Ph-G fault	42
Fig 4.12	$V_{rms}$ with indirect controlled STATCOM for L-G fault	43
Fig 4.13	3-Ph DC link voltage with indirect control for L-G fault	43
Fig 4.14	$I_q$ with indirect control for L-G fault	43
Fig 4.15	$V_{rms}$ with indirect controlled STATCOM for L-L fault	44
Fig 4.16	3-Ph DC link voltage with indirect control for L-L fault	44
Fig 4.17	$I_q$ with indirect control for L-L fault	44

Fig 4.18	$V_{rms}$ with indirect controlled STATCOM for LL-G fault	45
Fig 4.19	3-Ph DC link voltage with indirect control for LL-G fault	45
Fig 4.20	$I_q$ with indirect control for LL-G fault	45
Fig 5.1	Scheme of STATCOM direct controller	47
Fig 5.2	Optimized step response for direct Fuzzy controller	47
Fig 5.3	$V_{rms}$ during for 3Ph-G fault for direct control	48
Fig 5.4	3-Ph DC link voltage with direct control for 3Ph-G fault	48
Fig 5.5	Output 1 of direct controller (modulation index) for 3Ph-G fault	49
Fig 5.6	Output 2 of direct controller (delta) for 3Ph-G fault	49
Fig 5.7	$I_q$ with direct control for 3Ph-G fault	49
Fig 5.8	$I_d$ with direct control for 3Ph-G fault	50
Fig 5.9	$V_{rms}$ with direct controlled STATCOM for L-G fault	50
Fig 5.10	3-Ph DC link voltage with direct control for L-G fault	50
Fig 5.11	$I_q$ with direct control for L-G fault	51
Fig 5.12	$V_{rms}$ with direct controlled STATCOM for L-L fault	51
Fig 5.13	3-Ph DC link voltage with Direct control for L-L fault	51
Fig 5.14	$I_q$ with direct control for L-L fault	52
Fig 5.15	$V_{rms}$ with direct controlled STATCOM for LL-G fault	52
Fig 5.16	3-Ph DC link voltage with direct control for LL-G fault	52
Fig 5.17	$I_q$ with direct control for LL-G fault	53

# List of Tables

---

Table1.1	Typical Power Factor of Some Industrial Plant	2
Table1.2	Typical Voltage Fluctuation Standards	2
Table 2.1	Comparison of power component requirements per phase leg.	15
Table 2.2	Advantages and Disadvantages of different multilevel VSCs in a nutshell.	16
Table 2.3	The parameters for Genetic Algorithm	22
Table 4.1	Fuzzy logic Rule Base	39

**1.1 The Problem**

The electric power network is a very complex and dynamic system consisting of distributed generators, interconnected transmission and large number of reactive loads. As a result requirement of flexible control of electric power is essential to provide a better adaptation to varying operational conditions and improve the usage of existing installations. FACTS have been defined by the IEEE as follows [1]:

"A power electronic based system and other static equipment that provides control of one or more AC transmission system parameters to enhance controllability and increase power transfer capability."

The FACTS concept was originally created in the 1980s to solve operation problems due to the restrictions on the construction of new transmission lines, to improve power system stability margin and to facilitate power exchange between different generation companies and large power users.

FACTS devices can be applied for [2]

- Power flow control,
- Increase of transmission capability,
- Voltage control,
- Reactive power compensation,
- Stability improvement,
- Power quality improvement,
- Power conditioning,
- Flicker mitigation,
- Interconnection of renewable and distributed generation and storages.

Most of the industrial loads such as induction motors operate at moderately low power factor. Around 60% of the utility load consists of motors and hence the overall power factor of the power system is low. The typical load power factors are given in the Table1.1 [3]. So to prevent the transmission line and the generators from breaching their VA ratings, compensators are installed to maintain the required voltage support and the voltage profile.

**Table1.1: Typical Power Factor of Some Industrial Plant**

Industry	% of Power Factor	Industry	% of Power Factor
Chemical	80-85	Arc welding	35-60
Coal mine	65-80	Machine shop	45-60
Electroplating	65-70	Arc furnace	75-90
Hospital	75-80	Spraying	60-65
Office building	80-90	Weaving	60-75

The dynamic response of these compensators should be fast enough to cope up with the frequent incoming and rejection of reactive loads, as observed in Table1.2. In case of highly loaded line experiencing symmetrical faults, when the reactive current requirement increases which results high transient shaft torque and rotor acceleration on generators the problem become more severe. So this concludes that during faults the compensators are of critical importance with respect to transient stability.

**Table1.2: Typical Voltage Fluctuation Standards**

Load	Limits of Voltage Fluctuations
Large Motor starts	1-3% depending on frequency
Mine winders, excavators and large motor drives	1-3% at distribution voltage level $1/2 - 1 1/2$ % at transmission voltage level
Welding Plant	$1/4 - 2$ % dependent on frequency
Induction Furnace	Up to 1%
Arc Furnace	$< 1/2$ %

The evolution in the fabrication of semiconductor devices both in low power family like microprocessors which are used for mathematically complex digital control and also in the high power range for power stage of converters such as IGBT, ETO, IGCT, GTO etc. are increasingly finding places in FACTS technology. The high power electronic switches used should have the following characteristics [3]:

1. High forward and reverse voltage blocking ratings
2. High current during conduction states
3. Low off state leakage current



4. Low on-state voltage drop across the switch
5. Low turn-on and turn-off losses
6. Controlled switching characteristics during turn-on and turn-off
7. Capability to handle its rated voltage and current at the same time without the need for derating.
8. High  $dv/dt$  and  $di/dt$  ratings
9. Ability to operate in high temperatures
10. High input impedance.

The FACTS controllers can be divided into following categories

1. Series controllers
2. Shunt Controllers
3. Combined Series-Shunt Controllers

The Shunt controllers mainly the SVC (Static VAR Compensator) and STATCOM (Synchronous Static Compensator) have gained popularity in terms of reactive power support and dynamic response. Again the STATCOM is more superior to SVC in terms of V-I and V-Q characteristics, transient stability, dynamic response and capability to exchange real power.

## 1.2 STATCOM Operation

The STATCOM is a static counter part of the rotating synchronous condenser but it generates/absorbs reactive power at a faster rate because no moving parts are involved. The schematic of STATCOM is shown in Fig. 1.1(a). In principle, it performs the same voltage regulation function as the SVC but in a more robust manner because unlike the SVC its operation is not impaired by the presence of low voltages.

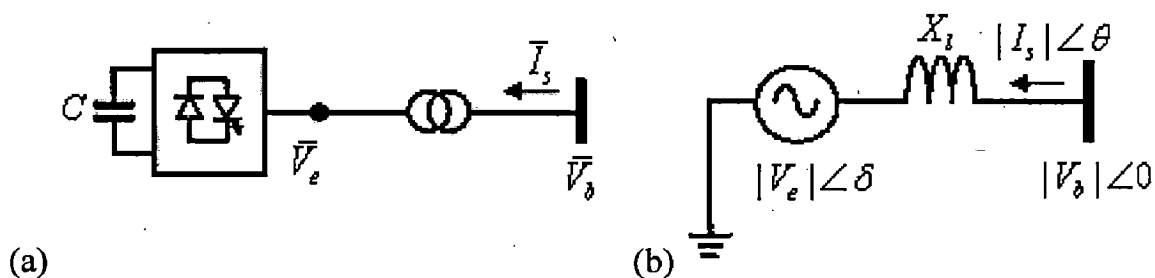


**Figure 1.1:** (a) VSC connected to ac network and (b) Equivalent Circuit.

The exchange of reactive power between the converter and the ac system can be controlled by varying the amplitude of the three phase output voltage  $V_e$  of the converter in Fig. 1.1(b). That is if the amplitude of the output voltage is increased above that of the utility bus voltage  $V_b$  then a current flows through the reactance from the converter to the ac system and the converter generates capacitive reactive power for the ac system. If the amplitude of the output voltage is decreased below the utility bus voltage then the current flows from the ac

system to the converter and the converter absorbs inductive-reactive power from the ac system as shown in Fig 1.2(a). If the output voltage equals the ac system voltage, the reactive power exchange becomes zero, in which case the STATCOM is said to be in floating state. Adjusting the phase shift between the converter output voltage and the ac system voltage can similarly control real power exchange between the converter and the ac system from its dc energy storage as shown in Fig 1.2(b). If the converter output voltage is made to lead the ac system voltage. On the other hand it can absorb real power from the ac system for the DC capacitor voltage if its voltage lags behind the ac system voltage.

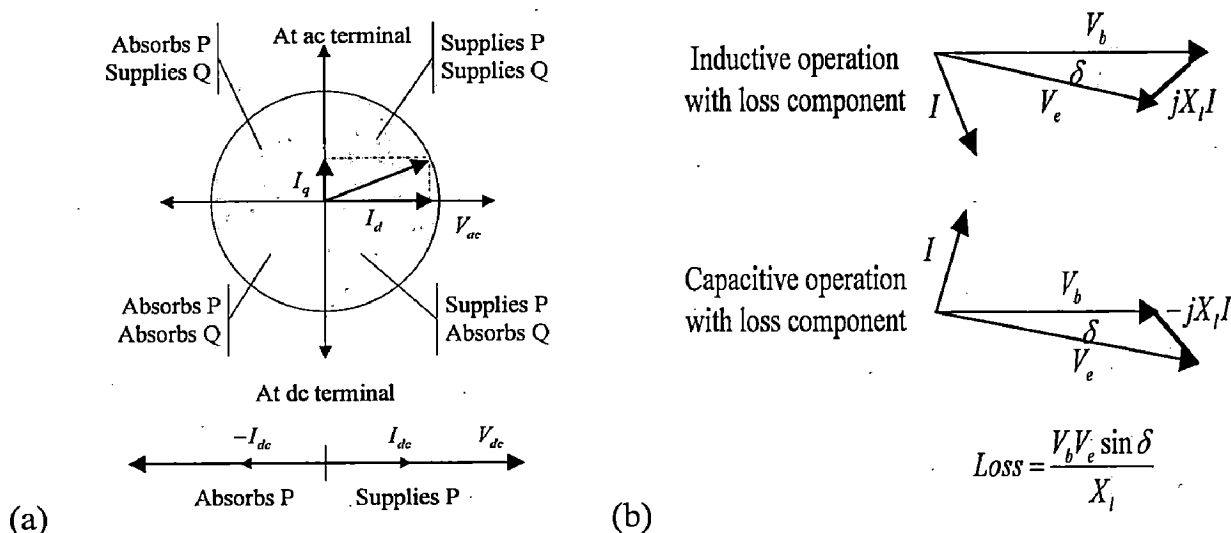
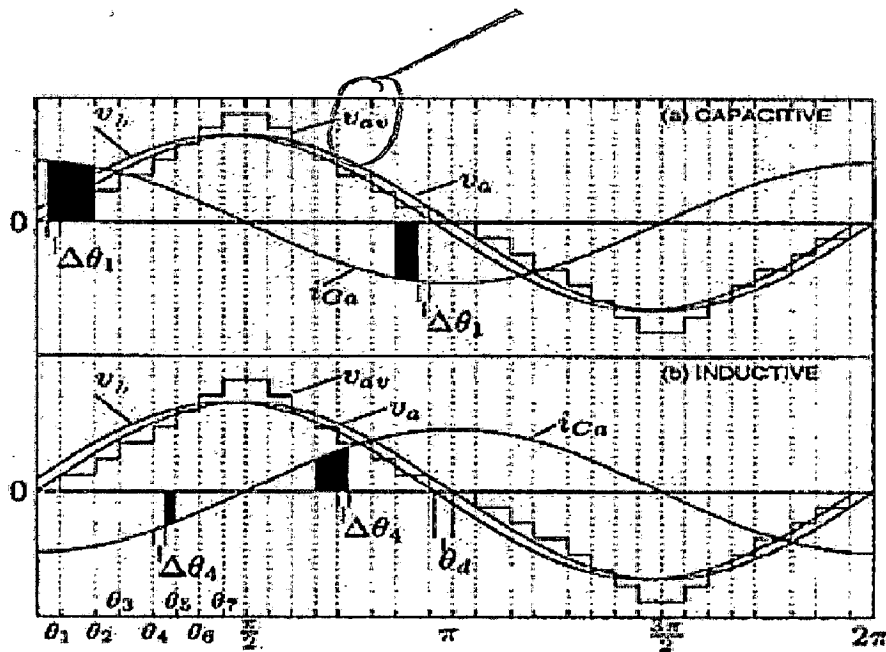


**Figure 1.2** (a) Power exchange between the STATCOM and the ac system. (b) Vectorial representation between voltage and current

### 1.3 Requirement of exchange of real power

In practice, the semiconductor switches of the conductor are not lossless, so the energy stored in the dc capacitor is eventually used to meet the internal losses of the converter, and the dc capacitor voltage diminishes. However when the STATCOM is used for reactive-power generation, the converter itself can keep the capacitor charged to the required voltage level. This task is accomplished by making the output voltages of the converter lag behind the ac system voltages by a small angle (usually in the  $0.1^\circ$ - $0.2^\circ$  range). In this way, the converter absorbs a small amount of real power from the ac system to meet its internal loss and keep the capacitor voltage at the desired level. The Fig 1.3 shows the average waveforms of the phase voltage  $V_{an}$ , the fundamental phase voltage, the system bus voltage  $V_b$  and the current  $I_{ca}$  flowing through the capacitors. The capacitor current either lags or leads the phase voltage by  $90^\circ$  depending on whether the converter acts capacitive or inductively. The average charge on each dc capacitor over every half cycle is equal to zero and because of this symmetric charge flow the voltage on all the dc capacitor remains theoretically balanced. However the power losses in the converter and an unbalanced operation of the three phase system the capacitor

voltage may drift away from their set levels. In principle the charge and hence the voltage across each capacitor is maintained by prolonging or shortening the current flow through it which is achieved by shifting the switching pattern. The first wave form depicts the extra charging of capacitor to raise its falling voltage when the converter is producing the leading VAR. In the positive half cycle of  $I_{ca}$ , C1 conduction is increased by  $\Delta\theta_1$  where as in the negative half cycle it is reduced by the same amount. Reflecting this behavior are shaded areas in which the positive half cycle is larger than in negative half cycle indicating extra charging of C1.

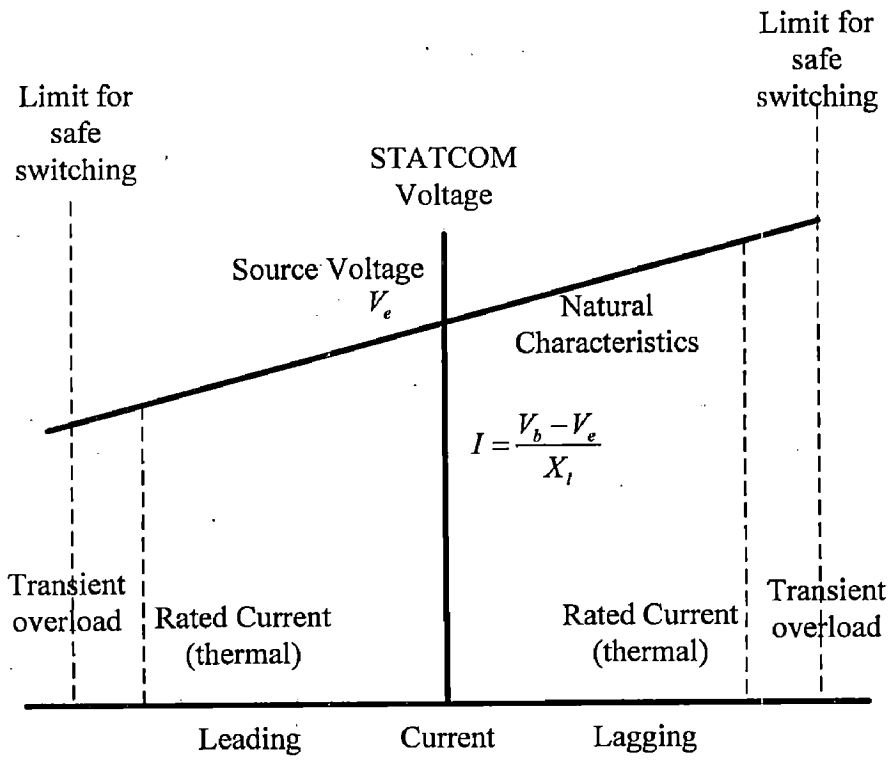


*Symbols do not match with text*

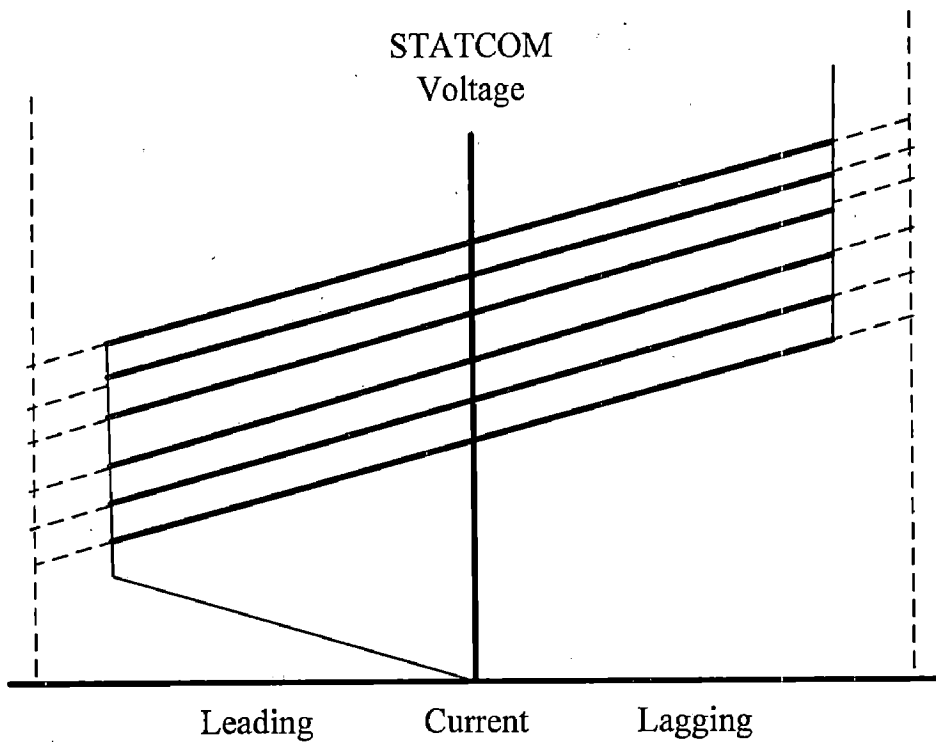
Figure 1.3 Modulating charge and discharge to of capacitor to control their voltages

#### 1.4 STATCOM operating characteristics – The regulation slope

STATCOM operate with a slope reactance typically between 2% and 5% as shown in Fig 1.5(a) which is much lower than the value of the coupling reactance given as natural characteristics in Fig 1.4 (a). Because the coupling reactance is fixed, the converter source voltage must therefore be changed i.e. raising it to  $V_e$  (high) to obtain the desired leading current condition or reducing it to  $V_e$  (low) for lagging conditions as shown in Fig 1.5 (a). This can be done by changing the switching pattern and then followed by changing the dc source voltage. At reduced voltage the STATCOM can continue to be operated at rated leading (or lagging) current with a constant transient overload current margin.



(a)



(b)

**Figure 1.4** (a) Natural V-I characteristics of a STATCOM. (b) Family of V-I characteristics of a STATCOM.

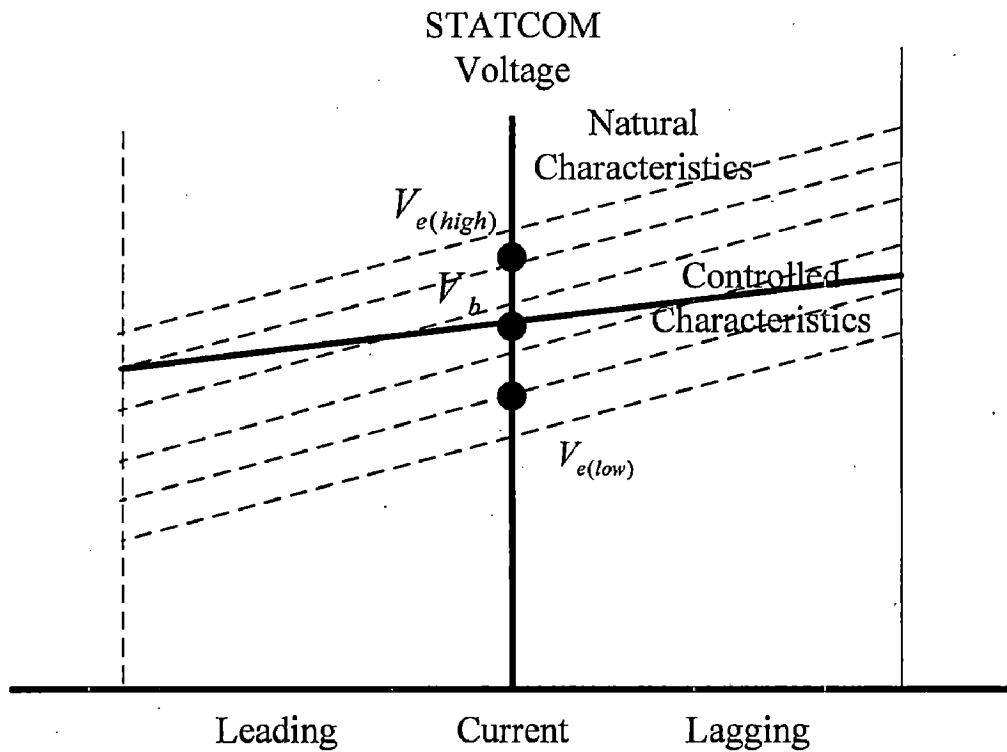
The STATCOM is not used as a perfect terminal voltage regulator, but rather the terminal voltage is allowed to vary in proportion with the compensating current. There are several reasons for this [4].

- 1) The linear operating range of a compensator with given maximum capacitive and inductive ratings can be extended if a regulation droop is allowed. Regulation droop means that the terminal is allowed to be smaller than the nominal no load value at full capacitive compensation and conversely, is allowed to be higher than the nominal value at full inductive compensation.
- 2) Perfect regulation (zero droop) could result in poorly defined operating point and a tendency of oscillation, if the system impedance exhibits a flat region in the operating frequency range of interest.
- 3) A regulation droop tend to enforce automatic load sharing between static compensator as well as other voltage regulating device normally employed to control transmission voltage.

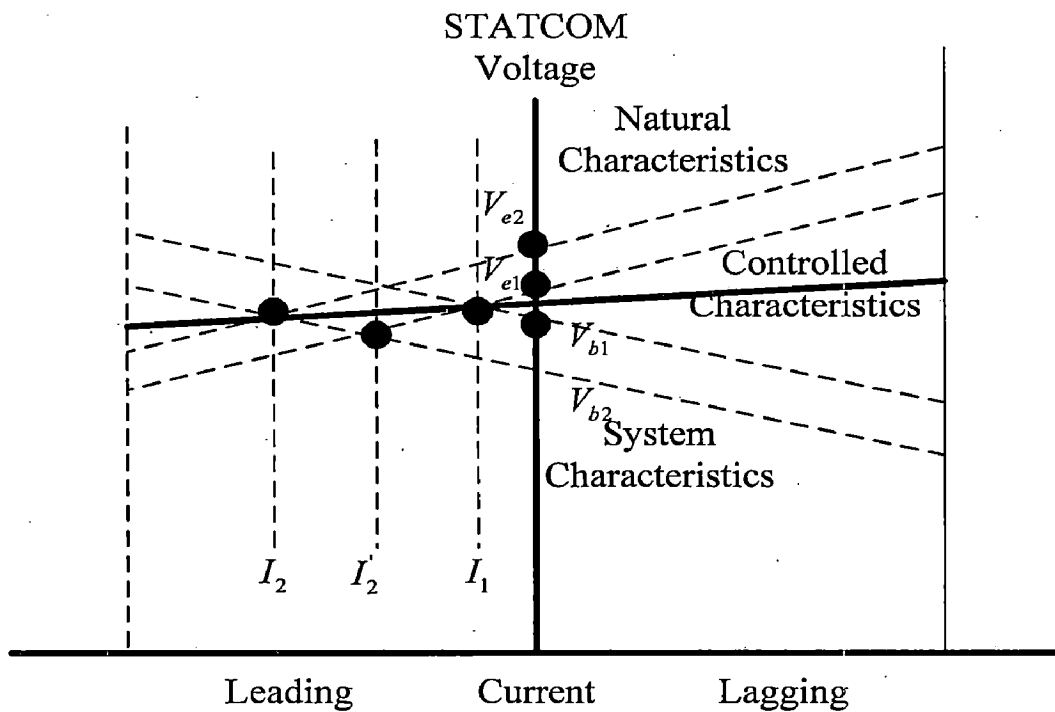
So the modulation index can be related to  $I_q(\text{req})$  as  $mV_{dc} = V_{d\_rated} + (\omega l)I_{q\_req}$  which is the equation of the natural characteristics.

### 1.5 Transient response

The steady state operating condition of a STATCOM is dependent on the system voltage and the STATCOM source voltage and its coupling impedance. Thus with an open circuit system voltage  $V_{b1}$  in Fig 1.5(b) slightly lower than the target voltage of the STATCOM steady state characteristics, the STATCOM draws a small capacitive current  $I_1$ . In order to generate this current the STATCOM source voltage  $V_{e1}$  must be slightly higher than the target voltage. If the system voltage is depressed due to a fault to a value  $V_{b2}$ , the point of intersection of the system characteristics and the STATCOM controlled characteristics demands a current  $I_2$ . Initially before there has been any change of STATCOM source voltage, the STATCOM current increases substantially from  $I_1$  to  $I_2$  this is increased by control action to the required value  $I_2$  by an increase of source voltage to  $V_{e2}$  normally within one half cycle.



(a)



(b)

**Figure 1.5** (a) Controlled V-I characteristics of a STATCOM. (b) Response of a STATCOM to a system voltage change



## 1.6 Literature Review

In 1995 a  $\pm 100$ MVA STATCOM was commissioned for the Tennessee Valley Authority (TVA) at the Sullivan Substation at North-Eastern Tennessee [5]. It is supplied by the 500 kV bulk power network and by four 161 kV lines. The Sullivan 500 kV feed supplies about 55 percent of the winter peak load of 900 MW. The 500 kV bus is tied to the 161 kV bus through a 1200MVA transformer bank. The STATCOM is connected to the 161 kV bus where it is required to regulate the voltage during the daily load cycle so that the tap changer on the transformer bank can be used less often. A standard 84 MVar switchable bank of capacitors are installed adjacent to the STATCOM and its switchings are normally coordinated with the STATCOM so as to reduce STATCOM loading and to provide an overall controllable VAr range from 100 MVar inductive to 184 MVar capacitive. Another example of  $\pm 100$ MVA STATCOM installed at SDG&E's Talega 138kV substation in October 2002[6]. It consists of two groups of Voltage Source Converter 50MVA each. Each 50MVA converter group consists of four sets of 12.5MVA modules plus a 5MVar harmonic filter, with a nominal phase to phase ac voltage of 3.2 kV and a DC link voltage of 6000V.

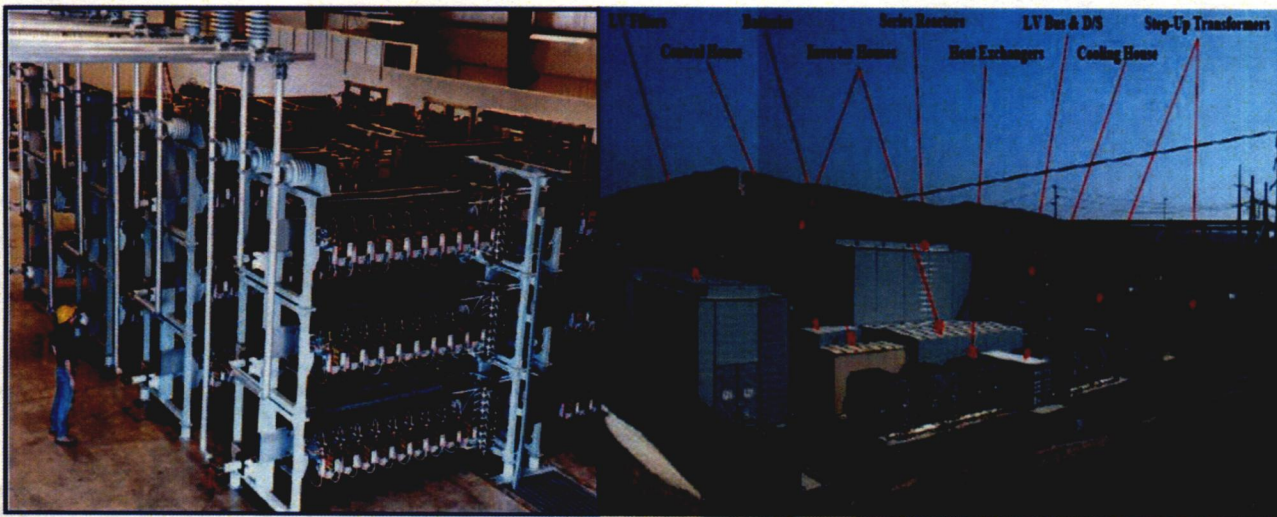


**Figure 1.6 (a) TVA STATCOM inverter valve layout. (b)  $\pm 100$  SDG&E Talega STATCOM**

But they suffered from many drawbacks like bulky zigzag transformers for 48 pulse output waveform, complex switching strategy and higher snubber losses, which encouraged the development of multilevel STATCOM.

The topology of Multilevel converter is further divided into 1) Diode clamped converter 2) Flying Capacitor converter 3) Cascaded Multilevel converter. The concept of the Cascade Multilevel Converter is put forward by Peng in 1996 [7] and concludes that Cascaded Multilevel Converter can be used as a STATCOM for reactive power control.



The Phase Shifted Multilevel Pulse Width Modulation and the capacitance requirement for acceptable ripple at full capacitive output is given by Nwanpa [8]. The initial charging of the capacitors by charging resistors is also designed for restricting the initial inrush current.

Shen et. al. [9] has performed the system calculations in per unit and designed PI controller for STATCOM application. The open loop time constant of the STATCOM has been shown to be operating point dependent in this paper.

Bacha et.al [10] has shown the poles of the STATCOM depend on operating point and proposed a nonlinear controller for robust STATCOM controlling.

The vector control for static VAR compensators with decoupled PI controller has been proposed by Mehta and Schauder [11]. They are classified as type I and type II control. The inverter is modeled in DQO reference frame and the state space representation is derived. In type I controller both the modulation index and the phase are the control input to the inverter. The second type deals with fixed modulation index and phase difference as the only control variable which has got application in transmission line ASVC's.

The exact linearization via state feedback for nonlinear control has been proposed by Qiang Song [12] and the controller is tested at  $\pm 30$ kVar prototype fabricated at Tsinghua University. The capacitor voltage unbalance is also minimized by THD minimization and fundamental voltage equalization and finally firing pattern swapping is employed. This is achieved by three times switching in a quarter cycles. The initial condition for the optimization problem is still to be decided for the best harmonic performance.

Tamer et.al.[13] have applied genetic Algorithm for solving SHEPWM for Cascaded Multilevel Converter. Binary coding system has been employed to perform selection, crossover and mutation in GA.

Soto et.al.[14] have successfully realized the nonlinear controller and applied pole placement to derive the controller gains. The validity of the controller is justified by 5 level STATCOM connected to infinite bus.

The fuzzy logic has been conceived by Lofti Zadeh, many versions of pi and pid [15] controller has been proposed for complex single input and single output system. Morris et.al [16] have employed two new structure fuzzy control algorithm. The control signal is obtained from a combination of generator speed deviation and STATCOM bus voltage deviation fed to the variable structure fuzzy controller. The controller evaluated in single machine and multi machine power system subject to a wide range of operating condition change.



## **1.7 Organization of the thesis**

Chapter 1 The Operation and state of the art technology available for STATCOM controller design has been explored.

Chapter 2 In this chapter a new initial condition algorithm by phase shift method has been applied and superior harmonic performance as compared to Song[9] has been achieved.

Chapter 3 The requirement of charging circuit for STATCOM has been highlighted and the Mathematical Model is derived.

Chapter 4 The fuzzy indirect control has been designed for STATCOM and the system performance during fault is evaluated. The control parameters are tuned by simplex optimization method.

Chapter 5 The indirect controller of chapter 5 together with an additional fuzzy controller is used for direct controlling of STATCOM. The performance is evaluated in distribution grid.

Chapter 6 Conclusion and future scope of this thesis have been discussed.



2.1 Types of Multilevel Converters

Multilevel Voltage Source Converters (VSCs) are emerging as a new breed of power converter options for high-power applications. The multilevel VSC typically synthesizes the staircase voltage wave from several levels of dc capacitor voltages. One of the major limitations of the multilevel converters is the voltage unbalance between different levels. The techniques to balance the voltage between different levels normally involve voltage clamping or capacitor charge control. In the past two decades, several multilevel VSC topologies have been reported and studied, i.e., diode clamped, flying capacitor and Cascaded-Multilevel Converter (CMC) [7] topologies.

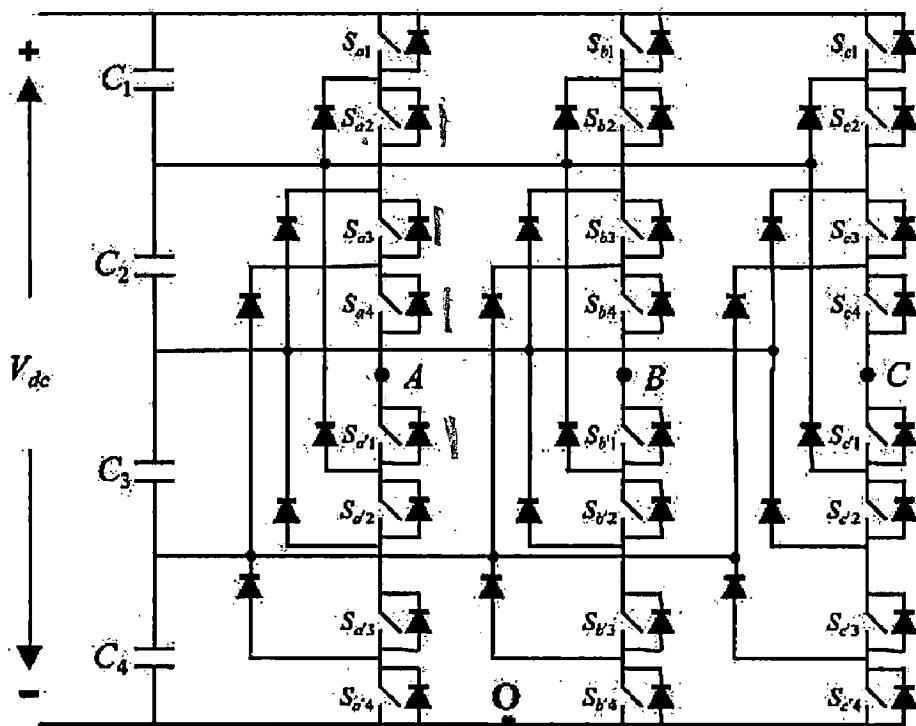
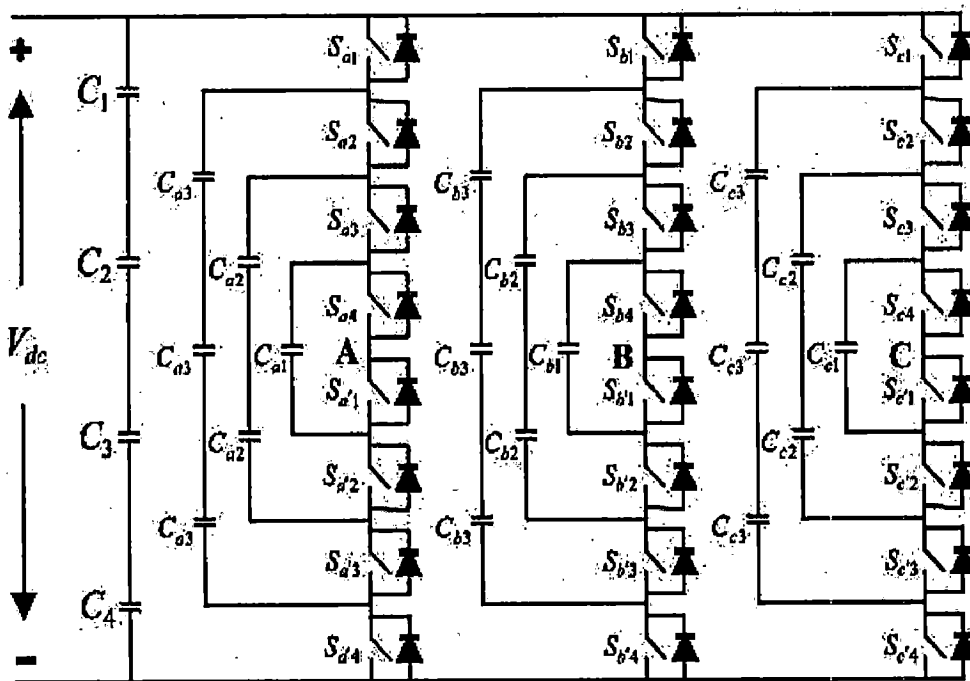


Figure 2.1 Diode Clamped Multilevel Converter

Fig. 2.1 shows a five-level Diode-Clamped Multilevel Converter (DCMC) in which the dc bus consists of four capacitors. For dc-bus voltage  $V_{dc}$ , the voltage across each capacitor is  $V_{dc} / 4$  and each device voltage stress will be limited to one capacitor voltage level through clamping diodes. With different switching combinations, multilevel voltages can be synthesized. For voltage level  $V_{dc}$ , turn on four upper switches; for voltage level  $3/4 V_{dc}$ , turn on  $S_{a2}$ ,  $S_{a3}$ ,  $S_{a4}$ ,  $S_{a'1}$ ; for voltage level  $1/2 V_{dc}$ , turn on  $S_{a3}$ ,  $S_{a4}$ ,  $S_{a'1}$ ,  $S_{a'2}$ ; for voltage level  $1/4 V_{dc}$ , turn on  $S_{a4}$ ,  $S_{a'1}$ ,  $S_{a'2}$ ,  $S_{a'3}$ ; for voltage level  $0 V_{dc}$ , turn on the lower four switches.

Fig 2.2 shows a five-level Flying Capacitor Multilevel Converter (FCMC) topology. The voltage level defined in the flying-capacitor converter is similar to that of the diode-clamp type converter. The voltage synthesis in a flying-capacitor converter has more flexibility than a diode-clamp converter. For voltage level  $V_{dc}$ , turn on all upper switches; for voltage level  $\frac{3}{4} V_{dc}$ , there are three combinations: (a)  $S_{a1}, S_{a2}, S_{a3}, S_{a'4}$ , (b)  $S_{a4}, S_{a'1}, S_{a'2}, S_{a'3}$ , (c)  $S_{a1}, S_{a3}, S_{a4}, S_{a'2}$ . For voltage level  $\frac{1}{2} V_{dc}$ , there are six combinations: (a)  $S_{a1}, S_{a2}, S_{a'3}, S_{a'4}$ , (b)  $S_{a3}, S_{a4}, S_{a'1}, S_{a'2}$ , (c)  $S_{a1}, S_{a3}, S_{a'2}, S_{a'4}$ , (d)  $S_{a1}, S_{a4}, S_{a'2}, S_{a'3}$ , (e)  $S_{a2}, S_{a4}, S_{a'1}, S_{a'3}$ , (f)  $S_{a2}, S_{a3}, S_{a'1}, S_{a'4}$ . For voltage level  $\frac{1}{4} V_{dc}$ , there are three combinations: (a)  $S_{a1}, S_{a'2}, S_{a'3}, S_{a'4}$ , (b)  $S_{a4}, S_{a'1}, S_{a'2}, S_{a'3}$ , (c)  $S_{a3}, S_{a'1}, S_{a'2}, S_{a'4}$ . For voltage level 0, turn on all lower switches.



**Figure 2.2** Flying Capacitor Multilevel Converter

The third type of multilevel converter, namely the Cascaded Multilevel Converter (CMC) is increasingly used at high power area due to its direct high voltage output with no need of transformer. Fig. 2.3 shows the topology of a CMC. The "level" in a cascaded-inverters based converter is defined by  $p=2N+1$ , where  $p$  is the output phase voltage level and  $N$  is the number of dc sources. For example, a 7-level cascaded-inverters based converter will have three DC sources. Compared to diode-clamped multilevel converters and flying capacitor multilevel converters, CMC is easy to design and assemble because of the uniform circuit structure of the converter units. Modularized circuit layout and packaging is possible in CMC topology, because each level has the same structure, and there are no extra clamping diodes or voltage-balancing capacitors, which are required in the DCMC and the

FCMC. The number of output voltage levels can then be easily adjusted by changing the number of full-bridge converters.

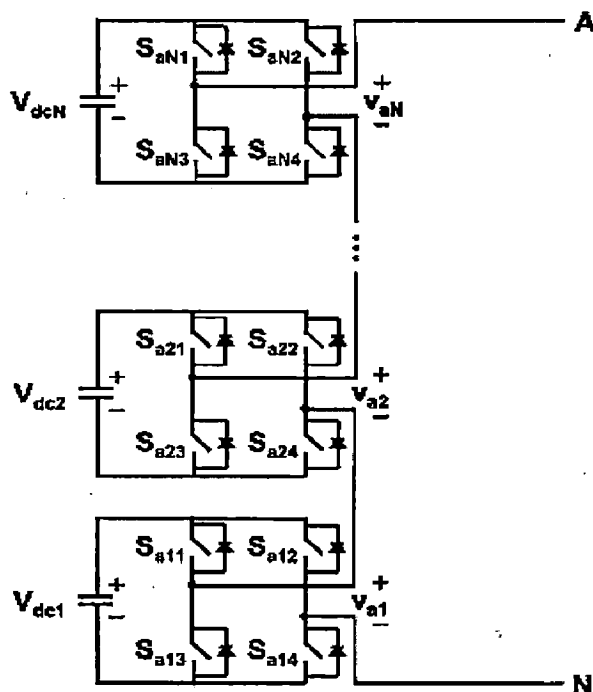


Figure 2.3 Cascaded Multilevel Converter

Table 2.1 [7] compares the main power component requirements per phase leg among these three multilevel VSCs, where  $p$  is the number of voltage levels. In Table 2.1, the number of main switches and main diodes needed by each converter to achieve the same number of voltage levels is the same. But DCMC (diode-clamp) needs extra clamping diodes, FCMC (flying-capacitor) needs extra balancing capacitors and CMC needs extra DC bus capacitors. So the number of total devices required for each converter is different. To synthesize the same number of voltage levels, the CMC requires the least number of total main components.

Table 2.1: Comparison of power component requirements per phase leg.

Converter Type	Diode-Clamp	Flying Capacitors	Cascaded Multilevel
Main switching devices	$2(p-1)$	$2(p-1)$	$2(p-1)$
Main diodes	$2(p-1)$	$2(p-1)$	$2(p-1)$
Clamping diodes	$(p-1)(p-2)$	0	0
DC bus capacitors	$(p-1)$	$(p-1)$	$2(p-1)$
Balancing capacitors	0	$(p-1)(p-2)/2$	0
Total	$p^2 + 2p - 3$	$(p^2 + 8p - 8)/2$	$(9/2)(p-1)$

**Table 2.2:** Advantages and Disadvantages of different multilevel VSCs in a nutshell.

Converter Type	Diode-Clamp	Flying Capacitors	Cascaded Multilevel
Advantages	<ul style="list-style-type: none"> <li>(1) DC-link capacitors are common to three phases.</li> <li>(2) Switching frequency can be low.</li> <li>(3) Reactive current and negative-phase-sequence current can be controlled.</li> </ul>	<ul style="list-style-type: none"> <li>(1) The clamping capacitor's voltage is automatically balanced.</li> <li>(2) Reactive current and negative-phase-sequence current can be controlled.</li> </ul>	<ul style="list-style-type: none"> <li>(1) No clamping components are necessary.</li> <li>(2) Low switching frequency can be used.</li> <li>(3) Low harmonics, small footprint and modular</li> <li>(4) Both real and reactive power can be exchanged</li> </ul>
Disadvantages	<ul style="list-style-type: none"> <li>(1) Many diodes are used for clamping.</li> <li>(2) Many diodes make physical layout difficult,</li> <li>(3) Problems with DC-link voltage control.</li> </ul>	<ul style="list-style-type: none"> <li>(1) Low switching frequency makes the clamping capacitors large.</li> <li>(2) An excessive number of capacitors is used for clamping.</li> <li>(3) Complicated selection of switch for real power conversion</li> </ul>	<ul style="list-style-type: none"> <li>(1) DC-link capacitors voltages are unbalanced for fundamental switching.</li> </ul>

Among these three types of converters, CMC has been studied in this thesis for its suitability to control voltage in a power distribution system. Now, for applying any multilevel VSC, proper switching scheme must be adopted for optimal performance of the converter. In the literature, following methods have been suggested for switching a CMC; 1) Sinusoidal PWM [17] 2) Space vector PWM [18] 3) Non Sinusoidal carrier PWM[19] 4) Mixed PWM[20] 5) Special structure of cell connection [21] and 6) Selected harmonic elimination PWM(SHEPWM)[22]. The SHEPWM methods can theoretically provide the highest quality among all the available techniques but suffers from the following drawbacks 1) high computational requirement 2) large look up table in flash ROM 3) non convergence at some modulation index and multiple solution at some modulation index. When SHEPWM is applied at fundamental switching frequency, the power sharing among the cells are unequal, as a result the capacitor voltage among the cells fluctuates in a particular phase. On the other hand, the

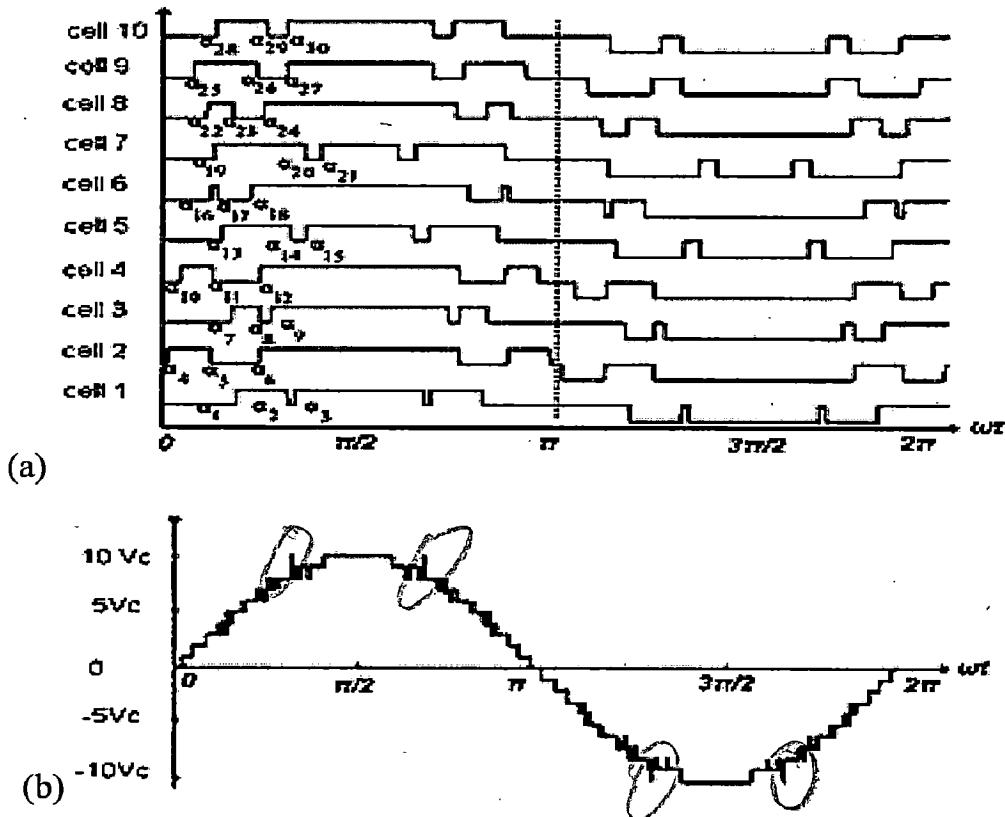
advancement in the power semiconductor device technology allows us to increase the switching frequency of the device to 150 Hz. [12]. In this thesis also, the switching frequency of the device has been assumed to be 150 Hz as shown in Fig 2.4(a). However, to decide the switching angles, an optimization based technique has been used, which is described in the next subsection.

## 2.2 Optimal Pulse Width Modulation

*Reference?*

The improvement in the power semiconductor device to operate at higher frequency, allow us to increase the switching frequency to 150 Hz with marginalized increase in the switching losses. This increase in the degree of freedom can be used to equalize the capacitor voltage by constrained optimization problem. The constrained formulation for equal power sharing is given by equal magnitude of fundamental voltage among the cells given by Eqns. (2.1)-(2.10). In this thesis, a 21 level CMC has been used. The 3 times switching in quarter cycle for ten cells H Bridge allow us to theoretically eliminate 41 order harmonics for solving 30 unknowns in 30 equations. The eliminated harmonics are given by Eqns. (2.11)-(2.30). The original harmonic elimination technique with equal fundamental voltage sharing can be modeled by the following equations, where  $\alpha_i$ 's are the firing angles in the first quarter of the sine wave.

*how?*  
*how?*



*how?*

Figure. 2.4 (a) Waveform of the output voltages of the inverter cells, and (b) synthesis of output phase voltage.

$$\cos \alpha_1 - \cos \alpha_2 + \cos \alpha_3 = m \frac{\pi}{4} \quad (2.1)$$

$$\cos \alpha_4 - \cos \alpha_5 + \cos \alpha_6 = m \frac{\pi}{4} \quad (2.2)$$

$$\cos \alpha_7 - \cos \alpha_8 + \cos \alpha_9 = m \frac{\pi}{4} \quad (2.3)$$

$$\cos \alpha_{10} - \cos \alpha_{11} + \cos \alpha_{12} = m \frac{\pi}{4} \quad (2.4)$$

$$\cos \alpha_{13} - \cos \alpha_{14} + \cos \alpha_{15} = m \frac{\pi}{4} \quad (2.5)$$

$$\cos \alpha_{16} - \cos \alpha_{17} + \cos \alpha_{18} = m \frac{\pi}{4} \quad (2.6)$$

$$\cos \alpha_{19} - \cos \alpha_{20} + \cos \alpha_{21} = m \frac{\pi}{4} \quad (2.7)$$

$$\cos \alpha_{22} - \cos \alpha_{23} + \cos \alpha_{24} = m \frac{\pi}{4} \quad (2.8)$$

$$\cos \alpha_{25} - \cos \alpha_{26} + \cos \alpha_{27} = m \frac{\pi}{4} \quad (2.9)$$

$$\cos \alpha_{28} - \cos \alpha_{29} + \cos \alpha_{30} = m \frac{\pi}{4} \quad (2.10)$$

$$\begin{aligned} & \cos 3\alpha_1 - \cos 3\alpha_2 + \cos 3\alpha_3 + \cos 3\alpha_4 - \cos 3\alpha_5 + \cos 3\alpha_6 \\ & + \cos 3\alpha_7 - \cos 3\alpha_8 + \cos 3\alpha_9 + \cos 3\alpha_{10} - \cos 3\alpha_{11} + \cos 3\alpha_{12} \\ & + \cos 3\alpha_{13} - \cos 3\alpha_{14} + \cos 3\alpha_{15} + \cos 3\alpha_{16} - \cos 3\alpha_{17} + \cos 3\alpha_{18} \\ & + \cos 3\alpha_{19} - \cos 3\alpha_{20} + \cos 3\alpha_{21} + \cos 3\alpha_{22} - \cos 3\alpha_{23} + \cos 3\alpha_{24} \\ & + \cos 3\alpha_{25} - \cos 3\alpha_{26} + \cos 3\alpha_{27} + \cos 3\alpha_{28} - \cos 3\alpha_{29} + \cos 3\alpha_{30} = 0 \end{aligned} \quad (2.11)$$

$$\begin{aligned} & \cos 5\alpha_1 - \cos 5\alpha_2 + \cos 5\alpha_3 + \cos 5\alpha_4 - \cos 5\alpha_5 + \cos 5\alpha_6 \\ & + \cos 5\alpha_7 - \cos 5\alpha_8 + \cos 5\alpha_9 + \cos 5\alpha_{10} - \cos 5\alpha_{11} + \cos 5\alpha_{12} \\ & + \cos 5\alpha_{13} - \cos 5\alpha_{14} + \cos 5\alpha_{15} + \cos 5\alpha_{16} - \cos 5\alpha_{17} + \cos 5\alpha_{18} \\ & + \cos 5\alpha_{19} - \cos 5\alpha_{20} + \cos 5\alpha_{21} + \cos 5\alpha_{22} - \cos 5\alpha_{23} + \cos 5\alpha_{24} \\ & + \cos 5\alpha_{25} - \cos 5\alpha_{26} + \cos 5\alpha_{27} + \cos 5\alpha_{28} - \cos 5\alpha_{29} + \cos 5\alpha_{30} = 0 \end{aligned} \quad (2.12)$$

$$\begin{aligned} & \cos 7\alpha_1 - \cos 7\alpha_2 + \cos 7\alpha_3 + \cos 7\alpha_4 - \cos 7\alpha_5 + \cos 7\alpha_6 \\ & + \cos 7\alpha_7 - \cos 7\alpha_8 + \cos 7\alpha_9 + \cos 7\alpha_{10} - \cos 7\alpha_{11} + \cos 7\alpha_{12} \\ & + \cos 7\alpha_{13} - \cos 7\alpha_{14} + \cos 7\alpha_{15} + \cos 7\alpha_{16} - \cos 7\alpha_{17} + \cos 7\alpha_{18} \\ & + \cos 7\alpha_{19} - \cos 7\alpha_{20} + \cos 7\alpha_{21} + \cos 7\alpha_{22} - \cos 7\alpha_{23} + \cos 7\alpha_{24} \\ & + \cos 7\alpha_{25} - \cos 7\alpha_{26} + \cos 7\alpha_{27} + \cos 7\alpha_{28} - \cos 7\alpha_{29} + \cos 7\alpha_{30} = 0 \end{aligned} \quad (2.13)$$

$$\begin{aligned} & \cos 9\alpha_1 - \cos 9\alpha_2 + \cos 9\alpha_3 + \cos 9\alpha_4 - \cos 9\alpha_5 + \cos 9\alpha_6 \\ & + \cos 9\alpha_7 - \cos 9\alpha_8 + \cos 9\alpha_9 + \cos 9\alpha_{10} - \cos 9\alpha_{11} + \cos 9\alpha_{12} \\ & + \cos 9\alpha_{13} - \cos 9\alpha_{14} + \cos 9\alpha_{15} + \cos 9\alpha_{16} - \cos 9\alpha_{17} + \cos 9\alpha_{18} \\ & + \cos 9\alpha_{19} - \cos 9\alpha_{20} + \cos 9\alpha_{21} + \cos 9\alpha_{22} - \cos 9\alpha_{23} + \cos 9\alpha_{24} \\ & + \cos 9\alpha_{25} - \cos 9\alpha_{26} + \cos 9\alpha_{27} + \cos 9\alpha_{28} - \cos 9\alpha_{29} + \cos 9\alpha_{30} = 0 \end{aligned} \quad (2.14)$$

$$\begin{aligned} & \cos 11\alpha_1 - \cos 11\alpha_2 + \cos 11\alpha_3 + \cos 11\alpha_4 - \cos 11\alpha_5 + \cos 11\alpha_6 \\ & + \cos 11\alpha_7 - \cos 11\alpha_8 + \cos 11\alpha_9 + \cos 11\alpha_{10} - \cos 11\alpha_{11} + \cos 11\alpha_{12} \\ & + \cos 11\alpha_{13} - \cos 11\alpha_{14} + \cos 11\alpha_{15} + \cos 11\alpha_{16} - \cos 11\alpha_{17} + \cos 11\alpha_{18} \\ & + \cos 11\alpha_{19} - \cos 11\alpha_{20} + \cos 11\alpha_{21} + \cos 11\alpha_{22} - \cos 11\alpha_{23} + \cos 11\alpha_{24} \\ & + \cos 11\alpha_{25} - \cos 11\alpha_{26} + \cos 11\alpha_{27} + \cos 11\alpha_{28} - \cos 11\alpha_{29} + \cos 11\alpha_{30} = 0 \end{aligned} \quad (2.15)$$









given in Eqns. (2.42). The nonlinear equality constraints are from Eqns. (2.1)-(2.10). The linear inequality constraints are Eqns. (2.31)-(2.41) and bound is given by Eqns. (2.41) Genetic Algorithm is used as a first attempt to obtain the global minimum of the constrained THD function for modulation index 0.550 to 1.000 in steps of 0.001. Two sets of parameters for Genetic Algorithm have been applied with different crossover function in the GA toolbox [23]. The results obtained are quite similar but far from being acceptable as the THDs obtained in these two methods, as shown in Fig. 2.5 and Fig 2.6., are unacceptably high.

**Table 2.2:** The parameters for Genetic Algorithm

GA parameter set	Details of set 1	Details of set 2
Initial Population range	0,90	0,90
Initial Population size	100	100
Crossover fraction	0.6	0.6
Migration direction	both	both
Generations	30	30
Selection function	roulette	roulette
Crossover function	Uniform	Heuristic 1.3165
Mutation	Adaptive feasible	Adaptive feasible

The fitness function which is to be minimized is the Total Harmonic Distortion given as:

$$\begin{aligned}
 THD = \sum_{n=3,5,\dots,41} & \left[ \frac{4}{n\pi} (\cos n\alpha_1 - \cos n\alpha_2 + \cos n\alpha_3 + \cos n\alpha_4 - \cos n\alpha_5 + \cos n\alpha_6 \right. \\
 & + \cos n\alpha_7 - \cos n\alpha_8 + \cos n\alpha_9 + \cos n\alpha_{10} - \cos n\alpha_{11} + \cos n\alpha_{12} \\
 & + \cos n\alpha_{13} - \cos n\alpha_{14} + \cos n\alpha_{15} + \cos n\alpha_{16} - \cos n\alpha_{17} + \cos n\alpha_{18} \\
 & + \cos n\alpha_{19} - \cos n\alpha_{20} + \cos n\alpha_{21} + \cos n\alpha_{22} - \cos n\alpha_{23} + \cos n\alpha_{24} \\
 & \left. + \cos n\alpha_{25} - \cos n\alpha_{26} + \cos n\alpha_{27} + \cos n\alpha_{28} - \cos n\alpha_{29} + \cos n\alpha_{30}) \right]^2 \quad (2.42)
 \end{aligned}$$

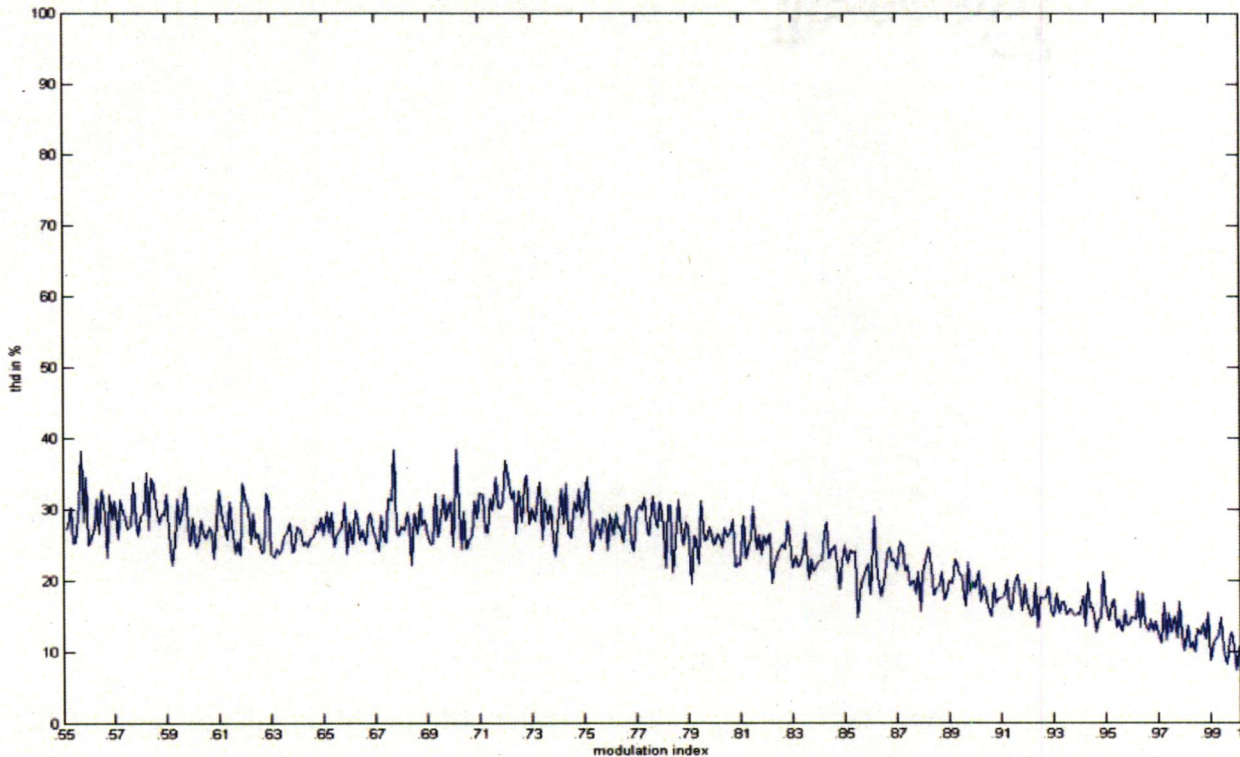


**Figure 2.5** Variation of %THD obtained by GA with set 1



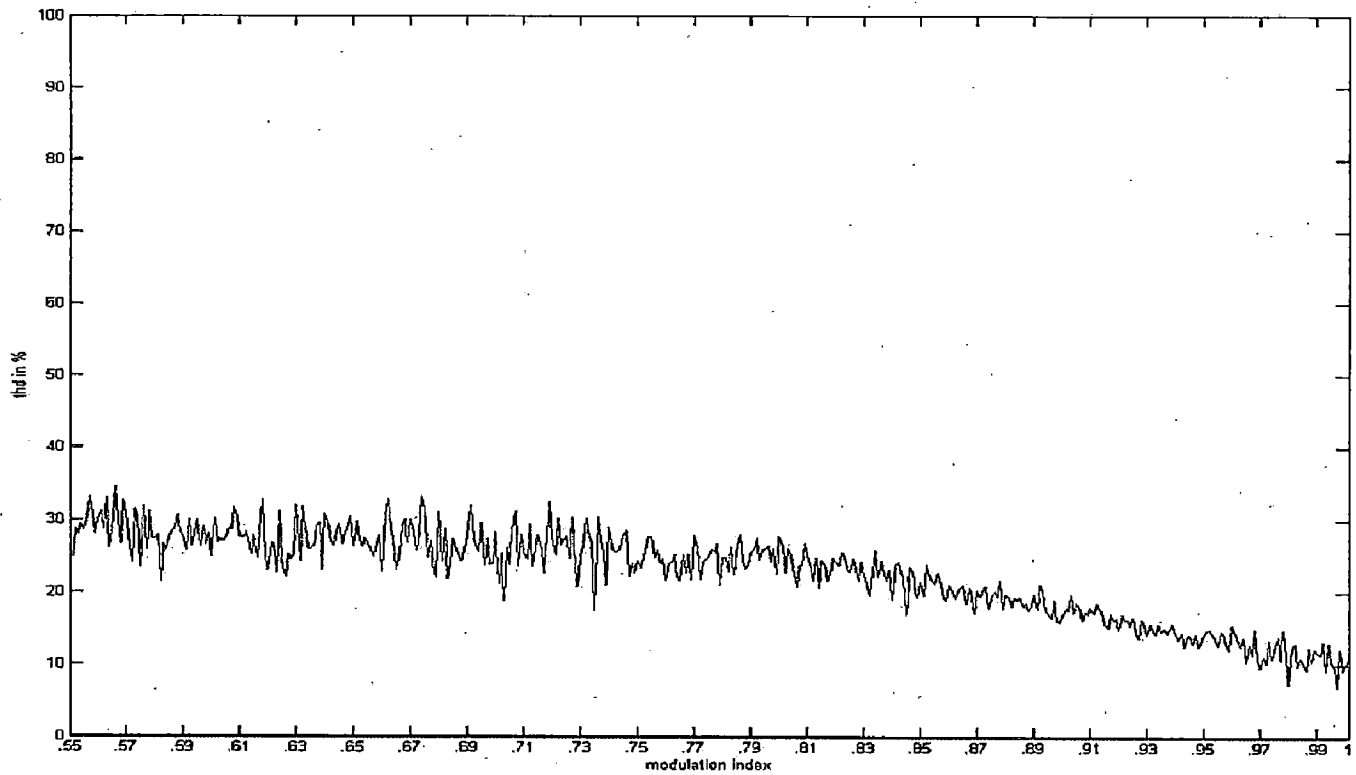


**Figure 2.6** Variation of %THD obtained by GA with set 2

The crossover function which generates new individual from the existing population has been applied are Uniform and Heuristic with fraction 1.13165. The Heuristic crossover creates children that lie on the line containing the two parents, a small distance away from the parent with the better fitness value in the direction away from the parent with the worse fitness value, but still the performance has not improved.

To find the switching angles with acceptable level of THD, the sequential quadratic programming (SQP) technique has been used. The initial conditions for SQP are computed by the algorithm described in next subsection.

#### **2.4 A new initial condition algorithm for THD minimization**

Elimination of lower order harmonics from only one cell which will be called a general SHEPWM method can be obtained by solving a system of 3 equation for three times switching in quarter cycle. Phase shift is an effective and simple method to decrease harmonic content in multilevel converter. Here phase shift together with 3 levels SHEPWM is used to obtain starting point for multilevel optimization. To preserve the high amplitude of the fundamental, the phase shift angle  $\beta$  among the 10 cells should be small. By 3 levels SHEPWM third and fifth harmonics are eliminated. For calculating phase shift harmonic order 11 is considered for which the value of  $\beta$  is  $3.273^\circ$  [24] as shown in appendix A. The 30 initial condition for each modulation index are obtained as follows, where a, b, c are the firing angles of the first cell in quarter cycle.



$$\cos a - \cos b + \cos c = m \frac{\pi}{4} \quad (2.43)$$

$$\cos 3a - \cos 3b + \cos 3c = 0 \quad (2.44)$$

$$\cos 5a + \cos 5b + \cos 5c = 0 \quad (2.45)$$

$$x0 = [a, b, c, a - \beta, b - \beta, c - \beta, a + \beta, b + \beta, c + \beta, a - 2\beta, b - 2\beta, c - 2\beta, \\ a + 2\beta, b + 2\beta, c + 2\beta, a - 3\beta, b - 3\beta, c - 3\beta, a + 3\beta, b + 3\beta, c + 3\beta, \\ a - 4\beta, b - 4\beta, c - 4\beta, a + 4\beta, b + 4\beta, c + 4\beta, a - 5\beta, b - 5\beta, c - 5\beta] \quad (2.46)$$

The alternative initial condition, which are

$$x0 = [a, b, c, a + \beta, b + \beta, c + \beta, a - \beta, b - \beta, c - \beta, a + 2\beta, b + 2\beta, c + 2\beta, \\ a - 2\beta, b - 2\beta, c - 2\beta, a + 3\beta, b + 3\beta, c + 3\beta, a - 3\beta, b - 3\beta, c - 3\beta, \\ a + 4\beta, b + 4\beta, c + 4\beta, a - 4\beta, b - 4\beta, c - 4\beta, a + 5\beta, b + 5\beta, c + 5\beta] \quad (2.47)$$

have not been consider because some initial condition results in angles greater than 90 degree. The %THD is plotted with modulation index from 0.550 to 1.000 in steps of 0.001. In Fig. 2.7 the MATLAB plot is the arithmetic function value for given modulation index and the PSCAD plot is the THD for the synthesized inverter voltage waveform. The optimization toolbox has been used to minimize the THD function. The algorithm used is Sequential Quadratic Programming Quasi Newton Line Search. The constrained satisfaction graph is also plotted in Fig 2.8 and the number of iterations for each modulation index optimization is plotted in Fig 2.9. This concludes the validity of the phase shift method by very good convergence and the satisfaction of the constraints which enlightens us to do away with the individual DC voltage controllers. In the next chapter STATCOM operation has been discussed in detail.

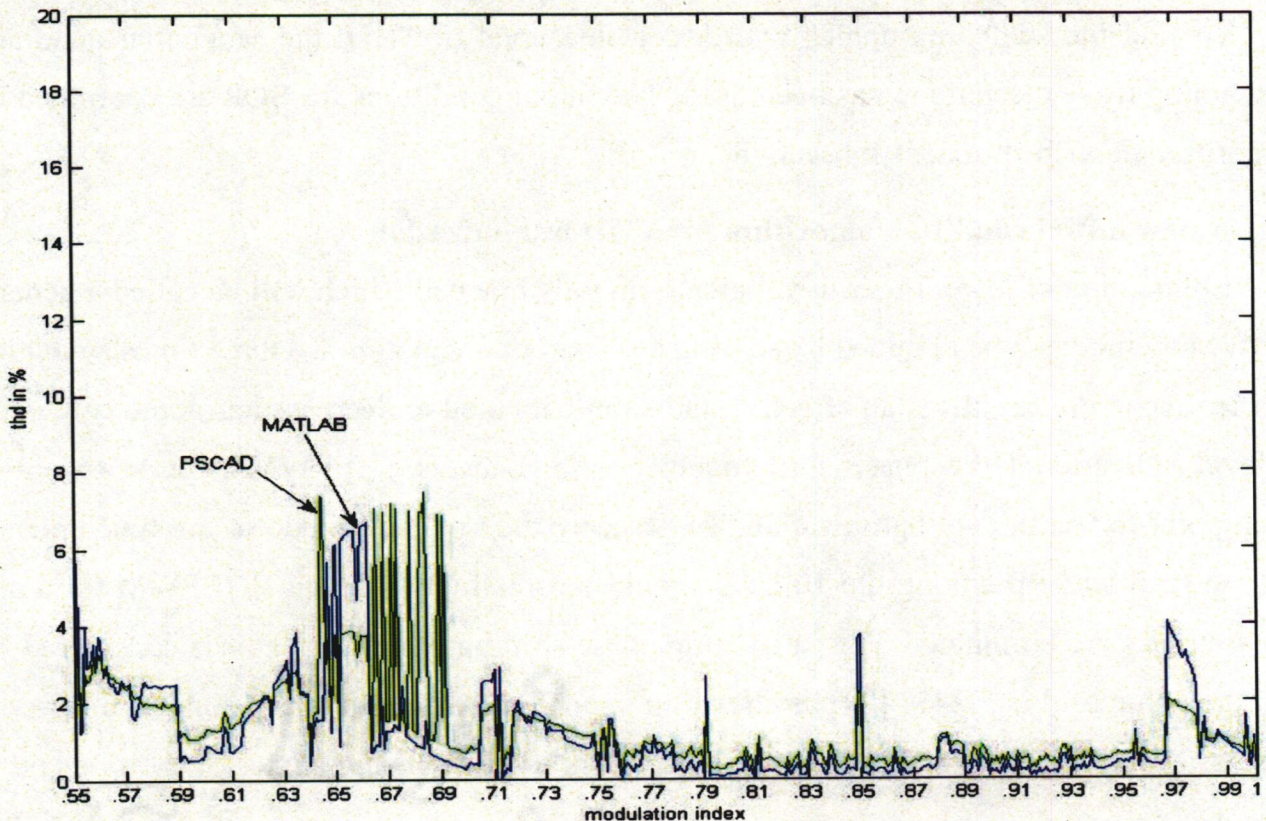
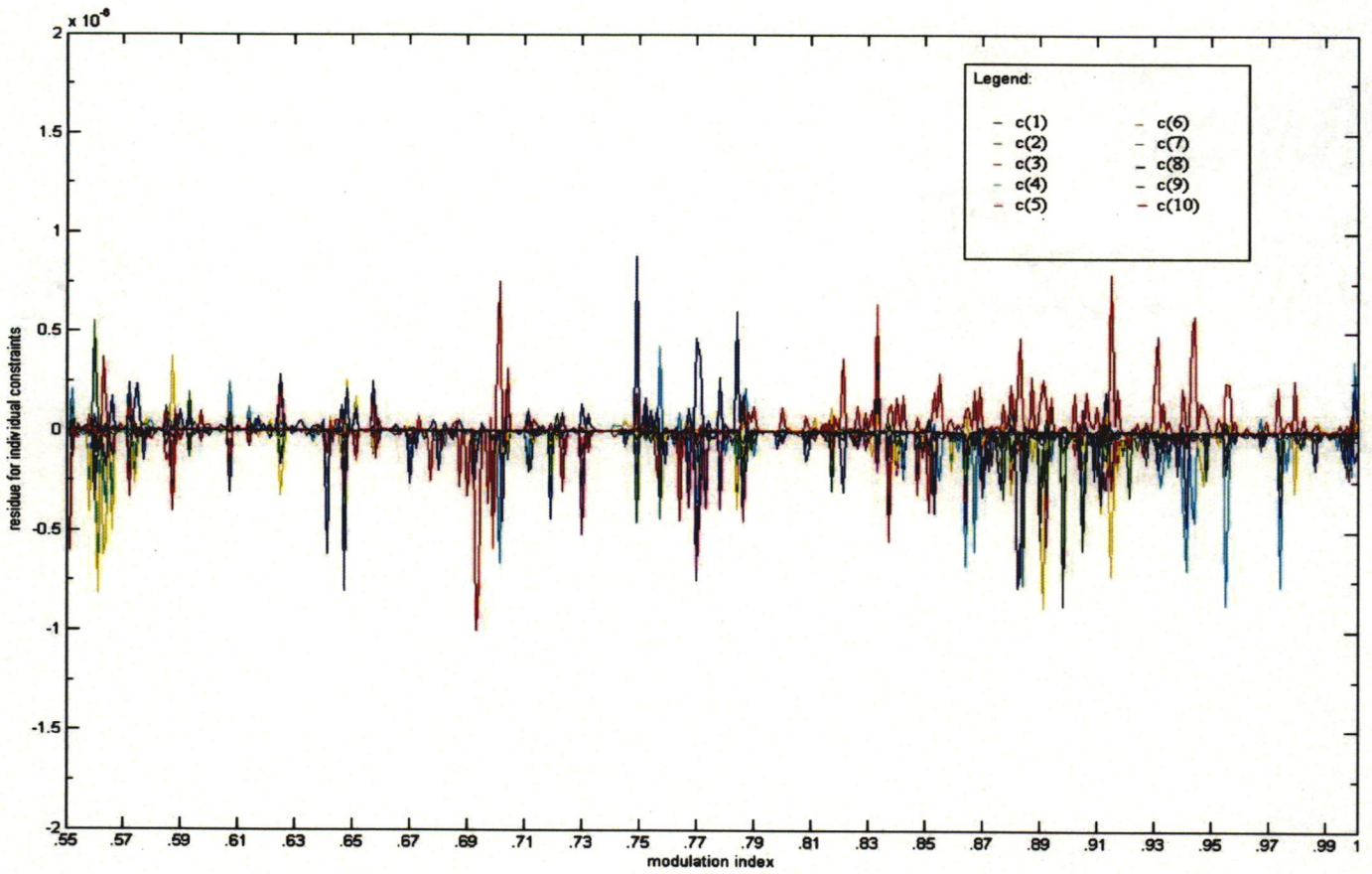
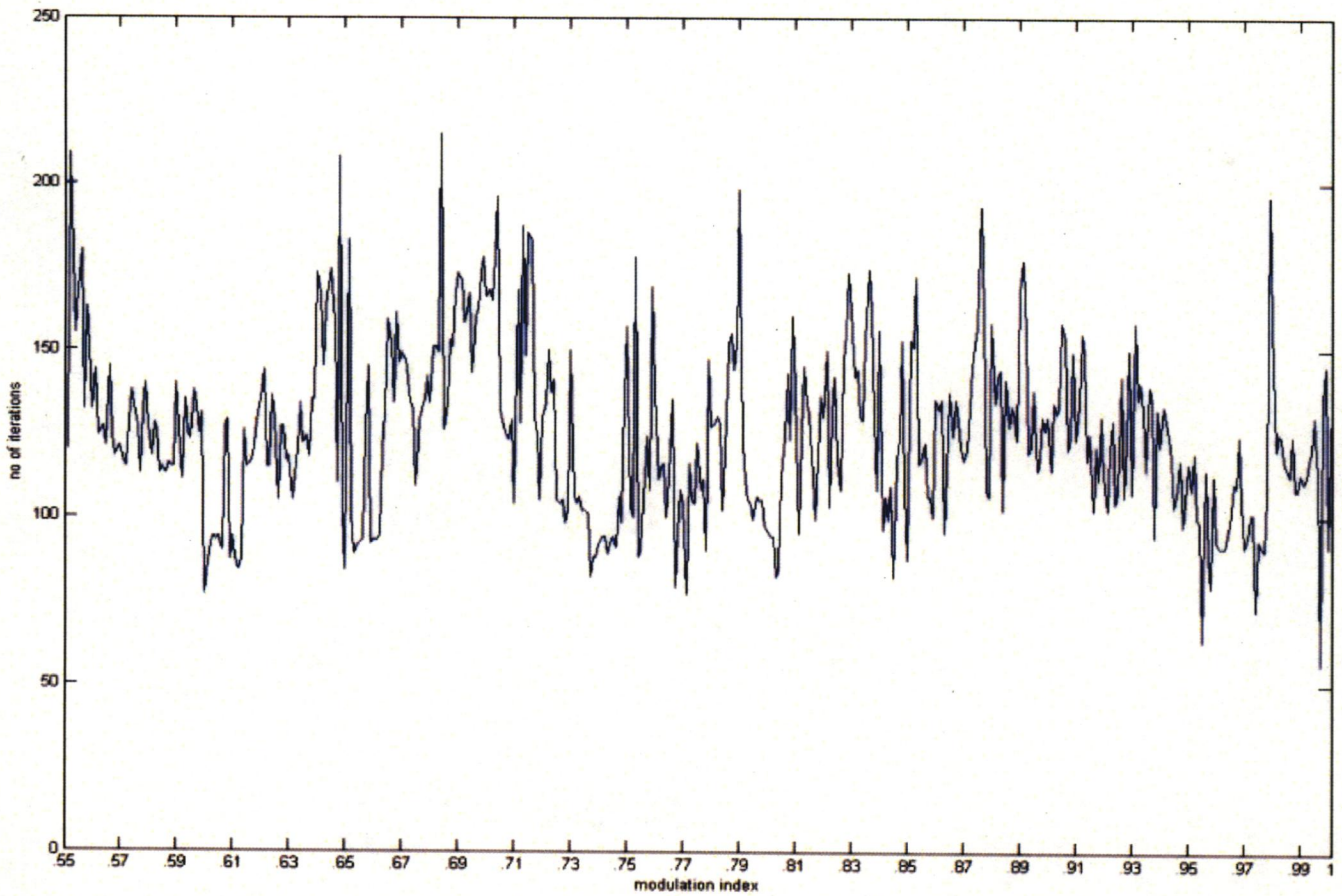


Figure 2.7 variation of % THD obtained by SQP





**Figure 2.8** constrained satisfaction



**Figure 2.9** No. of iterations of SQP





### 3.1 The Distribution system

The performance of STATCOM has to be evaluated in a practical grid. The 27 bus distribution system as shown in Fig 3.1[25] has been considered in this work and been simulated in PSCAD. The distribution system consists of single generator of 132 kV. The weak bus named 'Southery 11 BB' is identified to have a voltage of 0.92 pu during normal operation. As a result the STATCOM has been placed at this bus with a rating of  $\pm 30$  MVA.

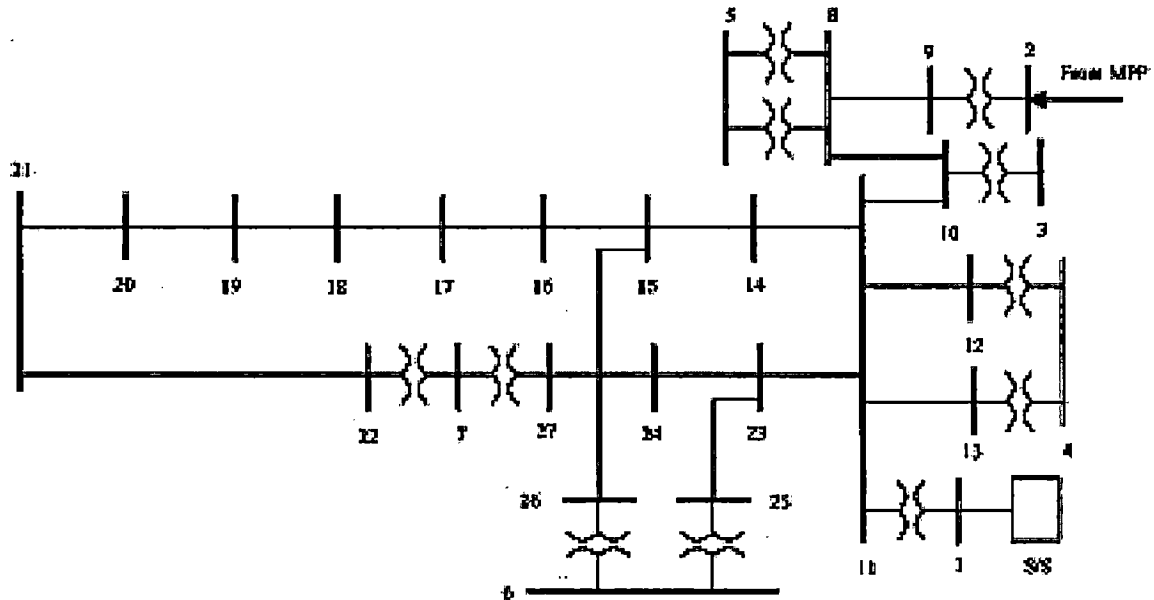


Figure 3.1 Single Line Diagram of Distribution system

### 3.2 System start up

The task of starting up the STATCOM is to bring the reactive power output to a certain level in a very short time, while maintaining all the switching devices within their ratings. The challenge of starting up the STATCOM lies in the fact that, before startup, the dc capacitor voltages are zero. It is observed, however, that when all the active switches are suppressed (no gating signals are supplied to these switches), the STATCOM system is actually composed of several cascading full-bridge rectifiers with no dc-side load except the dc capacitors. The balanced charging has been achieved without excessive absorption of the current above the transformer ratings.

The system is in rectifying mode from 0 to about 1.5s. At about 1.2s, the resistor is bypassed and the gating signals of the STATCOM active switches are enabled at 1.5s. The modulation index is ramped down from 1 to 0.656 to prevent the voltage dip when the power switches are enabled and the delta is fixed at 4.98 degree. This results in the increase in the capacitor voltage to 1.1547pu. At about 3.1s, the dc capacitor voltage reaches the required

level and the STATCOM is put into regulation mode. From 0 to 3.1s, the STATCOM is absorbing more real power than its total component loss. As a result, the capacitor voltage keeps increasing. After 3.1s the real power absorbed by the STATCOM equals its total component loss. Hence, the dc capacitor voltage maintains the same level as shown in Fig 3.2 (c). The next section deals with mathematical model and designing of nonlinear control system.

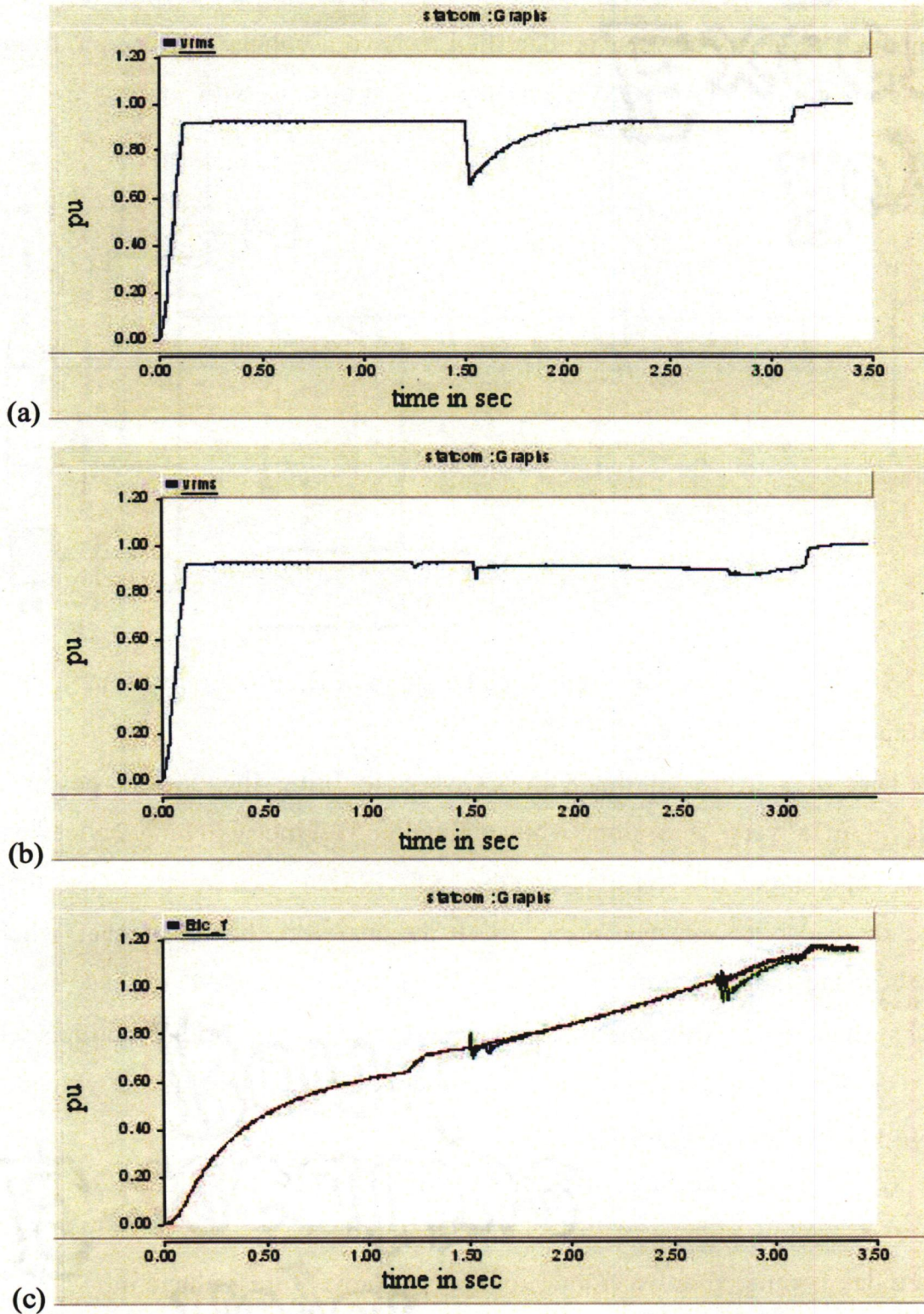


**Figure 3.2** (a) Vrms without modulation index ramp (b) (c) Vrms and Vdc(3 phase) with ramped modulation index

### 3.3 Vector representation of instantaneous three-phase quantities

The main function of the STATCOM is to regulate the transmission line voltage at the point of connection. It achieves this objective by injecting a controlled reactive current to the line. The STATCOM also has the intrinsic ability to exchange real power with the line. As there are no sizeable power sources or sinks associated with the inverter and its DC-side components, the real power must be actively controlled to a value which is zero on average and which departs from zero only to compensate for the losses.

A set of three instantaneous phase variables that sum to zero can be uniquely represented by a vector in orthogonal coordinates by Parks' transformation [6]. This is also called DQ transformation. The DQ transformation expresses synchronous three phase time varying quantity to a time invariant vector in synchronously rotating frame. The three phase voltage source as modeled in PSCAD can be expressed in DQ frame by the given transformation.

$$[c] = \frac{2}{3} \begin{bmatrix} \sin(\omega t) & \sin(\omega t - \frac{2\pi}{3}) & \sin(\omega t + \frac{2\pi}{3}) \\ \cos(\omega t) & \cos(\omega t - \frac{2\pi}{3}) & \cos(\omega t + \frac{2\pi}{3}) \end{bmatrix} \quad (3.1)$$

So that the voltage source

$$[v_a \ v_b \ v_c]^t = \left[ v_m \sin \omega t \quad v_m \sin(\omega t - \frac{2\pi}{3}) \quad v_m \sin(\omega t + \frac{2\pi}{3}) \right]^t \quad (3.2)$$

in DQ frame transforms to

$$\begin{bmatrix} v_d \\ v_q \end{bmatrix} = \frac{2}{3} \begin{bmatrix} \sin(\omega t) & \sin(\omega t - \frac{2\pi}{3}) & \sin(\omega t + \frac{2\pi}{3}) \\ \cos(\omega t) & \cos(\omega t - \frac{2\pi}{3}) & \cos(\omega t + \frac{2\pi}{3}) \end{bmatrix} \begin{bmatrix} v_m \sin(\omega t) \\ v_m \sin(\omega t - \frac{2\pi}{3}) \\ v_m \sin(\omega t + \frac{2\pi}{3}) \end{bmatrix} = \begin{bmatrix} v_m \\ 0 \end{bmatrix} \quad (3.3)$$

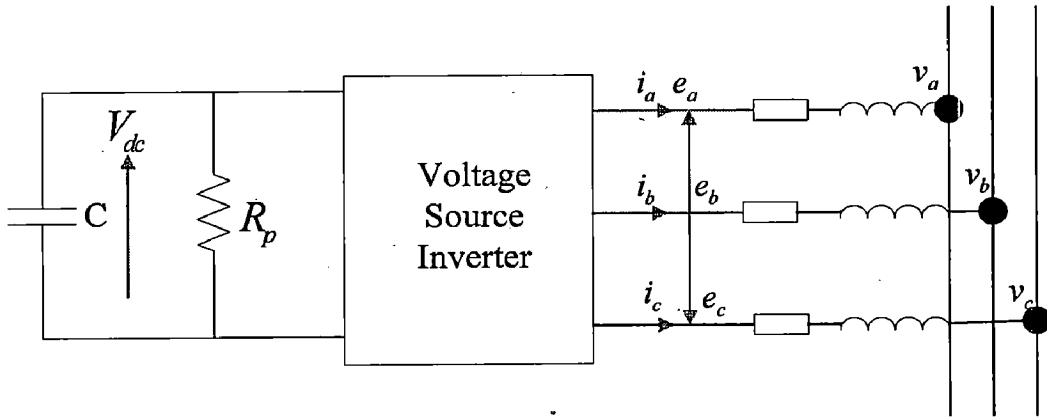
To use the inbuilt abc->dq transformation of PSCAD which is

$$[c] = \frac{2}{3} \begin{bmatrix} \cos(\omega t) & \cos(\omega t - \frac{2\pi}{3}) & \cos(\omega t + \frac{2\pi}{3}) \\ \sin(\omega t) & \sin(\omega t - \frac{2\pi}{3}) & \sin(\omega t + \frac{2\pi}{3}) \end{bmatrix} \quad (3.4)$$

Necessary correction has been done in the model by interchanging 'd' and 'q' signals [26].

### 3.4 Equivalent circuit and equations

Fig. 3.3 shows a simplified representation of the STATCOM, including a DC-side capacitor, an inverter, and series inductance in the three lines connecting to the transmission line. This inductance accounts for the leakage of the actual power transformers. The circuit also includes resistance in shunt with the capacitor to represent the switching losses in the inverter, and resistance in series with the AC lines to represent the inverter and transformer conduction losses. The inverter block in the circuit is treated as an ideal, lossless power converter.



Fig

Figure 3.3 Equivalent circuit of STATCOM

In terms of the instantaneous variables shown in Fig. 3.3, the AC-side circuit equations can be written as follows:

$$p \begin{bmatrix} i_a \\ i_b \\ i_c \end{bmatrix} = \begin{bmatrix} \frac{-R_s}{L} & 0 & 0 \\ 0 & \frac{-R_s}{L} & 0 \\ 0 & 0 & \frac{-R_s}{L} \end{bmatrix} \begin{bmatrix} i_a \\ i_b \\ i_c \end{bmatrix} + \begin{bmatrix} (v_a - e_a) \\ (v_b - e_b) \\ (v_c - e_c) \end{bmatrix} \quad (3.5)$$

where  $p = d/dt$ ,

Using the transformation of variables defined in Eqns. (3.1), Eqns. (3.5) can be transformed to the synchronously rotating reference frame as follows:

$$p \begin{bmatrix} i_d \\ i_q \end{bmatrix} = \begin{bmatrix} \frac{-R_s}{L} & \omega \\ -\omega & \frac{-R_s}{L} \end{bmatrix} \begin{bmatrix} i_d \\ i_q \end{bmatrix} + \frac{1}{L} \begin{bmatrix} (v_d - e_d) \\ -e_q \end{bmatrix} \quad (3.6)$$

where  $\omega = d\theta/dt$ .

The STATCOM dc-side circuit equation can be written as

$$q = C v_{dc} \quad (3.7)$$

$$\frac{dq}{dt} = C \frac{dv_{dc}}{dt} \quad (3.8)$$

$$i_{dc} = C \frac{dv_{dc}}{dt} \quad (3.9)$$

$$P_{dc} = v_{dc} i_{dc} = v_{dc} C \frac{dv_{dc}}{dt} \quad (3.10)$$

$$P_{ac} = \frac{3}{2} v_d i_d \quad (3.11)$$

$$\frac{dv_{dc}}{dt} = \frac{3v_d i_d}{2Cv_{dc}} \quad (3.12)$$

Where  $3/2$  is the reference frame transformation constant and  $e_d, e_q$  are defined as

$$e_d = mv_{dc} \cos \omega t \quad (3.13)$$

$$e_q = mv_{dc} \sin \omega t \quad (3.14)$$

Where  $m$  is the modulation index defined as

$$m = \frac{V_{phase\_peak}}{V_{dc}}$$

The state space model in R-I frame for the STATCOM circuit can be written as follows

$$p \begin{bmatrix} i_d \\ i_q \\ v_{dc} \end{bmatrix} = \begin{bmatrix} -\frac{R_s}{L} & \omega & \frac{v_d}{L} \\ -\omega & -\frac{R_s}{L} & 0 \\ \frac{3v_d}{2Cv_{dc}} & 0 & 0 \end{bmatrix} \begin{bmatrix} i_d \\ i_q \\ v_{dc} \end{bmatrix} - \frac{1}{L} \begin{bmatrix} v_{dc} & 0 \\ 0 & v_{dc} \\ 0 & 0 \end{bmatrix} \begin{bmatrix} m \cos \omega t \\ m \sin \omega t \end{bmatrix} \quad (3.15)$$

### 3.5 Exact linearization via feedback

The system described is a multi-input-multi-output with two input and two output. The system is coupled and nonlinear because it contains multiplication of states and the input variables. In order to decouple and linearize the model in Eqns. (3.15), the input-output linearization technique is applied [14][27]. The system is equivalent as two linear subsystems. These subsystems can be decoupled provided that the matrix in Eqns. (3.24) is not singular. In this case, the decoupling matrix is Eqns. (3.24) considering normal operating conditions, is not singular and the system can be transformed into two decoupled linear systems. The state variables in the linear and controllable system are defined as Eqns. (3.25). Eqns. (3.27) can be used to design a control law for the tracking of a desired trajectory. Comparing Eqns. (3.15) with Eqns. (3.16) the state space form



$$\begin{aligned}\dot{x} &= f(x) + g(x)u \\ y &= h(x)\end{aligned}\tag{3.16}$$

where  $x = [i_d \quad i_q \quad v_{dc}]^T$  then,

$$f(x) = \begin{bmatrix} -\frac{R_s}{L}x_1 + \omega x_2 + \frac{v_d}{L} \\ -\omega x_1 - \frac{R_s}{L}x_2 \\ \frac{3v_d x_1}{2Cx_3} \end{bmatrix}, \quad g(x) = \begin{bmatrix} -\frac{x_3}{L} & 0 \\ 0 & -\frac{x_3}{L} \\ 0 & 0 \end{bmatrix} = [g_1 \quad g_2] \quad \text{and} \quad y(x) = \begin{bmatrix} x_3 \\ x_2 \end{bmatrix} = \begin{bmatrix} h_1 \\ h_2 \end{bmatrix}$$

The Lie derivatives are as follows:

$$L_{f^1}h_1 = [0 \quad 0 \quad 1]f(x) = \frac{v_d x_1}{Cx_3}\tag{3.17}$$

$$L_{g^1}L_f h_1 = \left[ \frac{v_d x_1}{Cx_3} \quad 0 \quad -\frac{v_d x_1}{Cx_3^2} \right] g_1 = -\frac{v_d}{CL}\tag{3.18}$$

$$\begin{aligned}L_{f^2}h_1 &= \left[ \frac{v_d x_1}{Cx_3} \quad 0 \quad -\frac{v_d x_1}{Cx_3^2} \right] f(x) \\ &= \left( -\frac{R_s}{L}x_1 + \omega x_2 + \frac{v_d}{L} \right) \frac{v_d}{Cx_3} - \left( \frac{v_d x_1}{Cx_3^2} \right) \left( \frac{v_d x_1}{Cx_3} \right)\end{aligned}\tag{3.19}$$

$$L_{g^2}h_2 = -\frac{x_3}{L}\tag{3.20}$$

$$L_{g^2}L_f h_1 = 0\tag{3.21}$$

$$L_f h_2 = -\omega x_1 - \frac{R_s}{L}x_2\tag{3.22}$$

$$L_{g^1}h_2 = 0\tag{3.23}$$

$$\text{The decoupling matrix } E(x) = \begin{bmatrix} L_{g^1}L_f h_1 & L_{g^2}L_f h_2 \\ L_{g^1}h_2 & L_{g^2}h_2 \end{bmatrix} = \begin{bmatrix} -\frac{3v_d}{2CL} & 0 \\ 0 & -\frac{x_3}{L} \end{bmatrix}\tag{3.24}$$

The transformed state variables are defined as

$$z_1 = x_3 \quad z_2 = \frac{3v_d x_1}{2Cx_3} \quad z_3 = x_2\tag{3.25}$$

From this the following state space equation is obtained

$$\dot{z}_1 = z_2 \quad \dot{z}_2 = v_1 \quad \dot{z}_3 = v_2\tag{3.26}$$

Where  $v_1$  and  $v_2$  are the new control inputs

The final control laws are given by

$$u_1 = \frac{-L_f^2 h_1 + v_1}{L_{g1} L_f h_1} = \frac{-R_s x_1}{x_3} + \frac{\omega L x_2}{x_3} + \frac{v_d}{x_3} - \frac{L v_d x_1^2}{C x_3^3} - \frac{L C v_1}{v_d} \quad (3.27)$$

$$u_2 = \frac{-L_f h_2 + v_2}{L_{g2} h_2} = \frac{-\omega L x_1}{x_3} - \frac{R_s x_2}{x_3} - \frac{L v_2}{x_3} \quad (3.28)$$

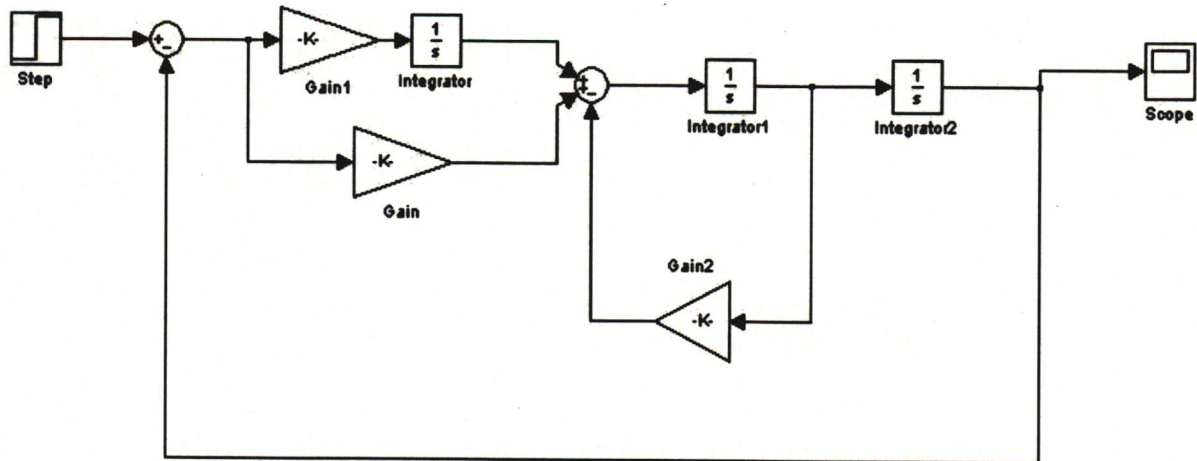


Figure 3.4 Control system for d-axis

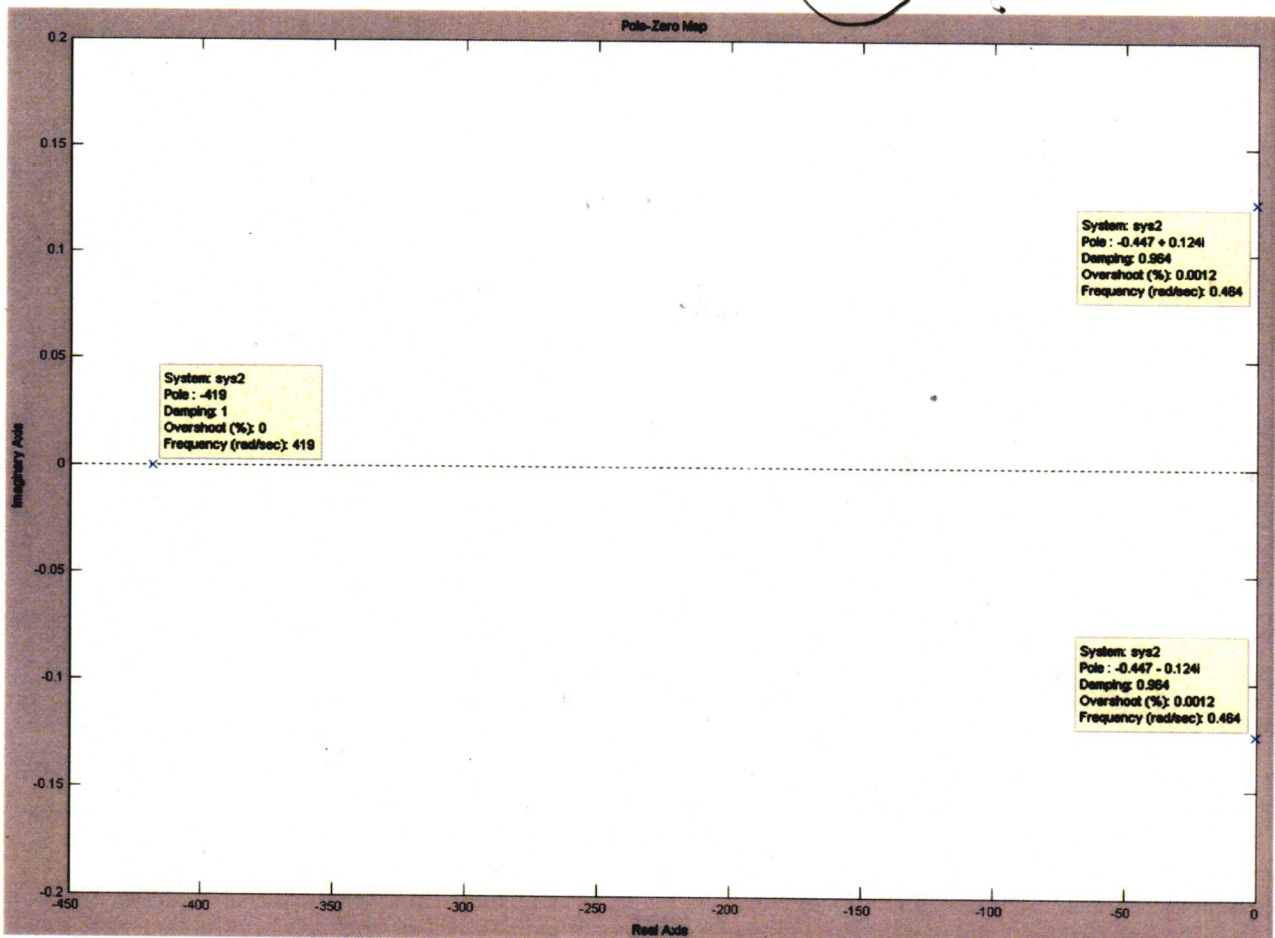


Figure 3.5 Pole placement for d-axis control system

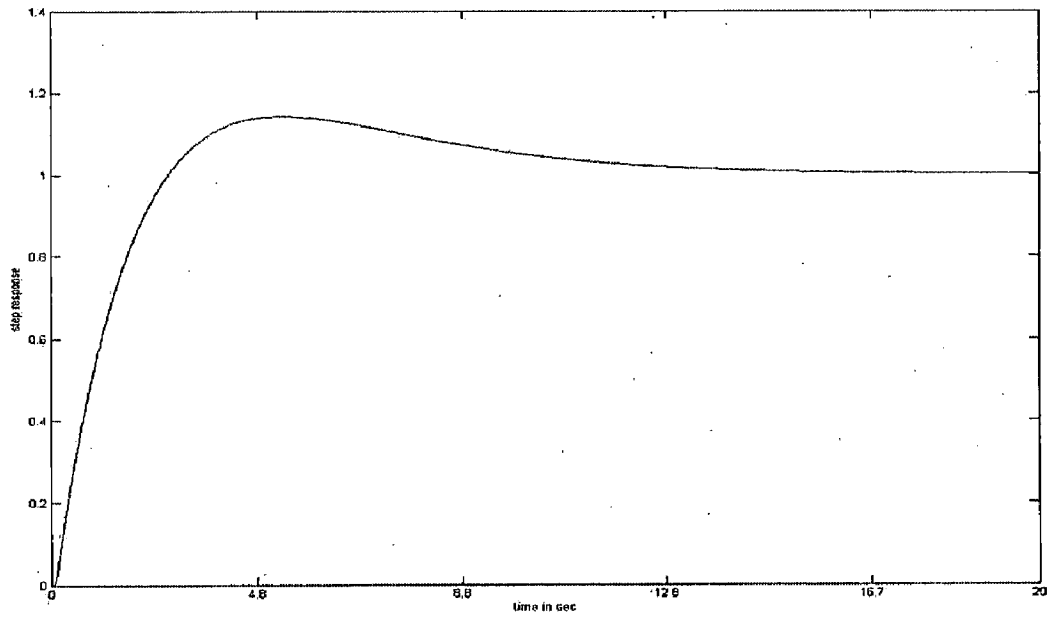


Figure 3.6 Step response for d-axis control system

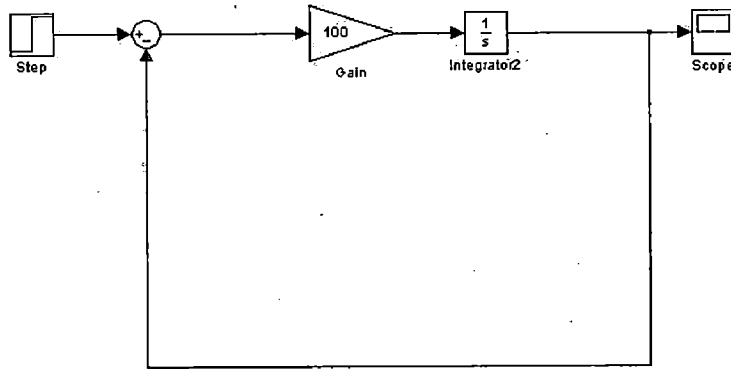


Figure 3.7 Control system for q-axis

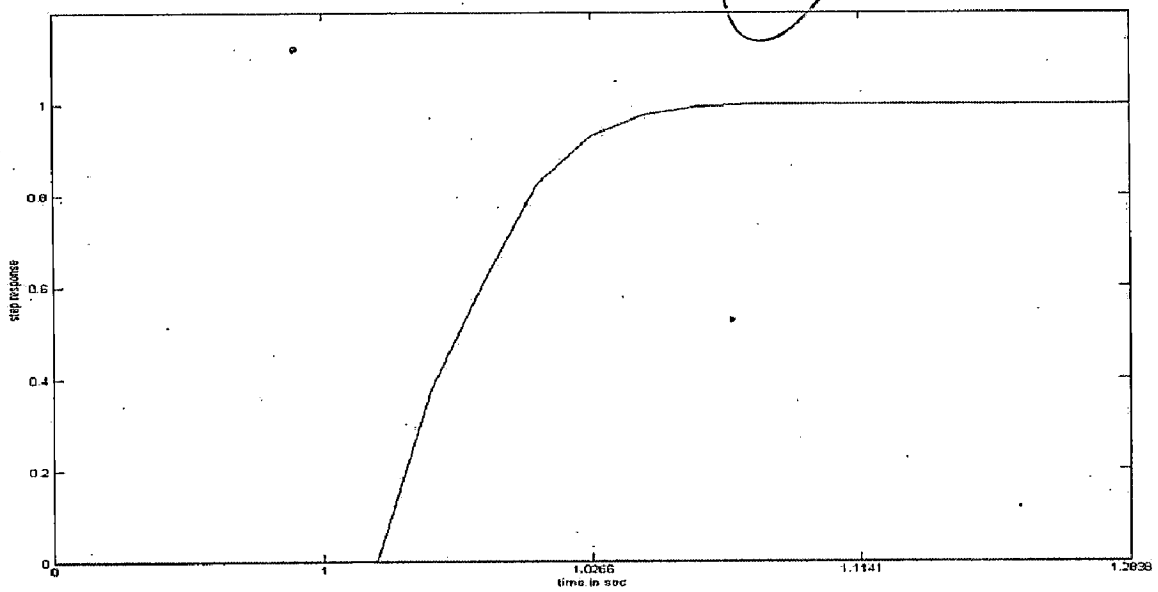


Figure 3.8 Step response for q-axis control system



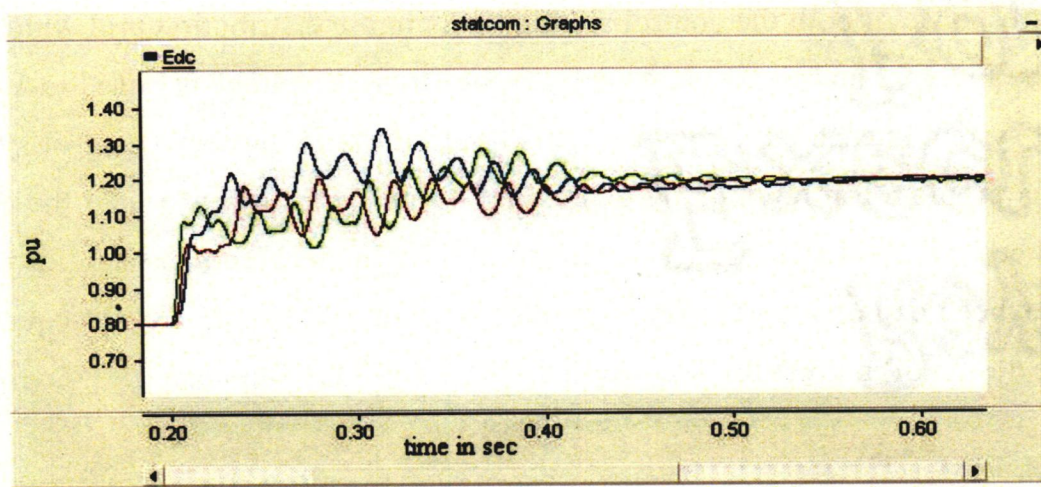


Figure 3.9  $V_{dc}$  response in infinite bus for exact linearization

The poles are placed at  $-0.477 \pm 0.124$  and  $-419$  to obtain the damping 0.964 at frequency 0.464 rad/sec and overshoot of 0.12% by adding a PI controller in the error input. The dc response at single machine infinite bus system is shown in Fig 3.9 for the obtained controller gains. It has to be noted that the obtained response highly in accordance to the proposed dynamics. The response is also compared with the approximate linearized equation proposed by Q. Song [12] which are stated below.

$$u_1 = \frac{-R_s x_1}{x_3} + \frac{\omega L x_2}{x_3} + \frac{v_d}{x_3} - \frac{L v_1}{x_3} \quad (3.29)$$

$$u_2 = \frac{-\omega L x_1}{x_3} - \frac{R_s x_2}{x_3} - \frac{L v_2}{x_3} \quad (3.30)$$

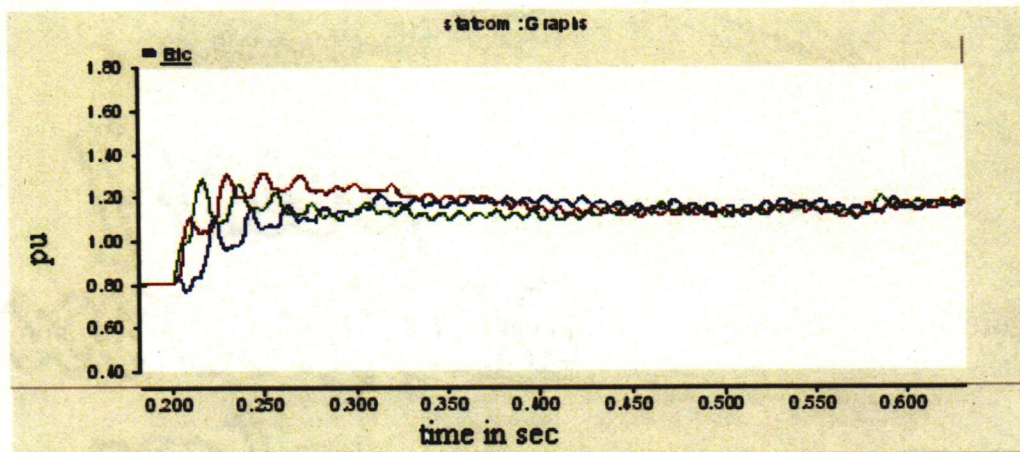


Figure 3.10  $V_{dc}$  response in infinite bus for approx linearization

Now both the controllers of Eqns. (3.27)-(3.28) and Eqns. (3.29)-(3.30) are evaluated in the distribution grid one at a time. The plot for  $V_d$  is observed in Fig 3.11 for Eqns. (3.27)-(3.28). The plot for  $V_d$  for Eqns. (3.29)-(3.30) is similar. Here  $V_d$  is considered to be constant in the State Space model of the STATCOM which is actually the case for infinite bus system. But for the finite distribution system the value of  $V_d$  is dependent on the reactive current requirement and hence the plot of  $V_d$  is not a constant as compared to the infinite bus system.



Naturally the response of both the control strategy fails in the distribution grid which has been observed in the Fig 3.12 and Fig 3.13. At 3.1 sec the DC link voltage is raised to 1.15 pu, but as the control system is enabled the voltage falls because of the defective control system. The remedy of this problem can be done by expressing  $V_d$  as a function of  $I_q$  and the decoupling matrix has to be re-evaluated for exact linearization. The model free approach for controlling the system has been explored and fuzzy logic control is one of them. The subsequent chapter deals with the design of indirect fuzzy controller for STATCOM application.

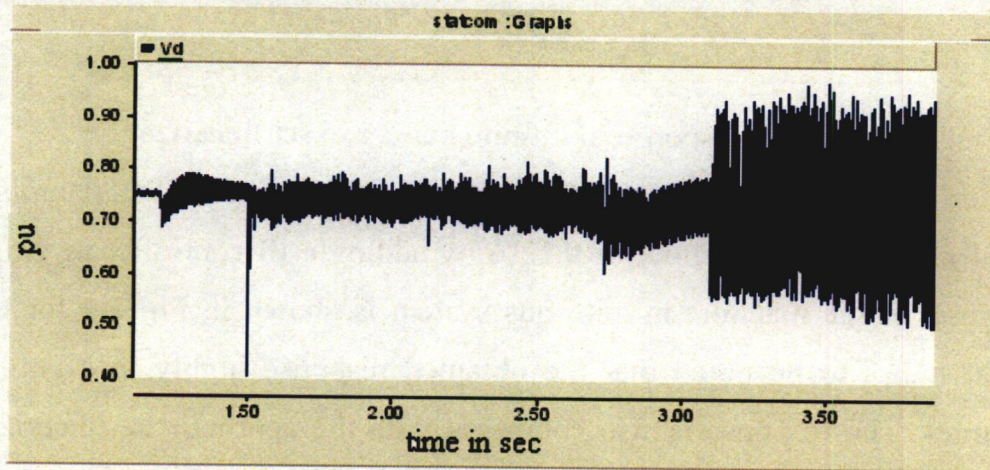


Figure 3.11  $V_d$  plot for the distribution grid

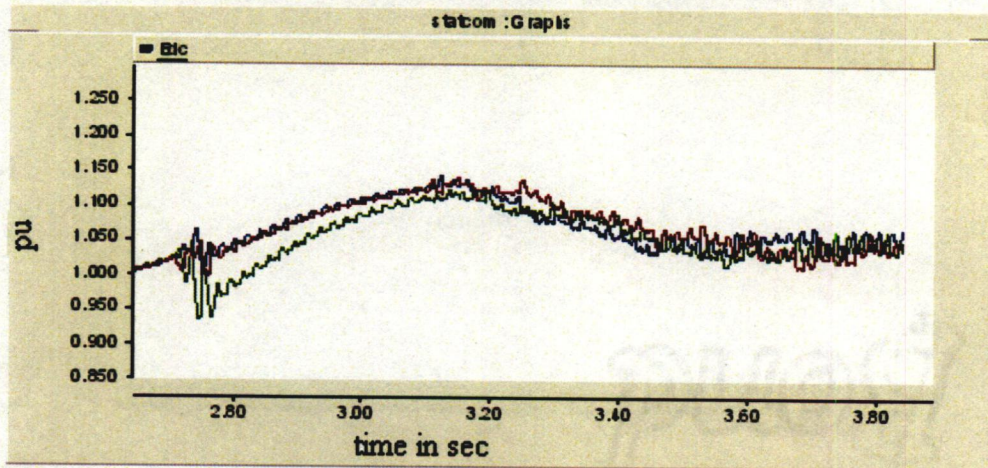


Figure 3.12  $V_{dc}$  in grid for exact linearization on enabling control system

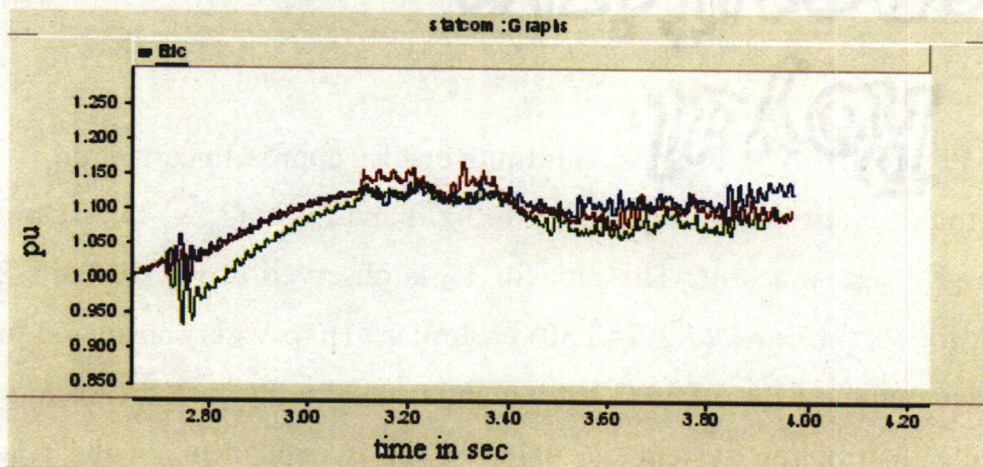


Figure 3.13  $V_{dc}$  in grid for approx linearization on enabling control system



The indirect fuzzy PI controller has been applied in this chapter. The modulation index is kept constant at 1.000 and the only control variable is delta. The input is the error between reference voltage and bus voltage  $V_{rms}$  as shown in Fig. 4.3 and the capacitor voltage level is allowed to vary to inject the required reactive current for bus voltage regulation.

#### 4.1 Fuzzy PI controller

The block diagram of the Fuzzy PI Controller (FPIC) is shown in Fig. 4.1 [15]. In this figure,  $e(k)$  is the error at the  $k$ -th sample and it can be written as  $e(k) = y_{sp} - y(k)$  where,  $y(k)$  is the actual system output and  $y_{sp}$  the set-point or desired system output at  $k$ -th sample respectively. The change in error is defined as

$$\Delta e(k) = e(k) - e(k-1)$$

The quantities  $e$  and  $\Delta e$  are converted to normalized quantities  $eN$  and  $\Delta eN$  respectively by using the Scaling Factors (SFs)  $G_e$  and  $G_{\Delta e}$ . These normalized quantities  $eN$  and  $\Delta eN$  are crisp in nature and therefore need to be first converted to their corresponding fuzzy variables. After fuzzification, the fuzzified inputs are given to the fuzzy inference mechanism which, depending on the given fuzzy rule base, gives the normalized incremental change in control output ( $\Delta uN$ ). The output  $\Delta uN$  is converted into actual incremental change in control output ( $\Delta u$ ) by using the scaling factor  $G_u$ . For implementing the fuzzy inference engine, the “min” operator for connecting multiple antecedents in a rule, the “min” implication operator, and the “max” aggregation operator have been used. Actually, the output  $\Delta uN$  from the inference mechanism is fuzzy in nature, hence, to determine the crisp output, these fuzzy outputs need to be defuzzified. The centroid defuzzification scheme has been used here for obtaining the output  $\Delta u$  as shown in Fig.4.1. Finally, the actual value of the controller output ( $u$ ) is computed by

$$u(k) = u(k-1) + \Delta u(k)$$

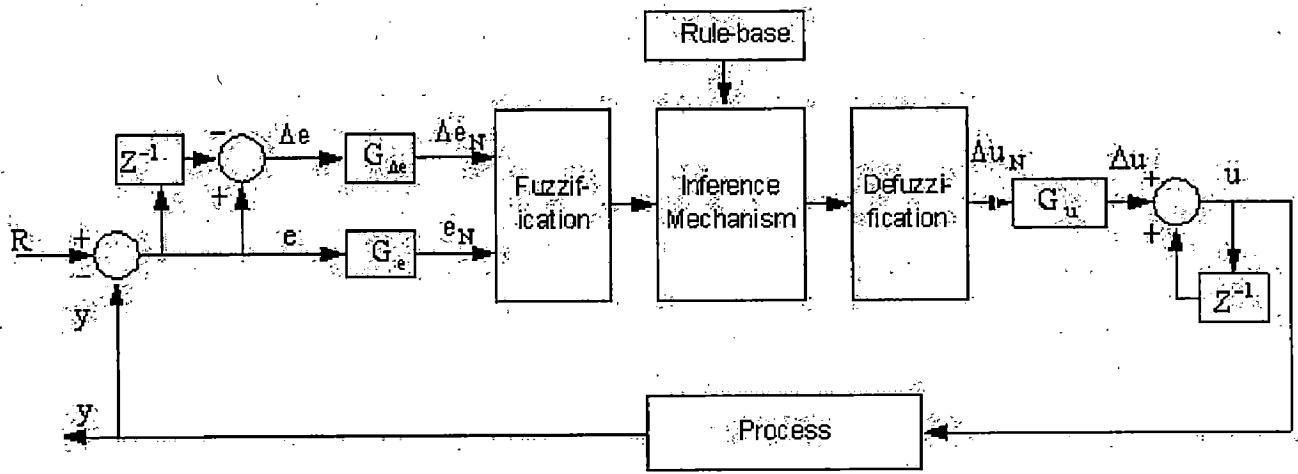


**Figure 4.1** Fuzzy PI controller

The relationships between the SFs ( $G_e$ ,  $G_{\Delta e}$  and  $G_u$ ) and the input and output variables of the FPIC are as follows:

$$e_N = G_e \cdot e$$

$$\Delta e_N = G_{\Delta e} \cdot \Delta e$$

$$\Delta u = G_u \cdot \Delta u_N$$

Here  $G_e$ ,  $G_{\Delta e}$  and  $G_u$  are the SFs for  $e$ ,  $\Delta e$  and  $\Delta u$  respectively and  $e_N$ ,  $\Delta e_N$  and  $\Delta u_N$  are normalized quantities.

The SFs are the main parameters used for tuning any Fuzzy Logic Controller (FLC) because variation of the SFs changes the normalized universe of discourse of input & output variables and their corresponding membership functions. Generally, selection of suitable values for  $G_e$ ,  $G_{\Delta e}$  and  $G_u$  are made based on the knowledge about the process to be controlled and sometimes through trial and error to achieve the best possible control performance. This is so because, unlike conventional non-fuzzy controllers, there is no well-defined method for selecting appropriate values of SFs for FLC. However, if required, it is possible to tune these parameters to achieve a given control objective using some optimization techniques. In this work, the appropriate values for  $G_e$ ,  $G_{\Delta e}$  and  $G_u$  have been determined by using Simplex Algorithm [26] as shown in Fig 4.4.

Each fuzzy control rule in the controller rule base is of the form

“ If  $e$  is  $E$  and  $\Delta e$  is  $\Delta E$ , then  $\Delta u$  is  $\Delta U$ ”

where  $E$ ,  $\Delta E$  and  $\Delta U$  are the fuzzy sets corresponding to error, change in error and the incremental change in the control output respectively. In this work, for both the inputs ( $e$  and  $\Delta e$ ) and the output ( $\Delta u$ ), seven fuzzy subsets have been used. These are: PB (positive big), PM (positive medium), PS (positive small), ZE (zero), NS (negative small), NM (negative medium) and NB (negative big). For each of these fuzzy sets, triangular membership function (MF) has been used. These membership functions have been defined on the common

normalized domain  $[-1, 1]$  and are shown in Fig. 4.2. From this figure it is observed that the triangles are symmetric with equal base having 50% overlap with neighboring MFs. As each of the two inputs has seven fuzzy sets, there are altogether 49 control rules in the FPIC. The rule base for computing the output  $\Delta u$  is shown in Table 4.1 which is a widely used rule base designed with a two-dimensional phase plane [28]. The control rules in Table 4.1 are built based on the characteristics of the step response. For example, if the output is falling far away from the set point, a large control signal that pulls the output toward the set point is expected, whereas a small control signal is required when the output is near and approaching the set point.

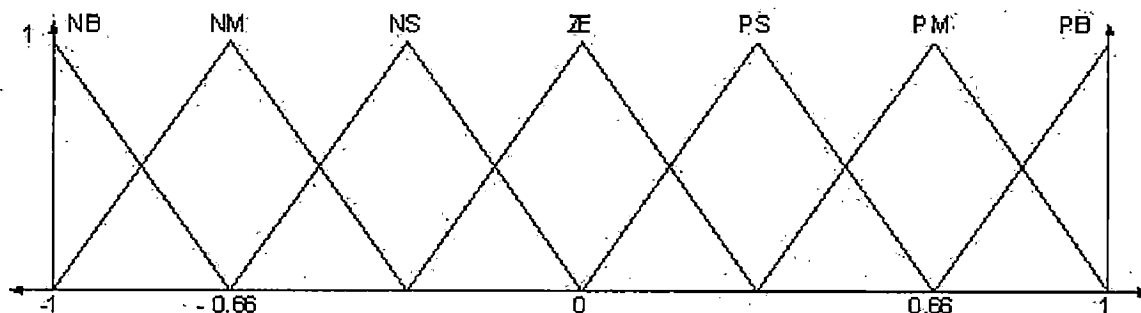


**Figure 4.2** Fuzzy Logic Rule Definition

**Table 4.1:** Fuzzy logic Rule Base

$\Delta e/e$	NB	NM	NS	ZE	PS	PM	PB
NB	NB	NB	NB	NM	NS	NS	ZE
NM	NB	NM	NM	NM	NS	ZE	PS
NS	NB	NM	NS	NS	ZE	PS	PM
ZE	NB	NM	NS	ZE	PS	PM	PB
PS	NM	NS	ZE	PS	PS	PM	PB
PM	NS	ZE	PS	PM	PM	PM	PB
PB	ZE	PS	PS	PM	PB	PB	PB

The scaling factors are tuned by simplex algorithm in PSCAD. The objective function

considered here is the integral square error defined as  $F = \int_0^{t_{sim}} e_p^2(t) dt$  for a step response. The

optimized step response is shown in the Fig 4.5. The optimized scaling factors are 4222 , 0.814815 and -0.0275035.



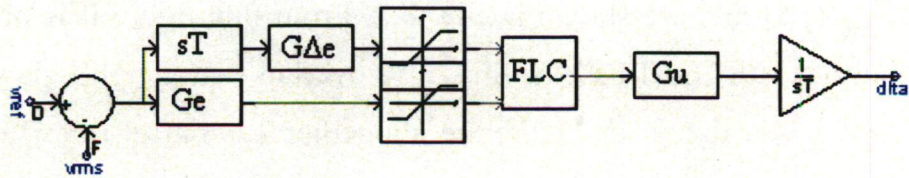


Figure 4.3 Indirect Fuzzy controller

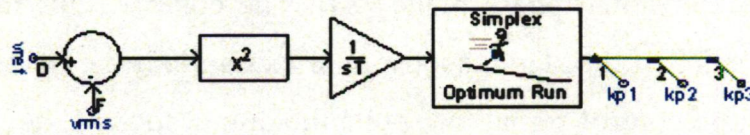


Figure 4.4 Optimization block for step response.

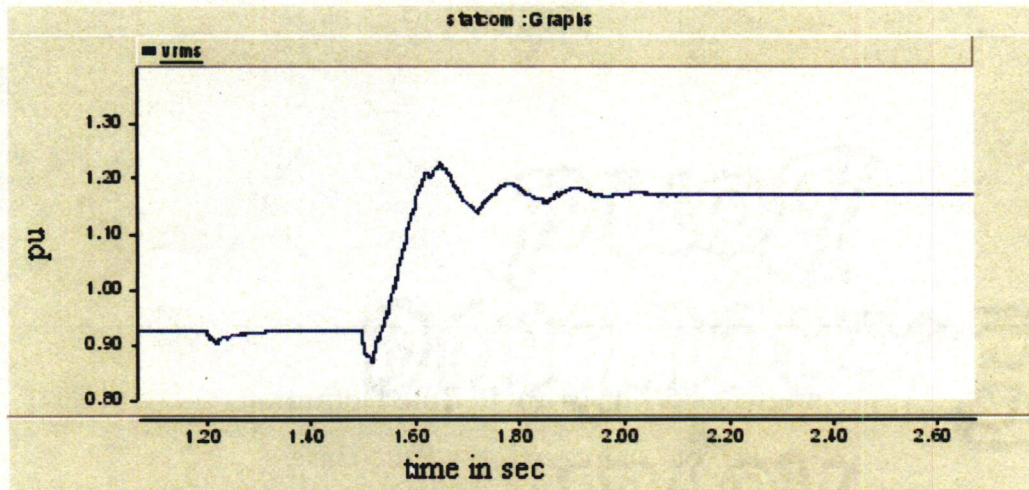


Figure 4.5 Optimized step response for indirect Fuzzy controller

#### 4.2 Performance of indirect fuzzy controller

The controller is then tested for voltage regulation and the response during three phase to ground fault at 'Southery 33 BB' is shown. The control signal delta varies according to the operating point and so the dc voltage of the capacitor changes. The bus voltage further dips to 0.81 pu during three phase to ground fault on the high side of the distribution transformer as shown in Fig 4.6. The  $\pm 30\text{MVA}$  STATCOM is to be installed at the load bus to provide the required voltage support during normal operation and during fault. The voltage sags and swells have to be reduced by installing the STATCOM. The inception of fault at 4 sec is accompanied by increasing the capacitor voltage to 0.9 pu and consequently the reactive current supplied by the STATCOM increases to 0.5 pu as shown in Fig 4.8 and Fig 4.10. The swapping [12] has been implemented to balance the individual capacitor voltage. The three phase total dc link voltage has been observed to be equal and hence there is no need for per phase dc voltage controller. It has been observed that the slow dynamics of the capacitor results in the low voltage dips at the occurrence of the fault. The clearing of the fault at 7.5 sec is also accompanied by large voltage swells to about 1.15 pu as shown in Fig 4.7. The controller designed in this chapter can now be successfully applied in capacitor voltage control in direct



fuzzy control for STATCOM. This is possible because the capacitor dynamics time constant is same in both the control.

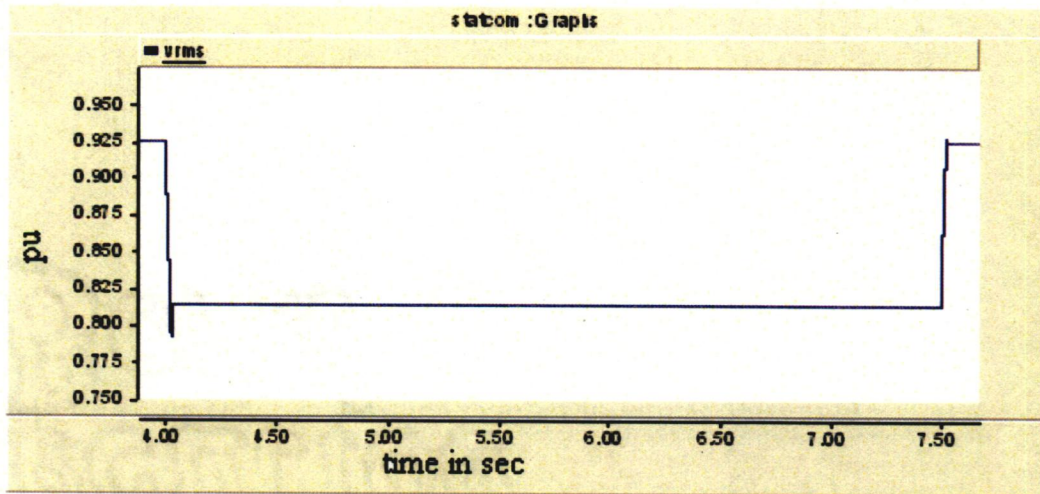


Figure 4.6 V<sub>rms</sub> without STATCOM for 3Ph-G fault

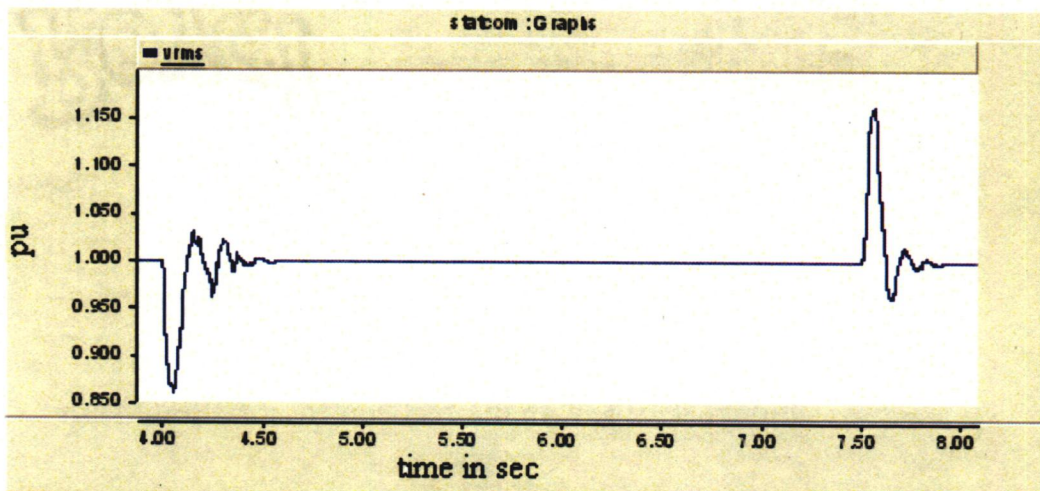


Figure 4.7 V<sub>rms</sub> with indirect controlled STATCOM for 3Ph-G fault

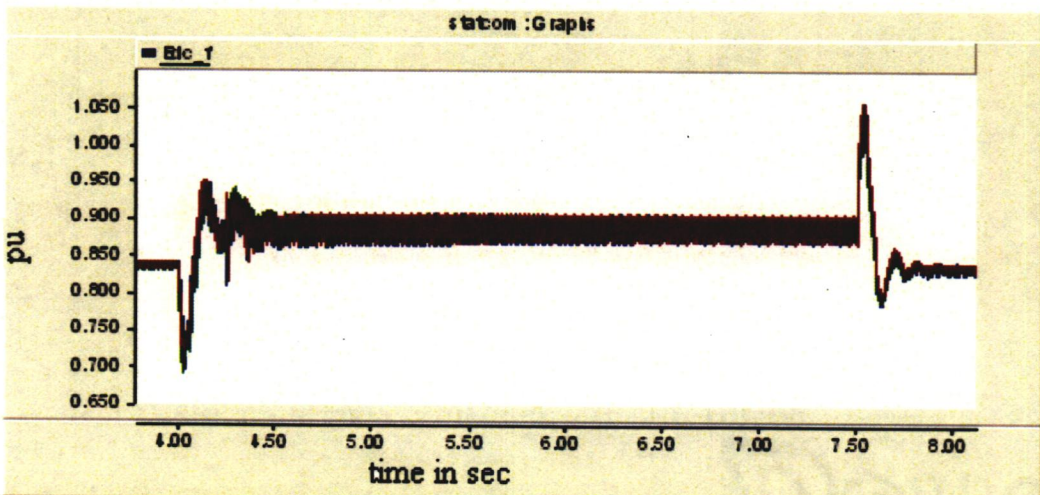


Figure 4.8 3-Ph DC link voltage with indirect control for 3Ph-G fault

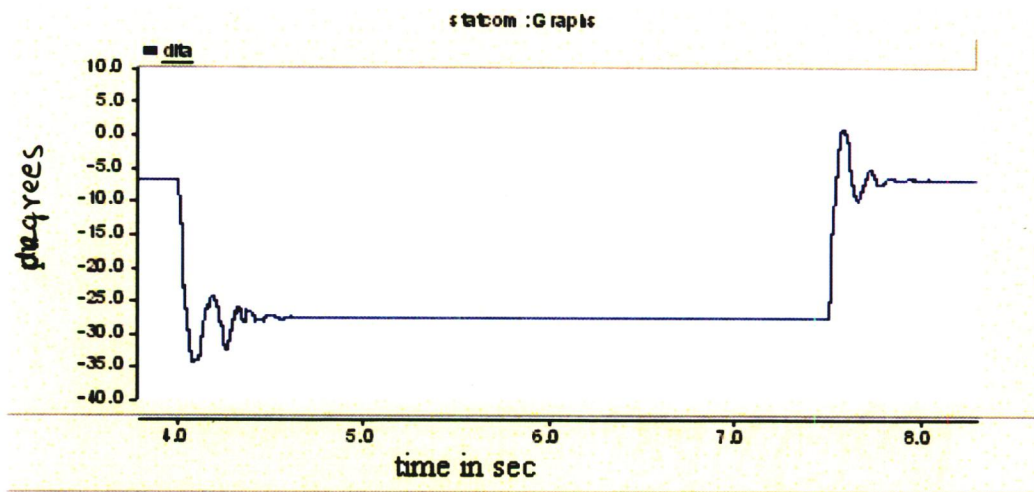


Figure 4.9 Output of indirect controller ( $\delta$ ) for 3Ph-G fault

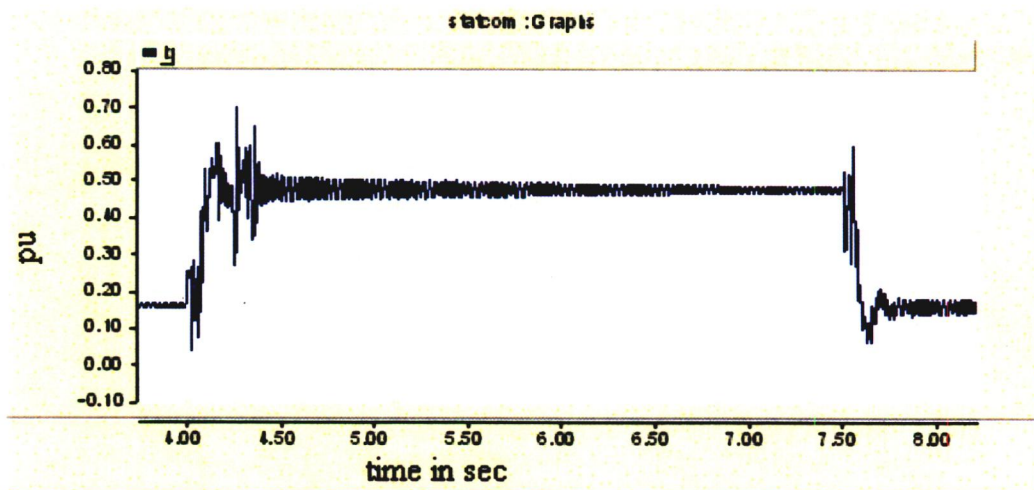


Figure 4.10  $I_q$  with indirect control for 3Ph-G fault

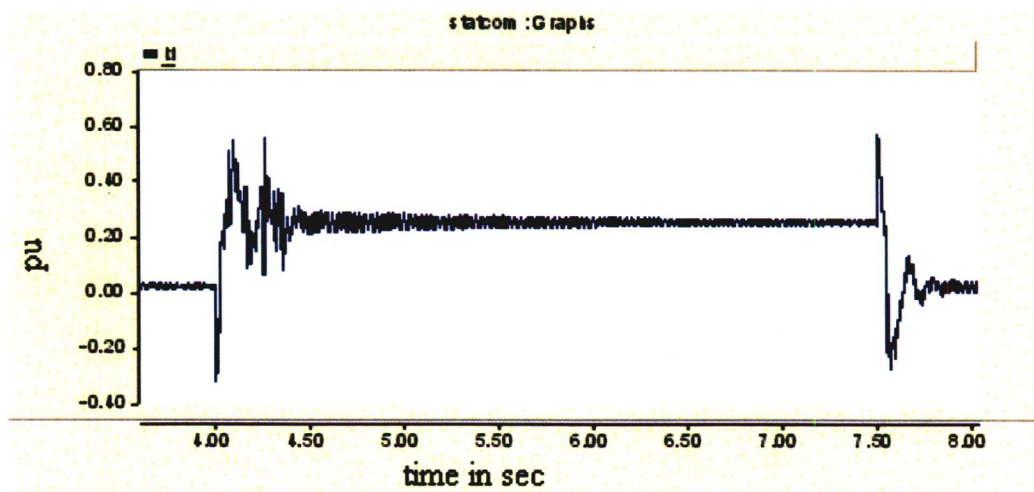


Figure 4.11  $I_d$  with indirect control for 3Ph-G fault



The responses of the indirect controller for Line to Ground (L-G) fault at same bus for 3.5sec are shown from Fig 4.12 to Fig 4.14. The DC link voltage corresponding to the faulted phase has been observed to be less than that of the healthy phases. The reactive current  $I_q$  supplied by the STATCOM oscillates with an offset. The bus voltage  $V_{rms}$  is maintained after small disturbance.

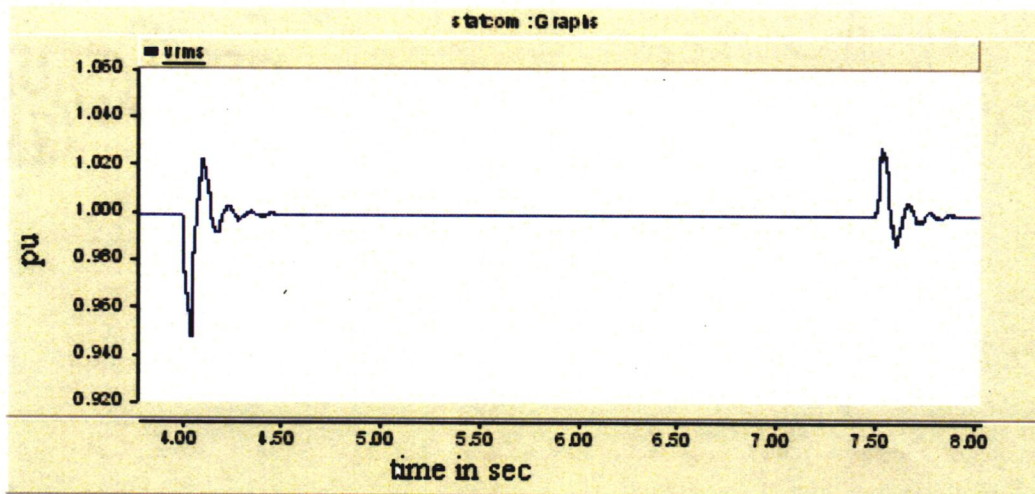


Figure 4.12  $V_{rms}$  with indirect controlled STATCOM for L-G fault

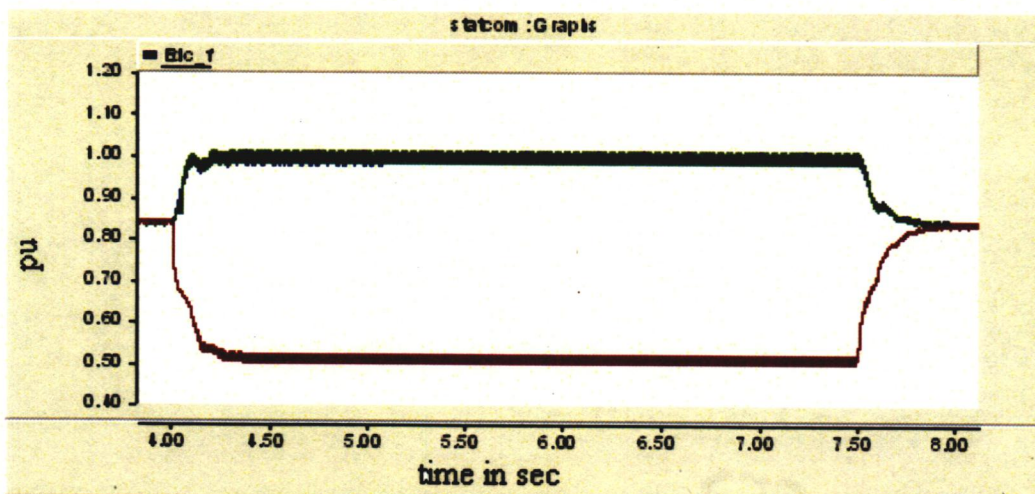


Figure 4.13 3-Ph DC link voltage with indirect control for L-G fault

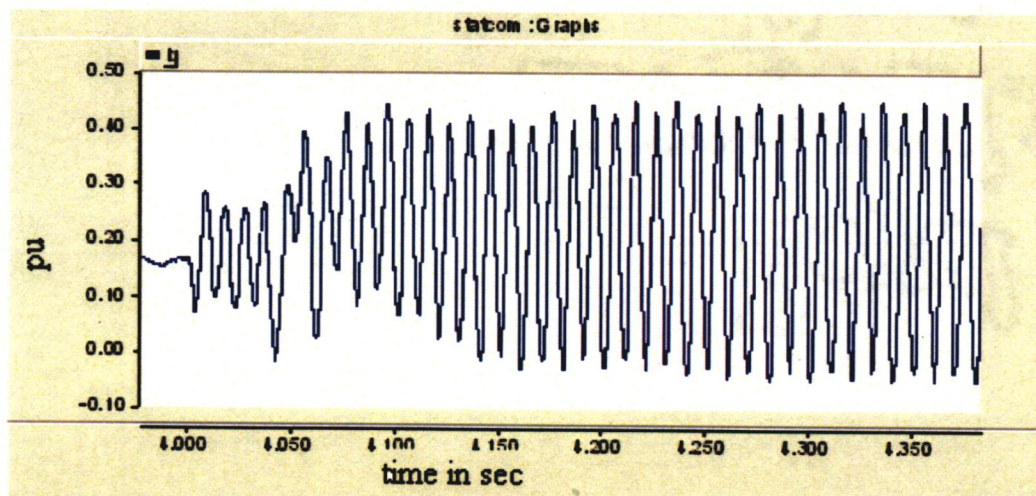


Figure 4.14  $I_q$  with indirect control for L-G fault



Fig 4.15 to Fig 4.17 are the response of the controller for Line to Line (L-L) fault at the same bus for 3.5 sec.

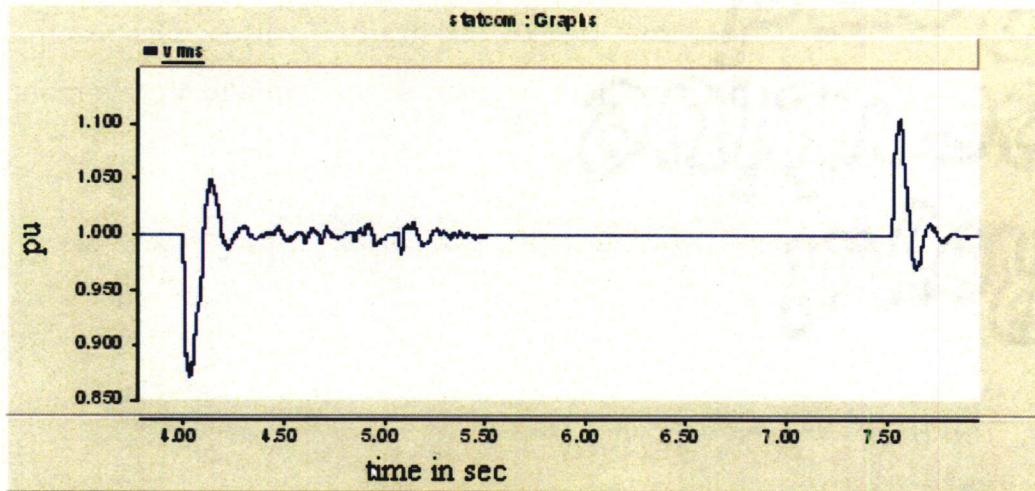


Figure 4.15  $V_{rms}$  with indirect controlled STATCOM for L-L fault

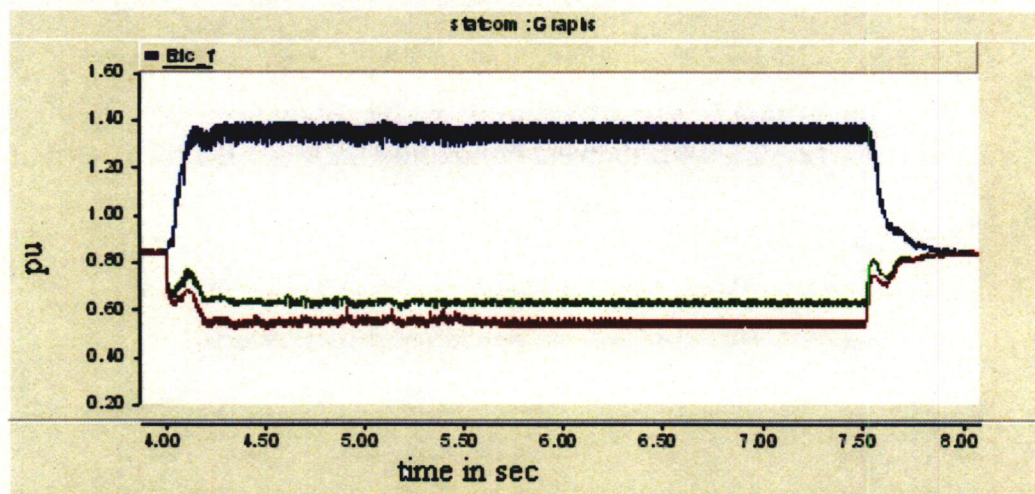


Figure 4.16 3-Ph DC link voltage with indirect control for L-L fault

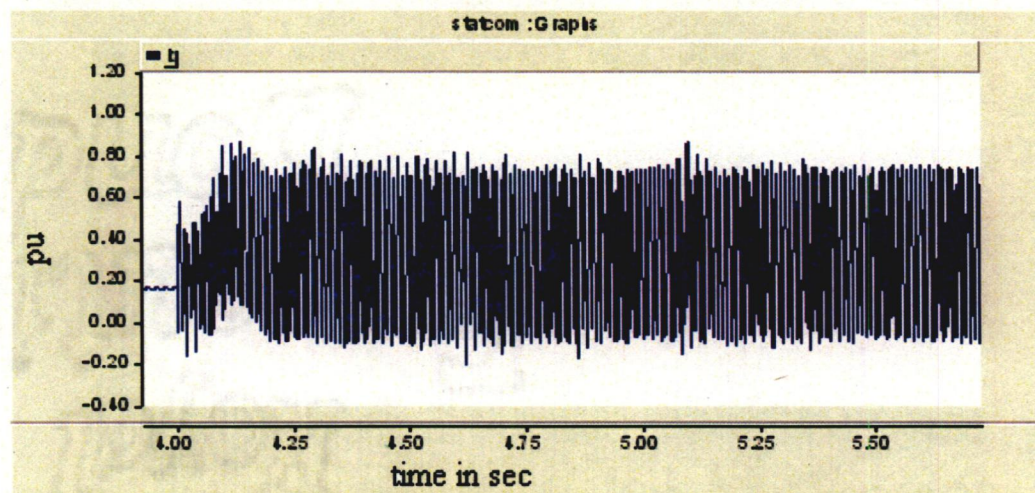


Figure 4.17  $I_q$  with indirect control for L-L fault



Figs 4.18 to Fig 4.20 are the response of the controller for Double Line to Ground (LL-G) fault at the same bus for 3.5 sec.

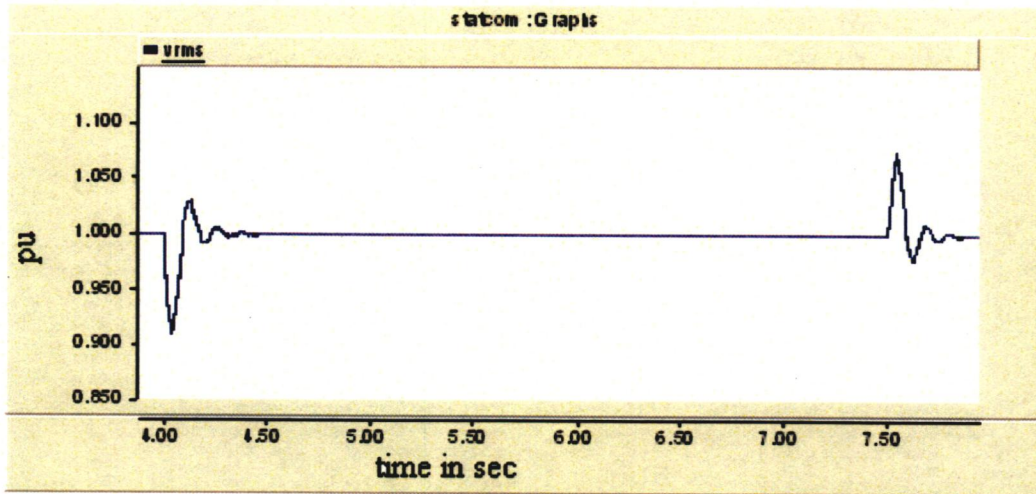


Figure 4.18 V<sub>rms</sub> with indirect controlled STATCOM for LL-G fault

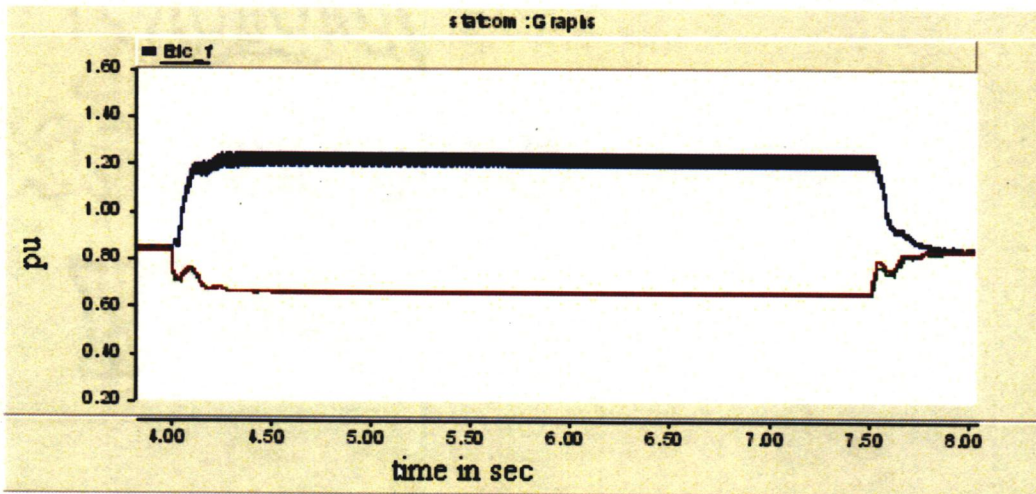


Figure 4.16 3-Ph DC link voltage with indirect control for LL-G fault

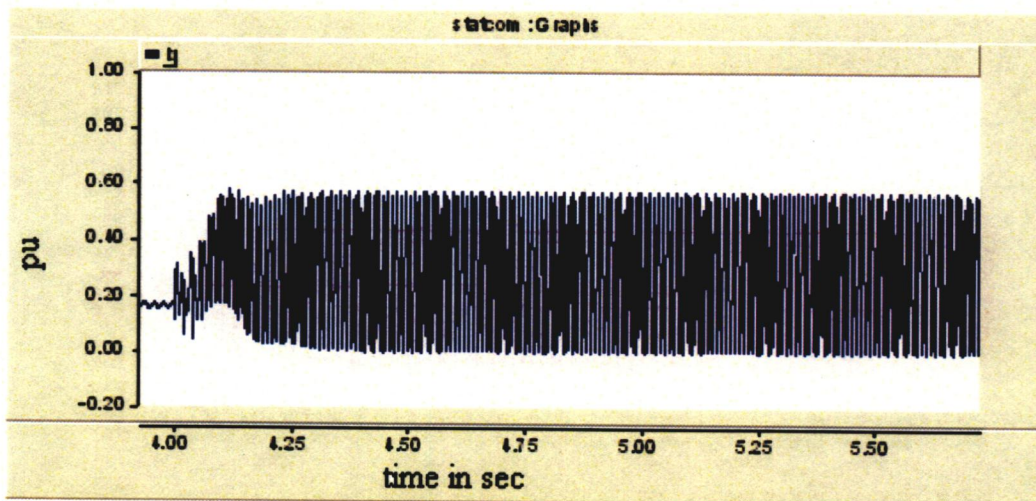


Figure 4.17 I<sub>q</sub> with indirect control for LL-G fault





5.1 Direct fuzzy controller design

The direct fuzzy controller design which has both the modulation index and the phase as output has been attempted. The dc capacitor voltage is maintained by controlling the delta of the inverter and the bus voltage support is achieved by controlling the modulation index. The controller for the dc voltage loop has been designed by the previous indirect controller by replacing the input as the error between reference and  $V_{dc}$ . This is justifiable because the time constant and the capacitor dynamics remain same. The bus voltage controller has been designed by considering the regulation slope as  $\omega l$  and the offset as  $V_d$  (rated) which is the equation of the natural characteristics of the STATCOM. The controller input is the error between reference and the bus voltage  $V_{rms}$  as shown in Fig 5.1. The output of the controller is  $I_q$ (required). The modulation index is calculated by the following equation

$$m = \frac{V_{d\_rated} + (\omega l)I_{q\_req}}{V_{dc}}$$

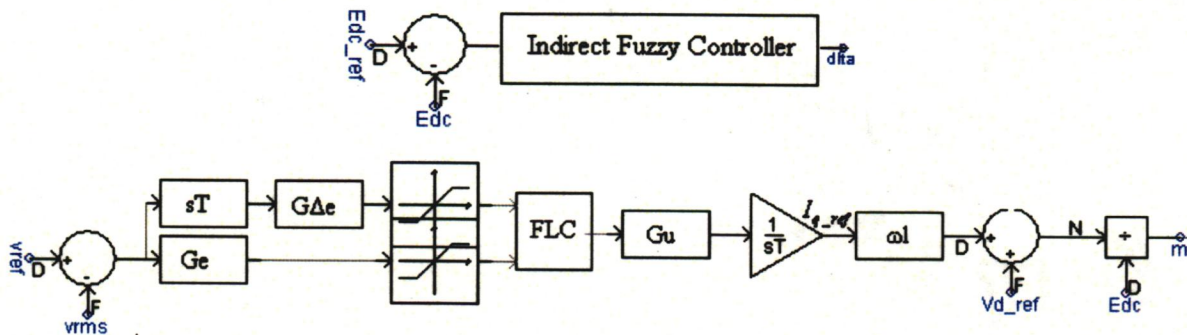


Figure 5.1 Scheme of STATCOM direct controller

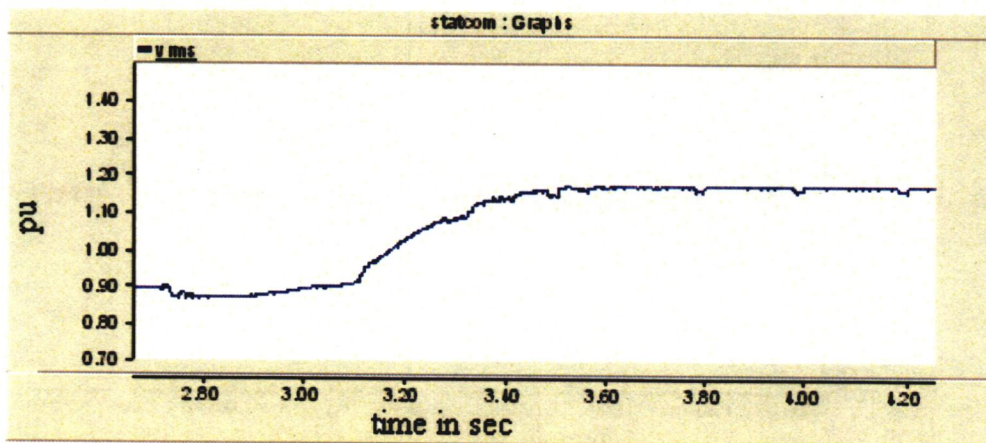


Figure 5.2 Optimized step response for direct Fuzzy controller

5.2 Performance of direct fuzzy controller

The controller gains are tuned for minimum integral square error by the simplex method. The optimized controller with STATCOM is then installed in the distribution grid for



performance evaluation. In the normal operation the STATCOM supplies 0.15 pu of reactive current to maintain the reference voltage level. The STATCOM also draws a small amount of real power in the form of  $I_d$  for required  $V_{dc}$ . The capacitor voltage ripple has been observed to be less while supplying 0.15pu of reactive current which subsequently increases on increasing the supplied  $I_q$  by the STATCOM. The inception of three phase to ground fault for 3.5sec at 'Southery 33 BB' is accompanied by increase in injected  $I_q$  by the STATCOM to 0.5pu and the capacitor voltage ripple as shown in Fig 5.7 and Fig 5.4. The capacitor voltage is maintained by the indirect controller independent of the bus voltage but has been noted by a slight dip for few cycles. This results in an increase modulation index to supply the reactive current at reduced capacitor voltage in Fig 5.5. The stabilization of capacitor voltage results in less fluctuation of the output of the modulation index controller. The voltage dips has been reduced to 0.92pu on the inception of the fault and is much better than the indirect controller. The response during the fault clearance is more remarkable as the maximum voltage swells is reduced to 1.05 pu in Fig 5.3.

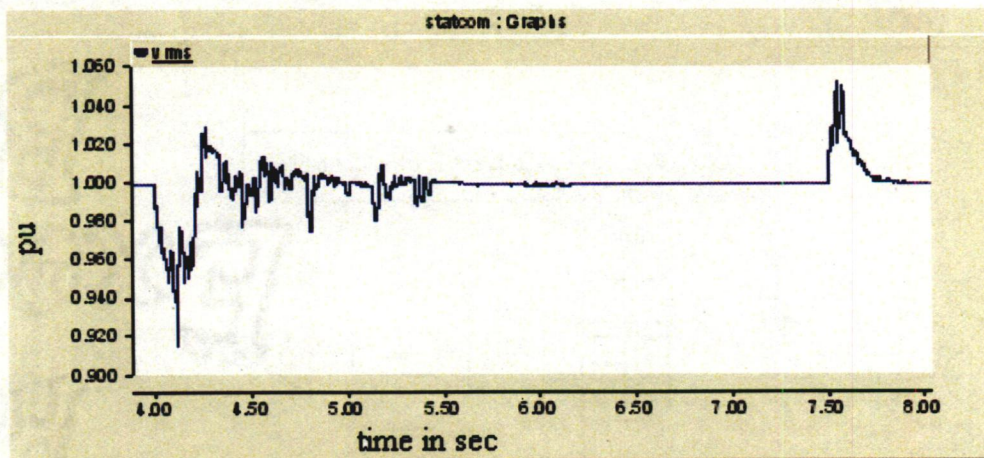


Figure 5.3  $V_{rms}$  during for 3Ph-G fault for direct control

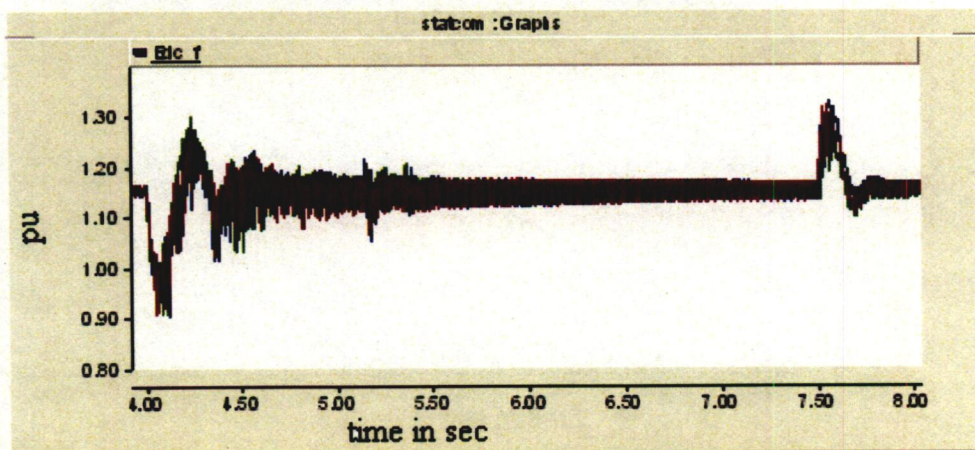


Figure 5.4 3-Ph DC link voltage with direct control for 3Ph-G fault



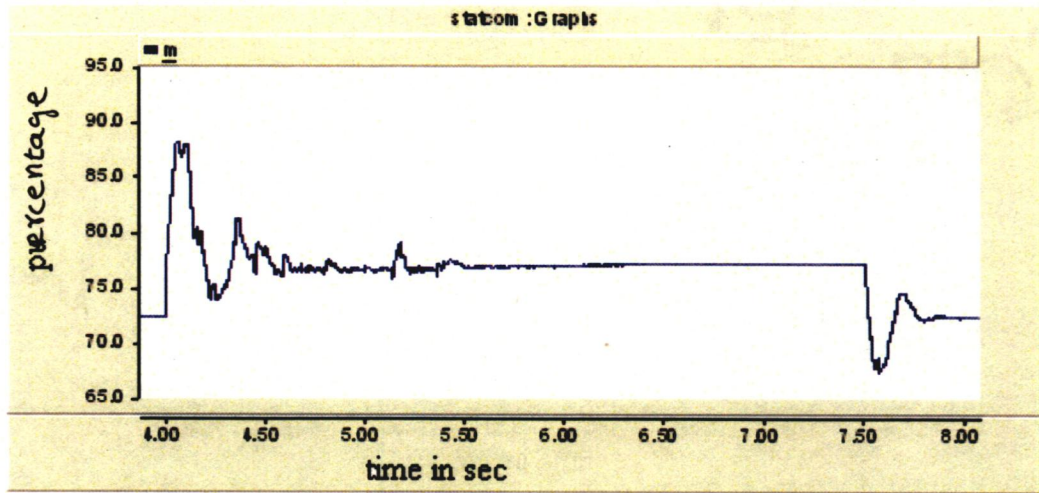


Figure 5.5 Output 1 of direct controller (modulation index) for 3Ph-G fault

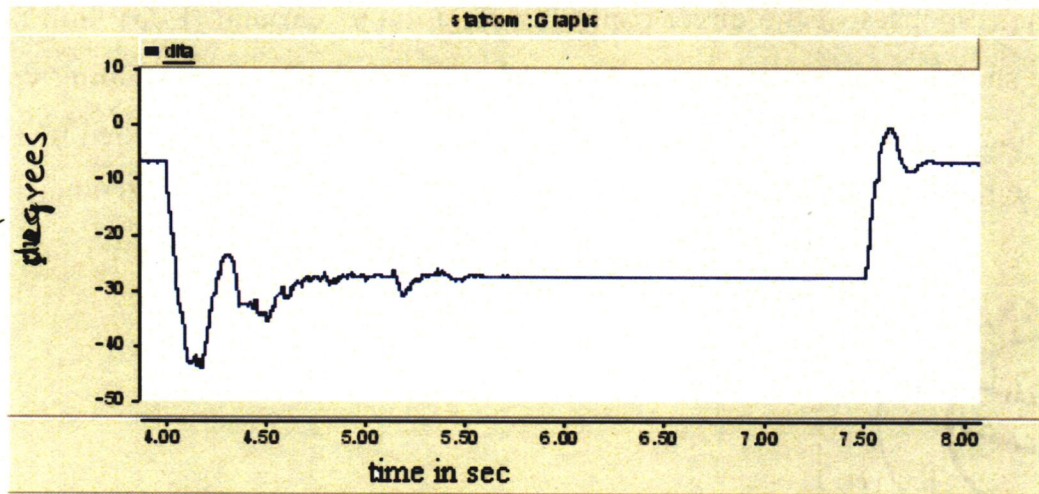


Figure 5.6 Output 2 of direct controller (delta) for 3Ph-G fault

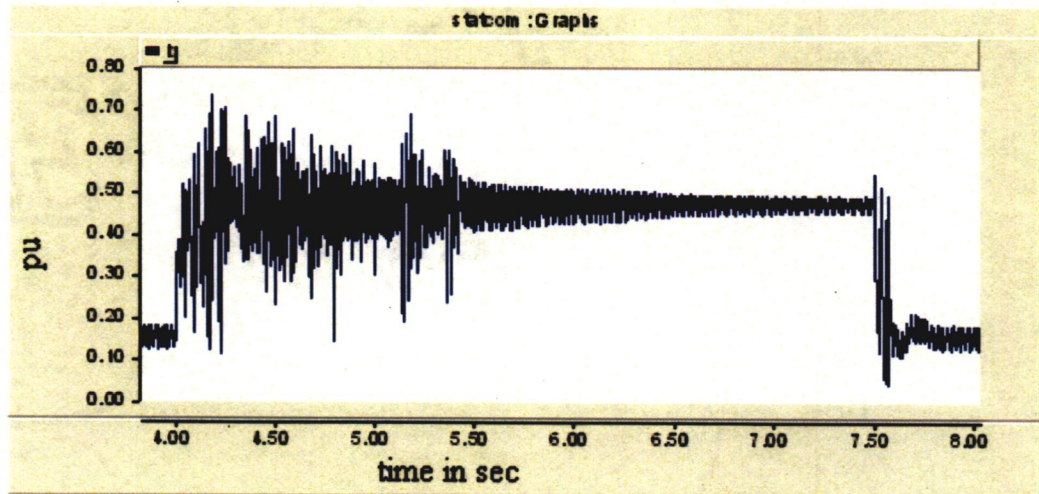


Figure 5.7  $I_q$  with direct control for 3Ph-G fault



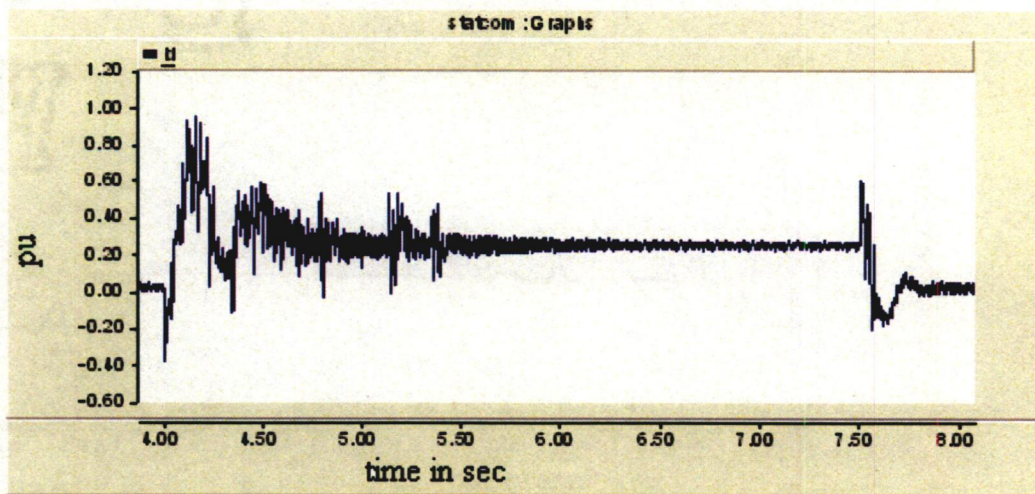


Figure 5.8  $I_d$  with direct control for 3Ph-G fault

The responses of the direct controller for Line to Ground (L-G) fault at same bus for 3.5sec are shown from Fig 5.9 to Fig 5.11. The faulted phase of the DC link voltage has been observed to be less than the healthy phases. The reactive current  $I_q$  supplied by the STATCOM oscillates with an offset. The bus voltage  $V_{rms}$  is restored with a dip of 0.99pu.

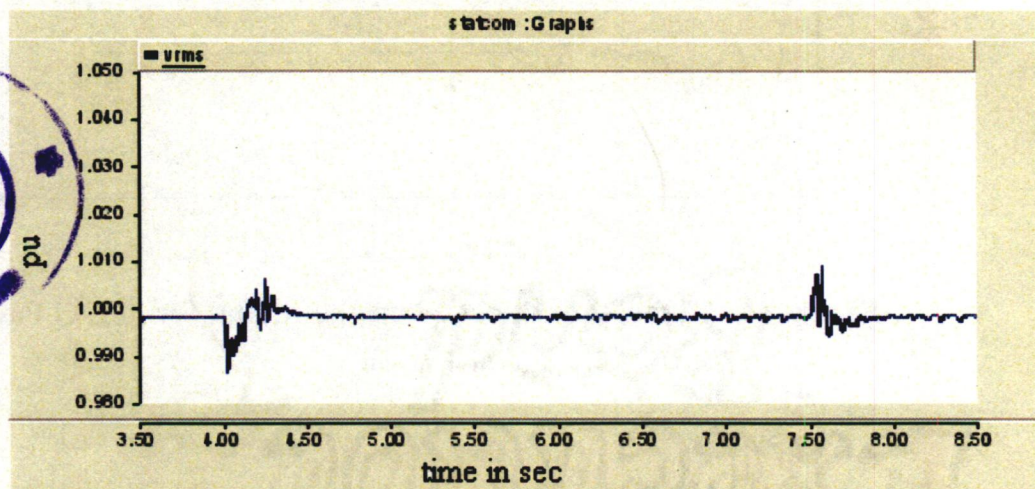


Figure 5.9  $V_{rms}$  with direct controlled STATCOM for L-G fault

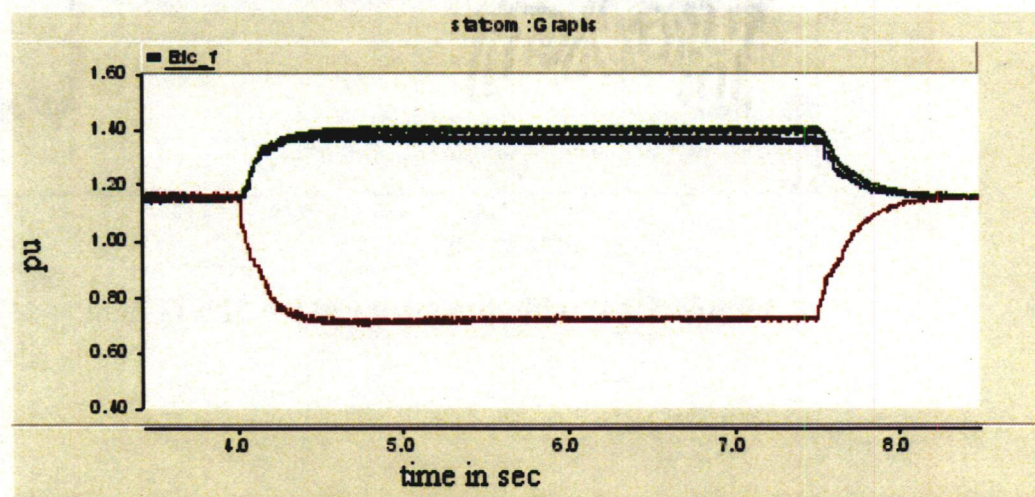


Figure 5.10 3-Ph DC link voltage with direct control for L-G fault



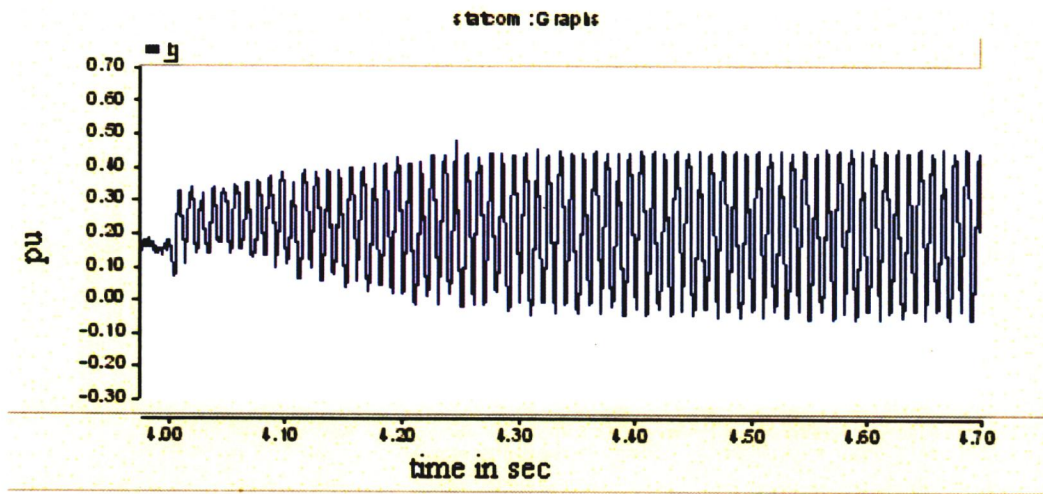


Figure 5.11  $I_q$  with direct control for L-G fault

Fig 5.12 to Fig 5.14 are the response of the controller for Line to Line (L-L) fault at the same bus for 3.5 sec.

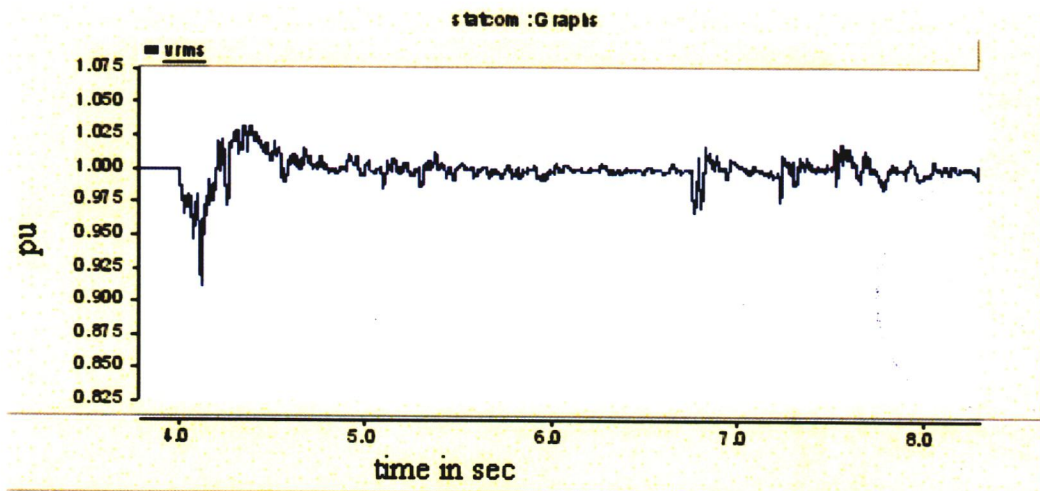


Figure 5.12  $V_{rms}$  with direct controlled STATCOM for L-L fault

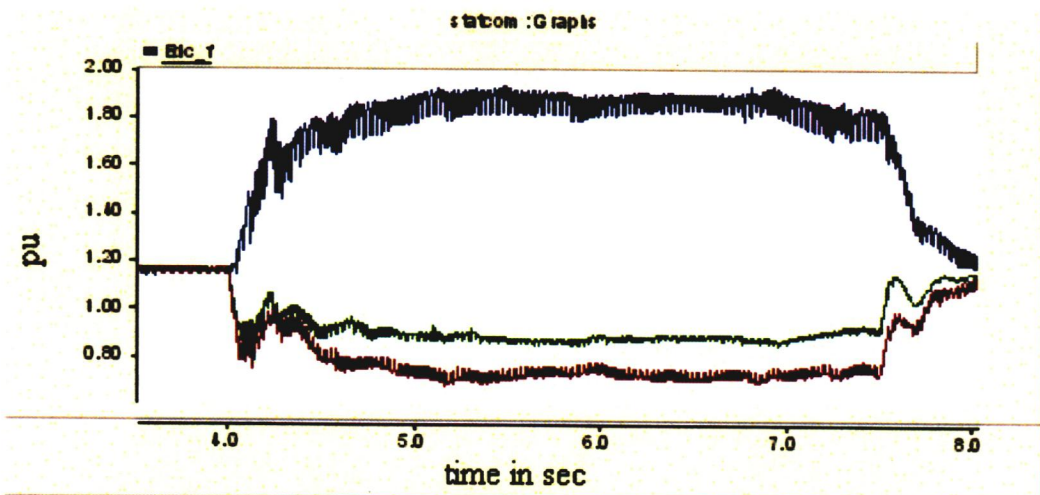
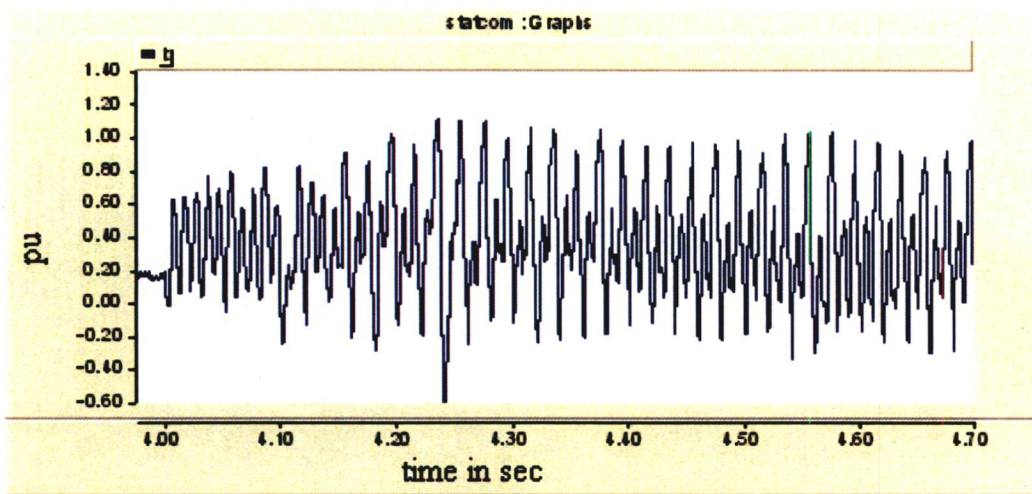
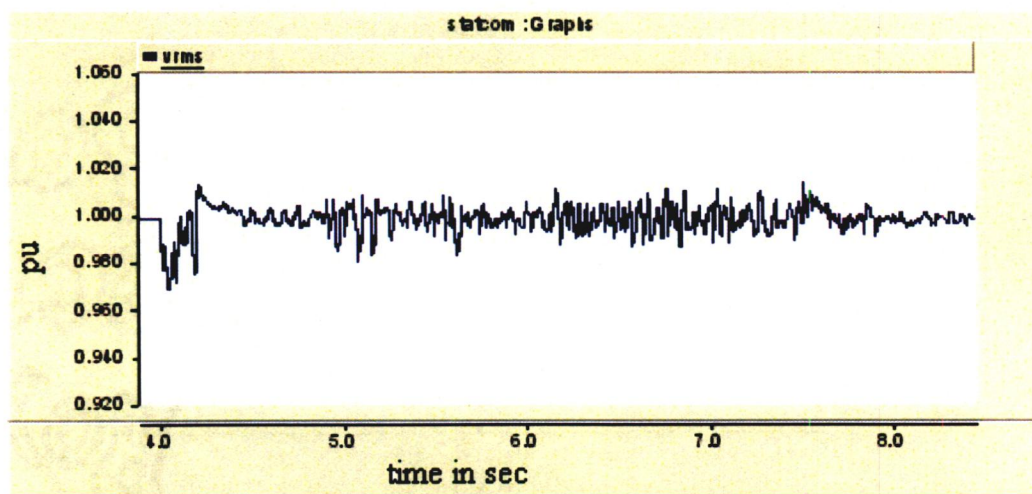


Figure 5.13 3-Ph DC link voltage with direct control for L-L fault



**Figure 5.14**  $I_q$  with direct control for L-L fault

Fig 5.15 to Fig 5.17 are the response of the controller for Double Line to Ground (LL-G) fault at the same bus for 3.5 sec.



**Figure 5.15**  $V_{rms}$  with direct controlled STATCOM for LL-G fault

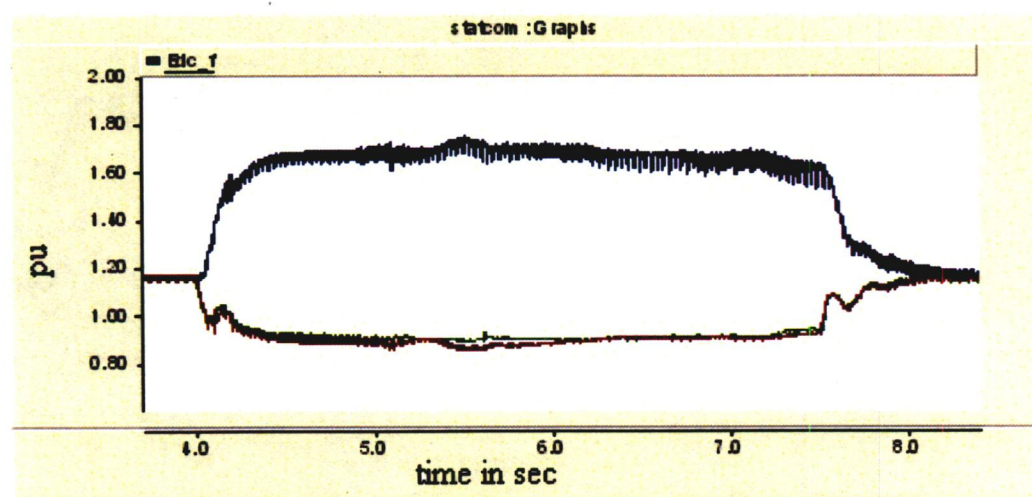


**Figure 5.16** 3-Ph DC link voltage with direct control for LL-G fault



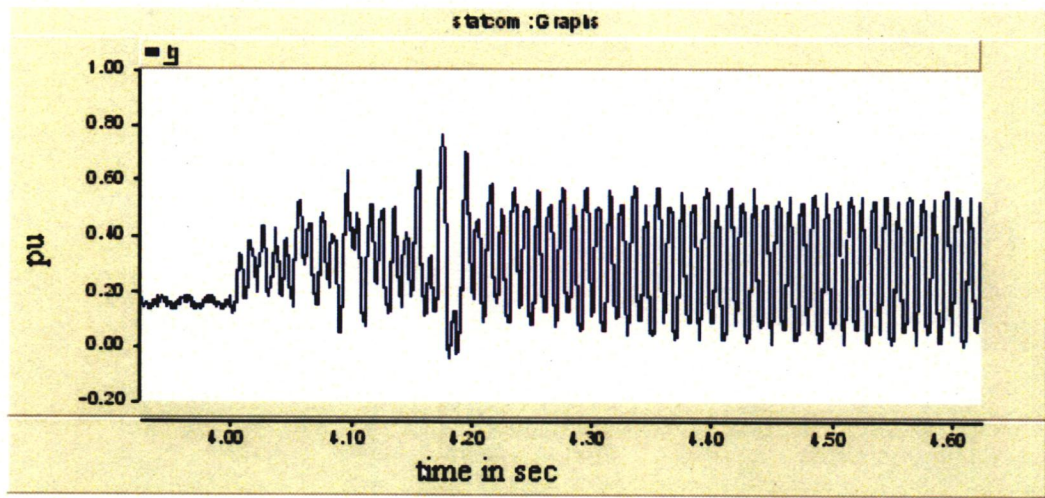


**Figure 5.17**  $I_q$  with direct control for LL-G fault



The main contribution of this dissertation is the development and tuning of Fuzzy Controller for STATCOM application. The direct control of STATCOM is a two input two output system as a result the designing of multi input multi output is quite difficult. This problem is solved by first designing the indirect Fuzzy controller which is a single input single output system, and then the design of direct Fuzzy controller has been achieved independently. The Optimization of the firing angles which has very low THD and good constrained satisfaction has been shown to be possible. The linear interpolation of modulation index has been done away as the look-up table has been stored with modulation index in steps of 0.001. The response of the controller for symmetrical fault is acceptable. In cases of unsymmetrical faults the problem with the unbalanced DC link capacitor voltages can be corrected by implementing per phase control of the DC voltage. The performance of the STATCOM for incoming and rejection of reactive load would be similar to the three phase to ground fault which has been observed to be satisfactory.

The membership function for the FPIC considered here is uniform, but the unequal voltage sag and swells during inception and clearing of faults provides the possibility to test the controller with non uniform membership function. The hardware and the computational requirements of the FPIC would be much simpler than the Exact nonlinear control system. The Fuzzy logic optimized PLC's from ABB and FANUC can be considered for the controller design. The complicated firing rule can be easily be fabricated by latest Field Programmable Gate Array (FPGA) from Xilinx or Altera. The power stage has to be designed considering the system rating and the switching loss. The latest family of Insulated Gate Commutated Thyristor (IGCT) and Emitter Turn Off (ETO) thyristors are viable options. In whole the thesis explored the possibility to use Fuzzy Logic for Cascaded Multilevel Converter based STATCOM successfully.



1957  
COMMUNICATIONS  
SECTION

- [15] Mudi R. K. and Pal N.R., "A robust self-tuning scheme for PI- and PD-type fuzzy controllers", IEEE Trans. on Fuzzy Systems, vol. 7, no. 1, Feb. 1999, pp. 2-16.
- [16] Stella Morris', P. K. Dash and K. P. Basu, "A fuzzy variable structure controller for STATCOM", Electric Power Systems Research, vol 65, issue 1 April 2003 pp. 23-24
- [17] B. Mwinyiwiwa, Z. Wolanski, and B. T. Ooi, "Microprocessor-implemented SPWM for multiconverters with phase-shifted triangle carriers," IEEE Trans. Industry Applications, vol. 34, pp. 487-494, May/June 1998.
- [18] S. M. Tenconi, M. Carpita, C. Bacigalupo, and R. Cali, "Multilevel voltage source converters for medium voltage adjustable speed drives," in Proc. IEEE International Symposium on Industrial Electronics, vol. 1, 1995, pp. 91-98.
- [19] P. W. Hammond, "Medium voltage PWM drive and method," U.S. Patent 5 625 545, Apr. 29, 1997.
- [20] S. Ito, K. Imaie, K. Nakata, S. Ueda, and K. Nakamura, "A series of PWM methods of a multiple inverter for adjustable frequency drive," in Proc. 5th European Conf. Power Electronics and Applications, vol. 4, 1993, pp. 190-195.
- [21] E. Cengelci, P. Enjeti, C. Singh, F. Blaabjerg, and J. K. Pederson, "New medium voltage PWM inverter topologies for adjustable speed ac motor drive systems," in Proc. IEEE APEC'98, vol. 2, 1998, pp. 565-571.
- [22] G. Carrara, D. Casini, S. Gardella, and R. Salutari, "Optimal PWM for the control of multilevel voltage source inverter," in Proc. 5th European Conf. Power Electronics and Applications, vol. 4, Brighton, U.K., Sept. 13-16, 1993, pp. 255-259.
- [23] MATLAB/SIMULINK [www.mathworks.com](http://www.mathworks.com)
- [24] L. Li, D. Czarkowski, Y. Liu, and P. Pillay, "Multilevel Selective Harmonic Elimination PWM Technique in Series-Connected Voltage Inverters," IEEE Trans Industry Applications, vol. 36, no. 1, Jan./Feb. 2000 , pp. 160-170
- [25] Biswarup Das and Bikash C. Pal, "Voltage Control Performance of AWS Connected for Grid Operation", IEEE Trans. on Energy Conversion, vol. 21, no. 2, June 2006 pp. 353-361
- [26] PSCAD/EMTDC, Manitoba HVDC research centre, Canada.
- [27] Qiang Lu, Y. Sun and Shengwei Mei "Nonlinear Control Systems and Power Systems Dynamics", Kulwer Academic Publisher.
- [28] Han-Xiong Li and H. B. Gatland , "Conventional Fuzzy Control and Its Enhancement", IEEE Trans. on Systems, Man, and Cybernetics- Part B: Cybernetics, vol. 26, no.5, October 1996, pp. 791-796.

# APPENDIX-A

## A.1 Calculations for Base values

$S_{base}$  =Rating of the STATCOM

$$= \pm 30 \text{MVA}$$

$V_{base}$  =Rated system voltage

$$= 11 \text{kV}$$

$$I_{base} = \frac{S_{base}}{\sqrt{3}V_{base}}$$

$$= \frac{30 \times 10^6}{\sqrt{3} \times 11 \times 10^3} = 1.57459 \text{ kA}$$

$$\begin{aligned} \text{DC link voltage in pu, } V'_{dc} &= \frac{\sqrt{2} \times V_{phase\_peak}}{V_{base}} \\ &= \frac{\sqrt{2} \times \sqrt{2} \times V_{line}}{\sqrt{3} \times V_{base}} = 1.1547 \end{aligned}$$

$$\begin{aligned} Z_{base} &= \frac{V_{base}}{\sqrt{3}I_{base}} = \frac{V_{base}^2}{S_{base}} \\ &= \frac{11^2}{30} = 4.03333 \end{aligned}$$

Coupling Resistance  $R=0.0605\Omega$

$$\text{Per-unit resistance } R' = \frac{R}{Z_{base}} = 0.015$$

Coupling Inductance  $L=0.00192576\text{H}$

$$\text{Per-unit reactance } X'_l = \frac{\omega L}{Z_{base}} = \frac{2 \times \pi \times 50 \times 0.00192576}{4.03333} = 0.15$$

Base voltage in DQ frame  $V_{DQ\_base} = V_{base}$

$$\text{Base current in DQ frame } I_{DQ\_base} = \frac{S_{base}}{V_{DQ\_base}} = \sqrt{3}I_{base} = 2.72727 \text{ kA}$$

## A.2 Phase shift for multilevel optimization

$$\beta = \frac{2 \times \pi}{N_{cell} \times h_{selected}} = \frac{2 \times \pi}{10 \times 11} = 3.273^\circ \text{ where } h_{selected} = \text{Harmonic to be eliminated by phase}$$

shift[24]

### A.3 Capacitor voltage ripple

$$\Delta V_c = 4.33\%V_{dc}$$
$$= \frac{4.33 \times \sqrt{2} \times \sqrt{2} \times V_{line}}{\sqrt{3} \times 100} = 550 \text{ V}$$

### A.4 Required total link Capacitance per phase

$$C_p = \frac{I_{peak}}{2\omega\Delta V_c} = \frac{\sqrt{2} \times 1574.59}{4 \times \pi \times 50 \times 550} = 0.006443768 \text{ F}$$

### A.5 Minimum modulation index for the system

$$Q = \frac{3}{2} (V_{ph\_peak}) \cos \delta \times \frac{(V_{ph\_peak}) \sin \delta}{R}$$
$$= \frac{3}{2} \sqrt{2} (V_{ph}) \cos \delta \times \frac{\sqrt{2} (V_{ph}) \sin \delta}{R}$$
$$= \frac{3}{2} \frac{(V_{ph})^2}{R} \sin 2\delta$$

For  $Q=30\text{MVA}$ ,  $R=0.0605\Omega$  and  $V_{ph} = \frac{11}{\sqrt{3}} \text{ kV}$

$$2\delta = -\sin^{-1} \frac{30 \times 2 \times 0.0605 \times \sqrt{3}^2}{3 \times 11^2}$$

$$\delta = -0.8595656^\circ$$

Now, using

$$mV_{dc} = \sqrt{2}V_{ph} (\cos \delta + \frac{x}{R} \sin \delta)$$

$$m_{\min} = \frac{\sqrt{2} \times 11}{\sqrt{3} \times 12.7} (\cos \delta - 10 \sin \delta)$$

$$m_{\min} = 0.601$$







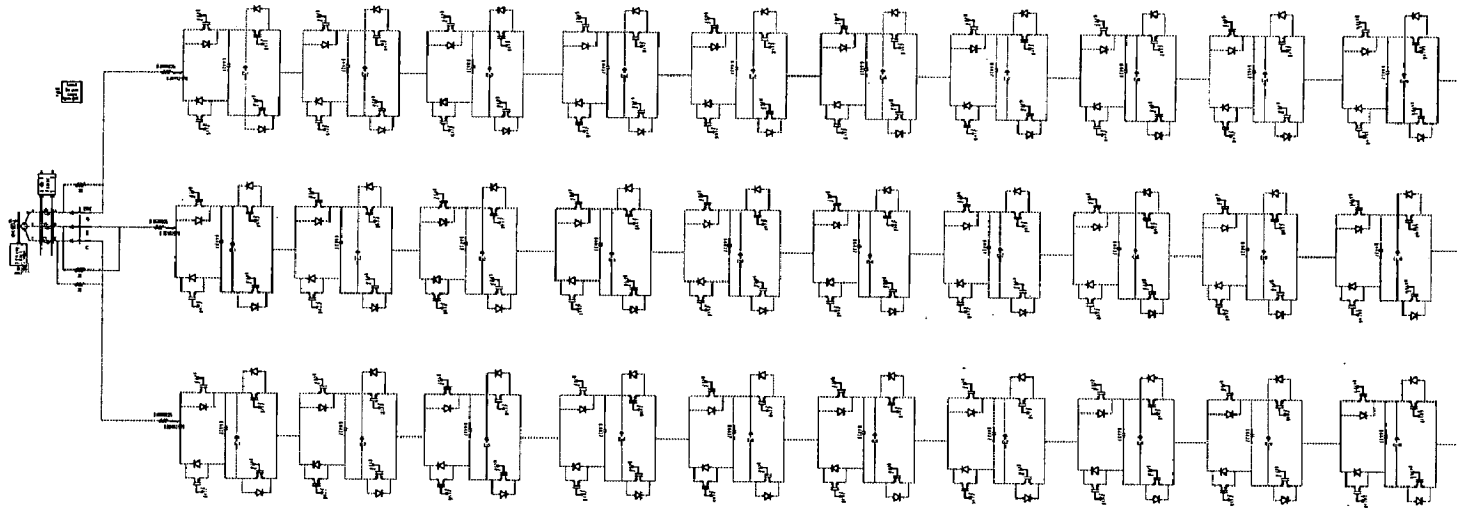
0.711	28.0192	67.8985	87.0263	33.6050	61.5843	77.2183	30.7925	62.9122	81.0979	32.0557	44.9829	70.1891	38.6539	75.9694	89.4675	19.4034	35.9918	64.8926	45.0823	81.3083	90.0000	11.8229	29.4917	63.1799	52.9394	16.7499	90.0000	3.9825	21.0178	60.3763
0.712	37.6347	74.5670	81.0863	33.7390	67.0010	83.2036	29.1575	59.3357	78.7011	20.6389	50.8229	75.2203	41.5166	78.5087	89.4466	16.9997	33.1234	63.8723	48.4381	84.0325	90.0000	12.2777	39.9704	69.6075	55.1131	16.9889	89.3414	4.0825	17.1393	58.8445
0.713	37.1873	66.3149	80.5004	29.2015	62.8485	81.7540	34.9887	70.8117	86.0206	22.8014	48.2392	72.2925	42.2650	79.6272	90.0000	20.4844	40.2698	67.2799	76.4657	82.8056	90.0000	12.2591	34.0194	65.6921	51.5190	85.8812	89.4524	4.0302	22.7019	60.9866
0.714	36.0477	65.0085	79.9370	29.2299	63.5964	82.5687	36.4829	71.2139	85.4818	20.3413	47.5766	72.6781	42.3986	79.7644	90.0000	23.5167	40.1850	65.9336	46.1791	82.4318	90.0000	12.1422	34.6395	66.0531	51.2760	45.9924	89.7081	4.0302	23.2287	61.1798
0.715	36.8237	71.1763	81.5201	35.6123	63.1201	79.8656	29.1917	63.1599	82.3634	20.4218	47.5448	72.5770	46.0342	80.3292	90.0000	23.5928	40.4129	66.0124	42.5169	79.8912	90.0000	12.1499	34.6420	66.1103	51.3167	16.7020	89.7446	4.0398	23.4040	61.1918
0.716	34.2654	63.7035	79.6936	33.5773	60.7273	77.3983	28.8853	66.7362	85.3051	19.0478	41.4385	68.4980	38.6735	77.1216	89.7417	12.1432	35.5049	63.5779	42.6817	80.0302	90.0000	11.9693	31.8492	64.2000	50.8362	16.6478	90.0000	3.9693	20.0014	59.7066
0.717	33.8673	62.4919	77.7443	32.9242	60.5955	77.9487	28.4413	66.5902	85.2465	18.7482	41.2080	68.3760	38.1236	77.0823	90.0000	20.9797	34.2440	62.8749	42.5980	79.7100	89.6768	11.9536	31.0321	63.7880	50.7984	16.8001	90.0000	3.9294	19.5150	59.4669
0.718	33.4440	60.5702	77.2010	30.2515	61.4089	79.7089	28.5606	66.9827	85.6062	18.0683	41.8215	68.9947	38.2254	76.7348	89.5535	20.2138	33.1719	62.4489	43.1287	80.4503	90.0000	12.2473	29.8573	63.0031	50.9991	16.2492	90.0000	4.1258	18.7339	58.8943
0.719	33.6142	63.2644	79.5235	33.3201	60.4466	77.1546	28.4482	66.1599	84.3163	18.2692	38.1206	78.3783	46.2692	81.2006	79.8082	23.3162	34.6512	63.1219	42.5705	80.0683	89.9584	11.9369	31.6842	64.6683	50.6893	16.6497	90.0000	4.1258	19.5126	59.1819
0.720	32.8214	60.3115	77.2670	31.5650	61.6656	79.1606	28.1473	66.0660	84.8690	18.5452	40.6079	67.8771	37.7155	76.9635	90.0000	20.4881	32.9012	62.0727	42.1843	79.7201	89.8307	11.9716	30.4602	63.2065	50.4222	16.6712	89.7760	3.9613	18.9733	59.0997
0.721	36.4851	60.9421	75.6435	27.2188	59.0448	78.9484	28.7391	65.9970	84.4677	15.2693	39.5878	68.1472	35.0179	73.1554	89.7802	20.3356	33.9888	62.7583	41.6297	79.4999	89.9396	12.1726	27.1383	61.4123	49.9089	16.2614	89.8204	4.0297	15.3905	57.7993
0.722	36.6315	61.7216	76.2124	27.7164	59.4520	79.0439	29.2128	66.1574	84.3490	16.8235	40.0785	67.9745	35.6896	73.8104	90.0000	20.3692	34.7959	63.2063	41.9210	79.6896	89.8870	12.0741	28.1109	61.8867	50.1461	16.5282	89.3603	3.9946	17.0152	58.2403
0.723	36.6099	61.1824	76.6014	27.3476	59.3990	79.1249	28.9607	65.9008	84.1815	16.6366	39.8149	67.8013	35.0448	73.6789	89.9939	20.3161	34.3092	62.8012	41.7193	79.6789	89.9659	12.0535	27.5777	61.5177	49.9384	16.5288	89.4758	3.9194	16.8098	58.1638
0.724	32.8649	61.0282	77.6985	27.8087	60.6514	79.9656	32.0572	66.9040	83.4897	18.0415	41.7989	68.6979	38.2527	77.4871	90.0000	20.3371	33.7392	62.4411	42.7608	80.4698	90.0000	11.9475	30.2007	62.9634	49.4478	16.4588	89.1377	3.8930	18.4693	58.7660
0.725	32.7115	61.1131	77.1816	27.7478	60.5875	79.8918	32.3094	66.9919	83.3453	17.8435	41.8385	68.7577	38.3076	77.6580	90.0000	20.2699	33.9095	62.5258	42.7078	80.4791	90.0000	11.9143	30.2595	62.9304	49.2930	16.4355	89.1064	3.8924	18.2277	58.5643
0.726	32.6691	61.2815	77.9145	27.6133	60.4352	79.6973	32.3238	67.0348	83.2698	17.7328	41.8758	68.7581	38.3628	77.6491	90.0000	20.1553	34.0340	62.6044	42.6272	80.4692	90.0000	11.8967	30.2399	62.8938	49.1626	16.4291	89.1050	3.9156	18.0582	58.4478
0.727	32.6575	61.3322	77.9278	27.6821	60.4939	79.7705	32.2649	67.0707	83.1969	17.5783	41.8767	68.6835	38.3034	77.6375	90.0000	20.1197	34.1106	62.6167	42.3004	80.4279	90.0000	11.8866	30.3444	62.9212	49.1566	16.4021	89.0675	3.9184	17.8862	58.3324
0.728	32.7158	61.0530	77.6192	27.6133	60.4718	79.7161	32.2271	66.7991	83.1203	17.5700	41.4513	68.4114	38.0887	77.5676	90.0000	20.1229	33.8614	62.4061	42.3111	80.1928	89.9755	11.8943	30.2001	62.7733	49.1349	16.4348	89.0715	3.8865	17.8902	58.2835
0.729	35.2317	59.4228	74.6671	28.0517	59.2408	78.3749	29.5735	64.4744	84.0032	16.2606	38.1094	65.4599	34.0966	74.4955	89.3253	19.9403	32.5256	61.5978	41.5496	79.2054	90.0000	11.8400	25.6510	60.3119	49.3283	16.4562	89.0000	3.9136	17.2018	57.6472
0.730	32.9321	59.9964	76.4637	27.7246	59.8249	79.4936	30.1175	65.4003	83.2973	17.2137	40.1628	67.5208	37.1084	76.7688	89.7292	20.0896	32.7955	61.6541	41.6304	79.9734	90.0000	11.9373	29.3517	62.1865	49.4348	16.4623	89.3043	3.9318	16.4103	57.9994
0.731	33.1472	59.9612	76.2642	27.4549	59.8722	79.1241	29.4044	65.6106	83.3453	16.4756	39.5938	67.3086	36.8147	76.5350	89.6333	19.9678	32.8086	61.6584	41.2028	79.7318	90.0000	11.9530	28.4201	61.6217	48.9618	16.4721	89.4558	3.9522	16.5677	57.6570
0.732	32.9403	60.1788	76.5280	27.4193	59.7442	78.9829	29.9425	65.7159	83.1283	16.5627	39.6718	67.3483	36.9446	76.8023	89.7704	19.9055	32.7966	61.6240	41.4629	79.5604	89.8237	11.9473	28.8607	61.8118	48.7836	16.4603	89.4287	3.9405	16.4404	57.3518
0.733	33.0817	60.8426	76.9263	27.9228	59.2203	78.4889	30.2841	65.8631	83.0456	16.0690	39.7060	67.4120	37.0005	77.1186	90.0000	19.8546	33.0920	61.7151	41.0901	79.1859	89.4473	11.8990	29.1303	61.9203	48.6997	16.4530	89.3161	3.9579	16.2225	57.4013
0.734	33.1677	61.4268	77.4692	27.8400	59.9530	78.4889	30.1175	66.1036	83.1283	17.2137	40.1628	67.5208	37.1084	76.7688	89.7292	20.0896	32.7955	61.6541	41.0846	79.9734	90.0000	11.9373	29.3517	62.1865	49.4348	16.4623	89.3043	3.9318	16.4103	57.9994
0.735	33.3127	62.0040	77.8195	27.3760	58.9334	78.1530	31.5831	66.3261	82.7083	16.1389	40.5029	67.7089	37.7499	77.6767	90.0000	19.7818	34.1891	62.3889	41.1272	79.0503	89.2001	11.8559	30.0359	62.3443	48.1190	16.4827	89.6661	3.9203	16.1402	57.3033
0.736	40.0799	67.6280	78.8415	35.5086	60.0588	74.7436	28.5164	64.4660	82.4880	26.9967	40.0523	65.0972	34.7882	73.3460	89.4404	19.9078	27.9589	58.2730	40.4931	79.4490	90.0000	11.8757	33.9526	64.5986	48.6560	16.4504	89.2537	3.9681	18.5045	68.1148
0.737	40.0511	67.6443	78.8298	35.4210	59.9631	74.6639	28.4739	64.2821	82.3140	26.8624	39.8817	65.9921	34.7364	73.3281	89.4075	19.9033	27.9756	58.1282	40.2802	79.3940	90.0000	11.8849	33.8222	64.4661	48.4102	16.4374	89.2394	3.9681	18.5007	68.6627
0.738	39.9299	67.6285	78.8485	35.2196	59.9631	74.6426	28.4073	64.1841	82.1788	26.7702	39.6999	65.8360	34.8882	73.4312	89.3779	19.8858	27.9699	58.0250	40.1244	79.3375	90.0000	11.8775	33.8214	64.4661	48.4102	16.4341	89.2278	3.9788	18.4183	68.5601
0.739	39.7712	67.6692	78.9447	35.0251	59.7491	74.6154	28.3606	63.9105	81.9401	26.6242	39.5655	65.6413	34.9797	73.5538	89.3970	19.8491	26.9139	57.8927	39.9833	79.2909	90.0000	11.8811	33.7911	64.3481	48.2400	16.4240	89.1563	3.9687	18.4132	68.5089
0.740	39.6233	67.7225	79.0440	34.8934	59.6514	74.5596	28.3871	63.6234	81.6217	26.5349	38.9264	65.4135	34.9950	73.6598	89.4459	19.8312	26.8683	57.7254	39.7475	79.1828	90.0000	11.9401	33.6870	64.2204	48.1006	16.4039	89.0379	3.9373	18.4850	68.5108
0.741	39.5411	67.6280	78.9644	34.8626	59.5961	74.4817	28.5126	63.6781	81.5656	26.1595	38.8040	65.3736	35.0466	73.6453	89.3572	19.7983	26.6298	57.6554	39.5467	79.0982	90.0000	11.9350	33.7778	64.2276	47.9400	16.4078	89.1270	3.9245	18.3771	68.3912
0.742	39.5622	67.6490	78.7745	35.0030	59.6328	74.3843	28.5432	63.8614	81.6710	26.2055	39.1725	64.9003	34.8882	73.5149	89.2810	19.8987	26.9390	57.6593	39.5104	79.1205	90.0000	11.9217	33.8214	64.2204	47.9400	16.4644	89.1196	3.9118	18.1472	68.3903
0.743	39.4738	67.4313	78.7304	35.1279	59.5995	74.2332	28.4738	63.8618	81.6596	26.0891	39.1199	65.5311	34.9887	73.4073	89.2925	19.7735	26.5840	57.5344	39.5591	79.1525	89.9554	11.9232	33.7047	64.0852	47.8902	16.4862	89.2107	3.9046	18.0704	68.0915
0.744	39.4406	67.4914	78.5																											



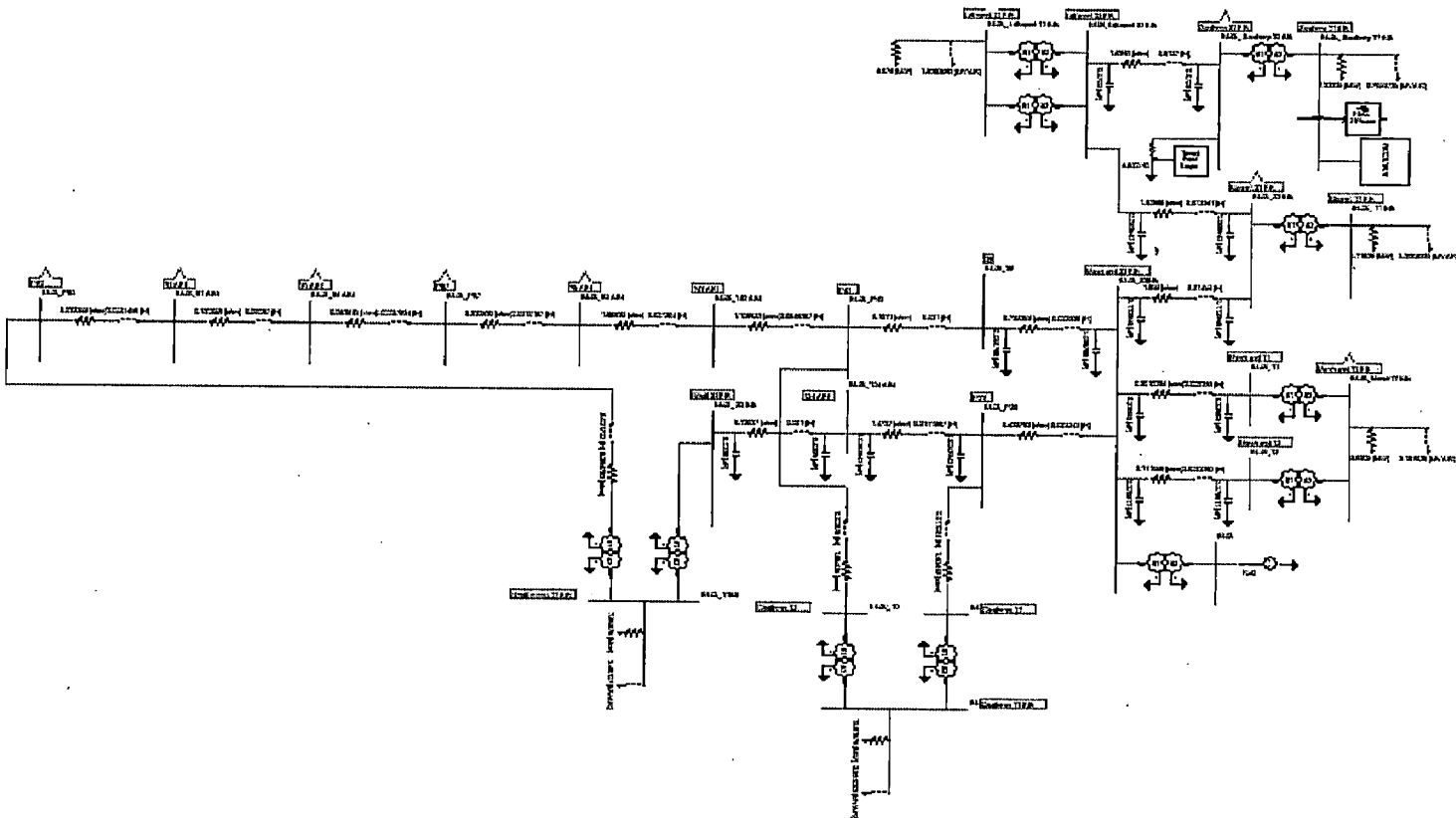
Table with 40 columns and 1000 rows of numerical data. The data is organized in a grid format, likely representing a dataset or a list of values. The first row contains values from 0.883 to 90.0000, and the last row contains values from 0.968 to 91.5708. The values are separated by commas and some are grouped by brackets.

Table with 31 columns and 1000 rows of numerical data, likely a coordinate list or a data table.

# APPENDIX C



STATCOM Circuit Layout



PSCAD Model of distribution grid